BREAKDOWN IN VACUUM DEPOSITED THIN FILM SILICON MONOXIDE CAPACITORS

By Paul J. Hayes
Directed by Paul P. Budenstein

Supplement to Final Report
on Contract NAS8-11279

Submitted to

National Aeronautics and Space Administration
George C. Marshall Space Flight Center
Huntsville, Alabama

August, 1966

A U B U R N U N I V E R S I T Y

Physics Department

BREAKDOWN IN VACUUM DEPOSITED THIN FILM SILICON MONOXIDE CAPACITORS

Supplement to Final Report
On Contract NAS8-11279

By Paul J. Hayes

Directed by Paul P. Budenstein

This report is a thesis
submitted to the Graduate Faculty
of Auburn University
in Partial Fulfillment of the Requirements
For the Degree of Master of Science.

Submitted to

NATIONAL AERONAUTICS AND SPACE ADMINISTRATION
GEORGE C. MARSHALL SPACE FLIGHT CENTER
HUNTSVILLE, ALABAMA

August, 1966

THESIS ABSTRACT

BREAKDOWN IN VACUUM DEPOSITED

THIN FILM SILICON MONOXIDE CAPACITORS

Paul Jackson Hayes

Master of Science, August 24, 1966
(B.E.P., Auburn University, 1960)

167 Typed Pages

Directed by Paul P. Budenstein

A technique is developed whereby thin film silicon monoxide capacitors are vacuum deposited and subsequently removed from the substrate intact. This development enables an electron microscope study of the capacitors while under electrical stress. Resulting from this study is the discovery of breakdown center defects of about one-half micron diameter. Furthermore, it is established that during breakdown the silicon monoxide decomposes, leaving free crystalline silicon. A number of types of breakdown patterns are observed in the electron microscope. Single breakdowns exhibit either a strong radial or concentric pattern, or both.

The breakdown strength is found to be relatively independent of temperature, at least between 80°K and 363°K. There is a slight increase in breakdown strength as the temperature is decreased. This is in marked contrast with the dc conductivity which is highly dependent on temperature.

A comparison of the breakdown strength data with published theories shows that the best agreement is with that attributed to electron ionization avalanche and developed by Forlani and Minnaja. Although their model is not an amorphous dielectric, the $1/W^{\frac{1}{2}}$ breakdown strength dependence on thickness roughly fits the experimental data of silicon monoxide capacitors. Other theories of breakdown (intrinsic, thermal, and avalanche) are not nearly in agreement with the experimental data. It is found that the voltage across the capacitor does not drop to zero volts during a breakdown, but to a value V_{MIN} which is a constant for a given polarity and a given capacitor; this voltage is independent of temperature over the range of measurements. It is of significance that no breakdowns were ever observed below a given capacitor's V_{MIN}. The field corresponding to the experimental value of V_{MIN} appears to depend on the reciprocal of dielectric thickness over the range investigated.

A study is made of the rate-of-breakdown as the voltage across a capacitor is steadily increased to and above the voltage corresponding to the breakdown strength. Since the rate-of-breakdown is thought to be closely related to the probability of a breakdown, the results are compared with tunnel-emission injection of current into the dielectric at the cathode, an inherent part of the electron ionization avalanche breakdown theory. Agreement is good in some cases, but not as good for higher voltages.

Several observations related to breakdown pulse characteristics and measurements are made.

A broad range of breakdown structure is discussed in connection with an optical photomicrographic examination of the breakdowns which occurred in the capacitors on glass slides.

No correlation between breakdown strength and deposition parameters is established. Neither is there any indication that breakdown is attributable to substrate irregularities.

ACKNOWLEDGEMENTS

The author is grateful to Dr. Paul P. Budenstein for the encouragement and many helpful suggestions given throughout this study. Appreciation is expressed to the National Aeronautics and Space Administration, Huntsville, Alabama, for the financial support which made this work possible.

The author wishes to thank J. W. Heptinstall for his help in reducing the data and W. T. Garrison for drawing the figures.

TABLE OF CONTENTS

LIST OF TABLES

LIST OF FIGURES

I. THE PROBLEM

A. History

The capacitor is one of the many circuital components readily fabricated by vacuum deposition methods. Because of ease of deposition, low cost of materials, and good temperature stability these components frequently have the construction of aluminum-silicon monoxide-aluminum sandwiches. The mechanical and electrical characteristics of such a device have been found to be very much dependent on the deposition conditions. In particular, studies by Novice[1,2], Priest, Caswell, and Budo[3,4], and Holland[5] have shown that stresses within silicon monoxide films are dependent on the source temperature and the amount of oxygen in the atmosphere of the evaporant. Novice has indicated that proper control of these two parameters will yield practically stress-free films when they are exposed to atmospheric pressure.

Several studies of the electrical characteristics of silicon monoxide capacitors have been made[6-8] but with the intention of shunning the conditions for dielectric breakdown. On the other hand, Siddall[9] found that capacitors having a dielectric thickness of 5500 Å to 17,200 Å possessed a greater dielectric strength if the silicon monoxide were deposited at a slower rate. More recently, Hartman, Blair, and Bauer[10] have observed breakdown strengths of 4×10^5 to 2×10^6 volts/cm in agreement with Siddall. Siddall's data also show that for a given dc voltage on a capacitor, the breakdown rate decreases with the time of

voltage application. This decrease in breakdown rate was not so great at higher electric fields and thus the effect was interpreted as follows: defects in the capacitor influence the occurrence of breakdown below the dielectric strength and hence the minimum breakdown voltage in a capacitor does not yield a realistic value of dielectric strength. These defects at which breakdown occurred were thought to be either pinholes in the film, due to dust on the substrate or spitting of the evaporant source, or some type of dielectric fault. Replicas of the silicon monoxide films observed in an electron microscope showed an occasional irregular structure of about one-half micron diameter; However, this was thought to be an aggregation of the shadow material (gold/palladium alloy) used in the replica.

Siddall also mentions the occurrence of spontaneous short circuits which may be destroyed by a forming process in which a large (few microfarads) capacitor is suddenly discharged through the shorted capacitor. Budenstein[11] has shown that the temperature coefficient of resistivity of the capacitor while in such a low resistance state is positive and 3/4 that of the aluminum electrodes. He interprets the shorting spots to be due to highly doped regions of the dielectric rather than direct aluminum shorts. The destroyed regions generated when the capacitor is formed are similar in appearance to the breakdowns which occur in low-leakage capacitors. This indicates the same type of process for both--i.e., a local high current path at the instant of breakdown.

Chaikin and St. John[12] concluded that the presence of substrate blemishes contributed significantly to a low breakdown strength. The electrode material was also found to be important in this respect. A bottom

copper electrode with a matte surface resulted in a lower breakdown strength than smooth copper or aluminum electrodes. Their study indicated that steps in the dielectric were highly vulnerable to breakdown.

Many parameters are thought to contribute to the dielectric strength of vacuum deposited silicon monoxide capacitors. From the literature mentioned above one would strongly suspect that the following would substantially effect the breakdown strength:

1) Temperature of silicon monoxide evaporant
2) Rate of deposition of dielectric
3) Cleanliness of substrate
4) Construction of capacitor
5) Substrate temperature
6) Pressure and constituency of vapors in vacuum chamber.

Tests made early in this breakdown study indicate that the following factors also influence the breakdown strength:

1) Polarity of applied voltage
2) Previous electrical history of the capacitor
3) Humidity
4) Electrode materials.

B. Purpose of This Study

The purpose of this study is to investigate the breakdown mechanism in vacuum deposited thin film silicon monoxide capacitors. The study encompasses an investigation of the onset of breakdown in both its electrical and visual aspects. These two aspects are combined in a unique, as far as can be determined, experimental arrangement whereby the capacitors are electrically energized and simultaneously observed by transmission

electron microscopy. Development of the specimen preparation techniques for this experimental arrangement is a secondary purpose of the study.

C. Organization of the Remainder of the Thesis

The method of capacitor fabrication and the techniques for stripping the capacitors for electron microscopy are described in Chapter II. The testing methods and setups for both electron microscopy and ramp voltage tests are discussed in Chapter III. Chapter IV contains the results of the visual and electrical observations and the interpretation of these in regard to the breakdown mechanism. The last chapter gives a summary of the results along with suggestions for future work.

II. CAPACITOR FABRICATION BY VACUUM DEPOSITION

A. Deposition Preliminaries

Primarily because of its smooth surface, chemical inertness, rigidity, and ease of cleaning, glass was chosen as the substrate onto which the capacitors would be deposited. Some effort was made to use thin colloid films as substrates for capacitors to be studied in the electron microscope. However, little success was realized and these attempts were abandoned after a method was established for stripping capacitors from glass slides.

In order to prevent pinholes and obtain good film adherence to the glass substrate, the substrate must be thoroughly cleaned prior to deposition. The substrate preparation procedure is as follows:

1) Silver contact tabs are painted at the edges of the glass slides. The slides are then heated to 600°C to "fire-on" the silver. (This step is not required when depositing capacitors for electron microscopy.)
2) The slides are washed with deionized water and detergent for approximately fifteen minutes in an ultrasonic cleaner.
3) The slides are rinsed twice with deionized water in the ultrasonic cleaner. Each rinsing lasts about fifteen minutes.
4) Finally, the slides are rinsed with isopropyl alcohol and vapor-degreased in a manner similar to that discussed by Holland.[13]

The basic design of the capacitor for electron microscopy is shown in Fig. 1. The dielectric thickness is of the order of 2000 Å; however, this parameter has varied from 800 Å to 3000 Å. The aluminum electrodes are about 300 Å to 400 Å thick. The bottom electrode and dielectric are made 1/8 inch diameter to fit the specimen holder of the RCA-EMU-2D electron microscope. The upper electrode is 1/16 inch diameter to prevent shorting at the edges. The effective area of the capacitor is that of the upper electrode--0.02 cm^2. On top of the upper electrode is deposited another metallic layer which is several thousand Angstroms thick. This layer, generally aluminum or silver, is 1/64 inch in diameter and serves as the contact point of the upper electrode. The purpose of such a thick contact point is to reduce the likelihood of scratching through the dielectric while establishing contact to the electrode. The edges of the different layers are not as sharp as is shown in Fig. 1. Rather, each edge slopes off over a distance of approximately ten microns.

The larger capacitors, which are not made for electron microscopy, but are to remain on the glass slide, are constructed similarly but the contact layer is omitted and the effective area of the capacitor is over 100 times larger; this area is about 9.0 cm^2.

The two electrode and dielectric masks are shown in Fig. 2. Each fabrication yields a batch of twenty-seven capacitors suitable for electron microscopy and one larger capacitor. For notational purposes the capacitors of each batch are numbered in the order in which they are studied (e.g., 1000-1, 1000-2, etc.). The larger capacitor is designated by the same number but with the suffix T (e.g., capacitor 1000-T).

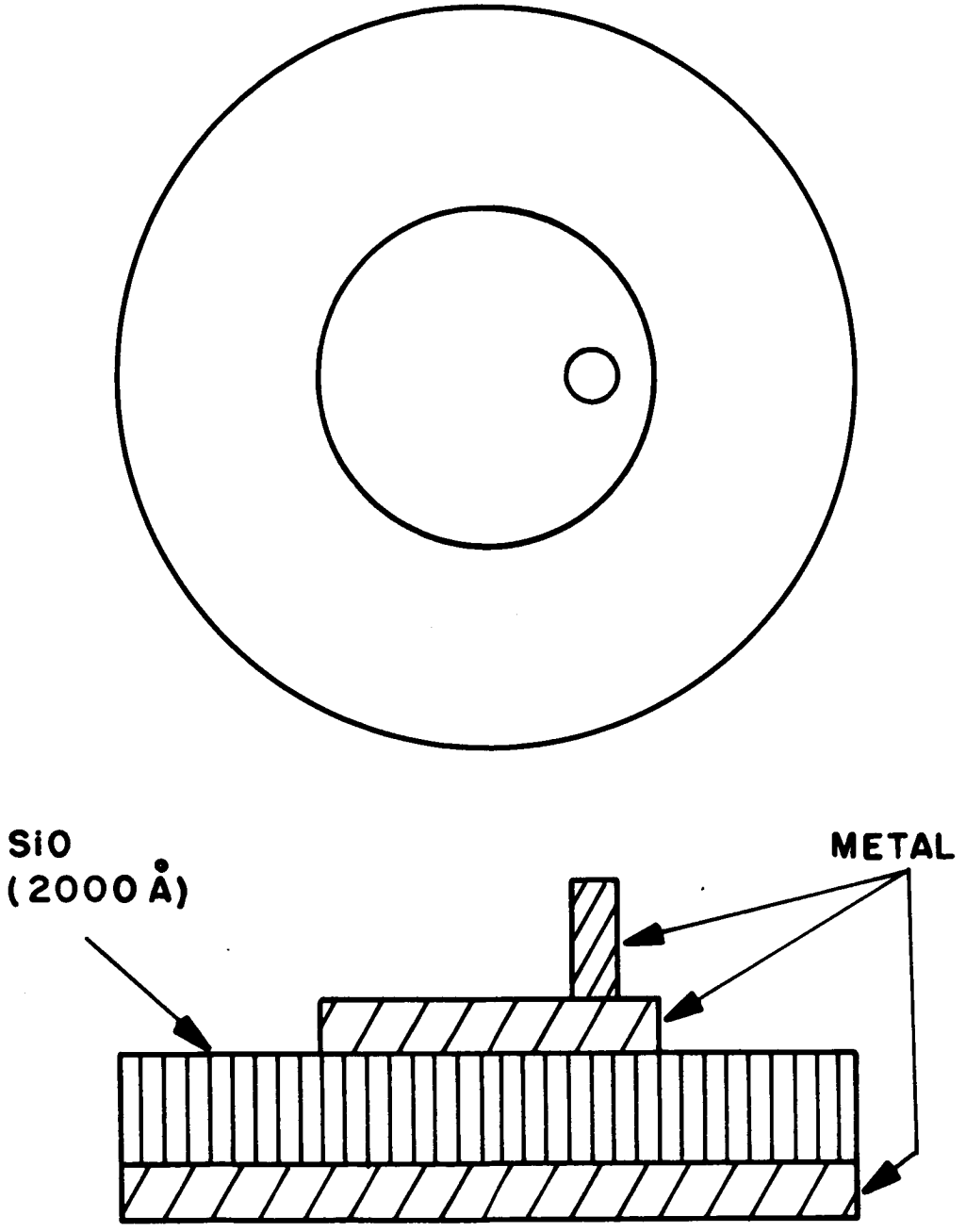

Figure 1. Capacitor design.

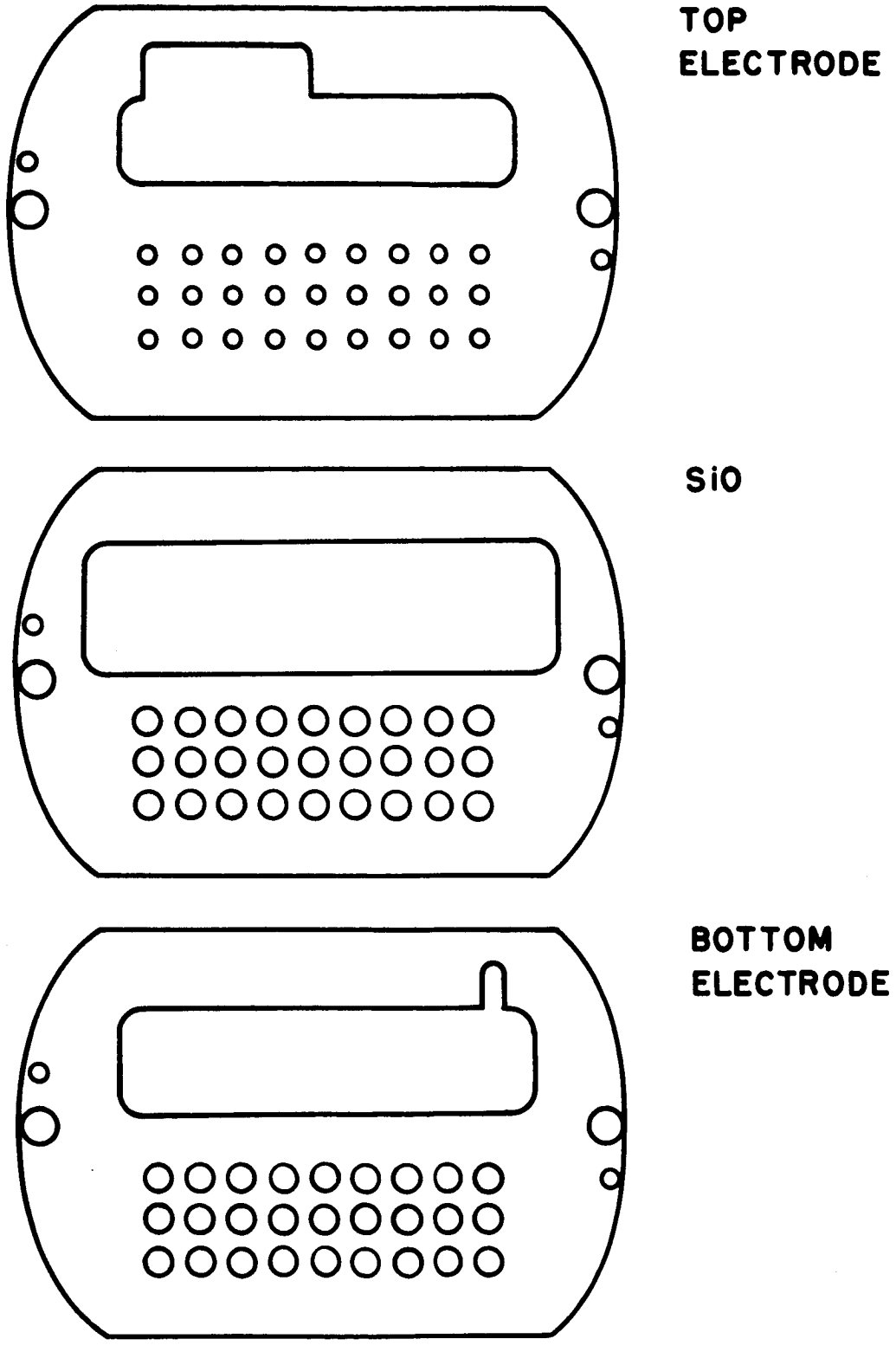

Figure 2. Masks used for capacitor fabrication.

B. Evaporation Setup and Procedures

Vacuum system and evaporation unit

To obtain high quality vacuum deposited films, it is generally desirable to evacuate the deposition chamber to about 10^{-6} Torr. The system constructed, shown in Fig. 3, consists of a four-inch silicone oil diffusion pump with a water-cooled baffle backed by a mechanical pump. Two to three hours are usually required to pump the system down to about 2×10^{-6} Torr while over-night pumping will reduce the pressure to about 6×10^{-7} Torr. A thermal switch on the cooling coil of the diffusion pump and a relay are arranged to turn the system off in the event of either a loss of cooling water or a temporary loss of electrical power.

Immediately above the baffle is an aluminum collar which provides six ports into the chamber. The five ports in use provide for an air inlet valve, a thermocouple gauge, an ionization gauge, and two fifty ampere feed-through terminals. The deposition chamber is a Pyrex cross which rests on the collar. The two side openings are provided with quarter-turn fasteners so that quick entry may be made without removing the flanges. Feed-through terminals (3/8 inch diameter) capable of handling 300 amperes continuously and 400 amperes for twelve minute alternate intervals are mounted in an aluminum cover which is secured to the flange at the entry seen on the left side in Fig. 3. Extension rods are bolted to the feed-through terminals to center the evaporant in the vacuum chamber. As seen in Fig. 4, the evaporation source is enclosed by a stainless steel box which is isolated from the glass chamber by ceramic insulators. A tubular stainless steel shield is placed on top of the box with

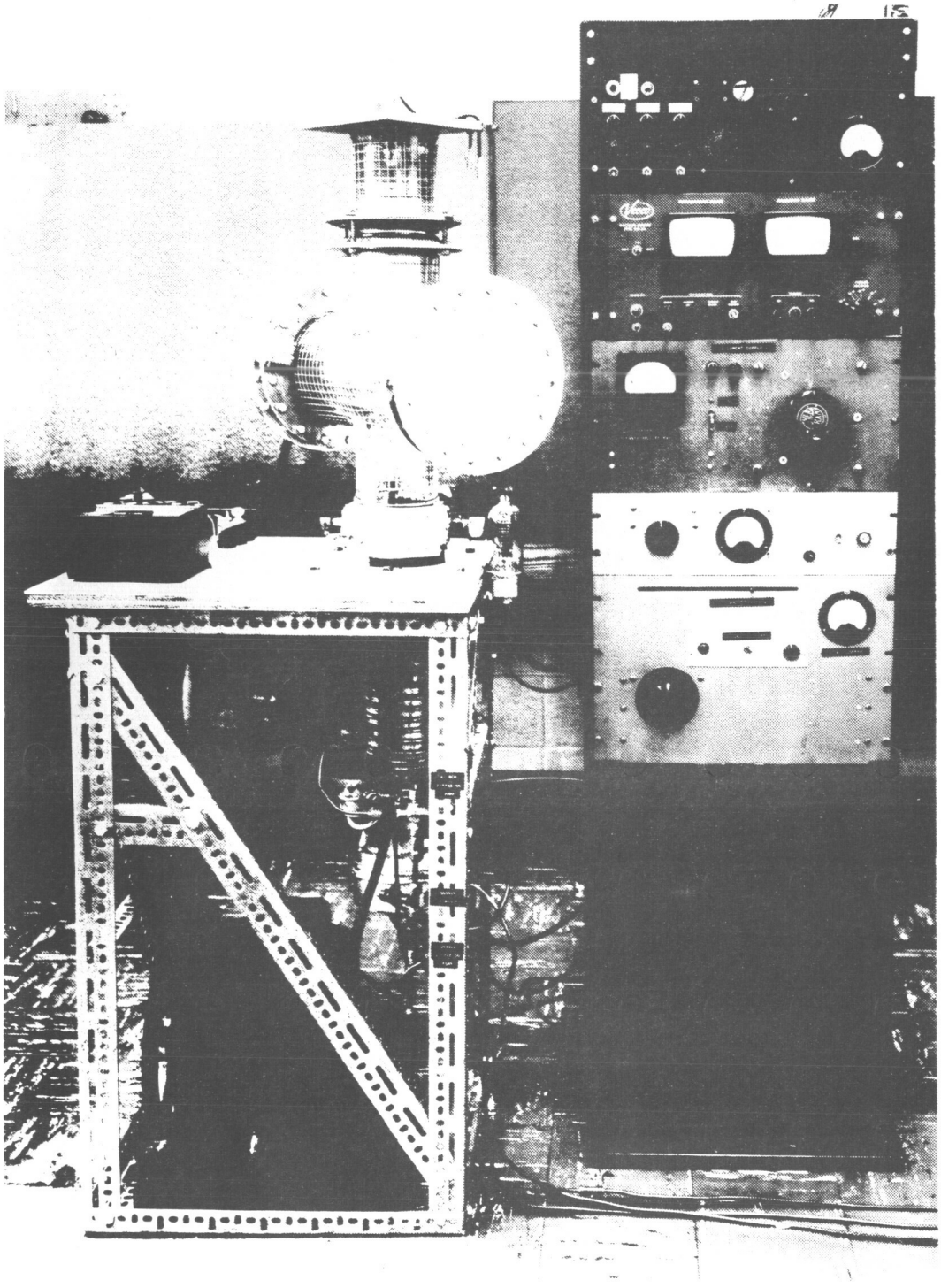

Figure 3. Vacuum evaporation system.

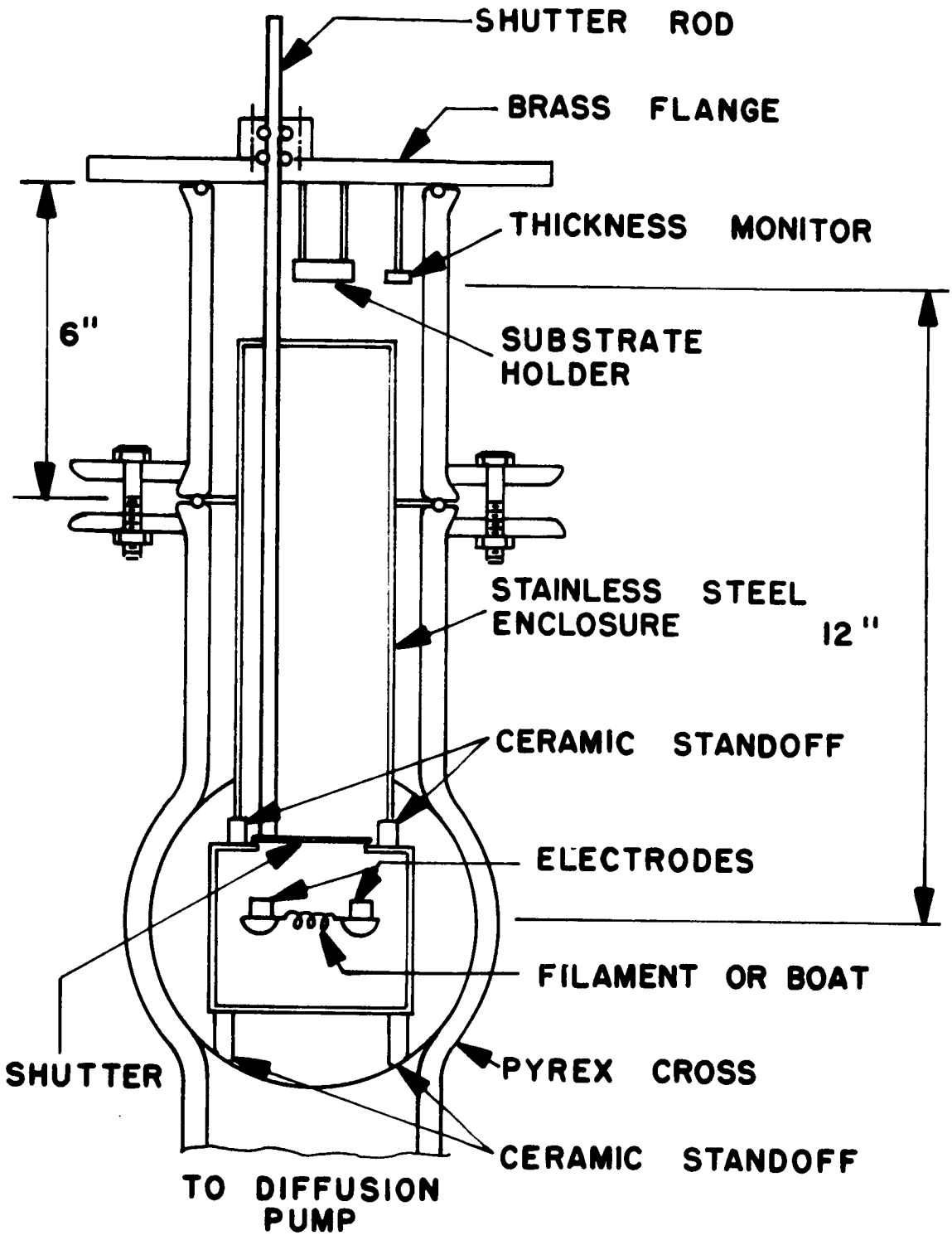

Figure 4. Diagram of vacuum evaporation chamber.

sufficient vertical clearance for movement of a shutter. The shutter is attached to the top brass plate, but is located about $\frac{1}{4}$ inch above a $1\frac{1}{2}$ inch diameter hole in the center of the box which encloses the evaporation source. These shields reduce the heating of the glass chamber and prevent dirtying of the chamber by the evaporants.

The shutter, substrate, and film-thickness monitor-crystal are mounted to the brass plate which rests on an O-ring at the top of the chamber. The substrate and monitor-crystal are nominally twelve inches above the evaporating source. Some capacitors were made without the six inch extension on top of the Pyrex cross. The source-to-substrate distance for that arrangement was about six inches. The instrumentation and pressure meter (Veeco Type RG-3A) are mounted on the panel rack beside the vacuum chamber as shown in Fig. 3.

The electrical circuit of the evaporation unit is shown schematically in Fig. 5. The twenty ampere variac and 2 KVA transformer are standard parts provided with certain Consolidated Vacuum Corporation evaporation units. The ac meter M2 (Westinghouse Type PA-151) is paralleled with three precision shunts to expand the highest scale from 200 amperes to 400 amperes full-scale reading. In Fig. 3 this meter is shown on the table in front of the evaporation chamber.

Film thickness monitor

A quartz crystal is employed to measure film thickness and rate of evaporation continuously during the deposition process. The change in the natural frequency of oscillation of such a crystal is related to the change in thickness of a film deposited onto it through the equation[14]

$$\frac{\Delta f}{f} = \left[\frac{\rho(F)}{\rho(Q)}\right]\frac{\Delta T_o}{T_o} \qquad (1)$$

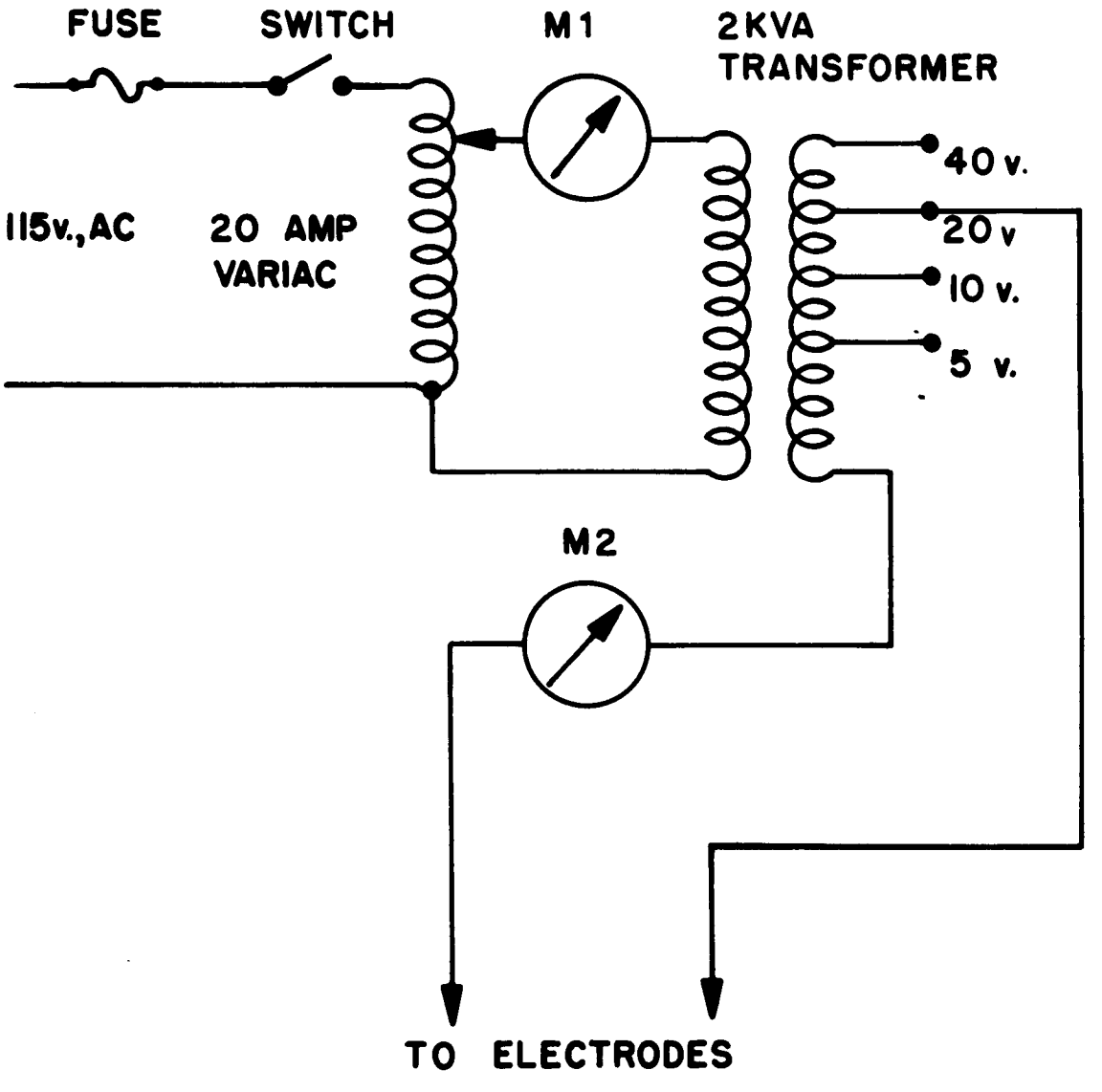

Figure 5. Schematic of evaporation unit.

where f and Δf are, respectively, the resonance frequency and the change in frequency corresponding to a change in film thickness ΔT_o. T_o is the total thickness of the quartz crystal and the deposited film; $\rho_{(Q)}$ and $\rho_{(F)}$ are the densities of the crystal and the deposited film respectively. From the results of Wolter, one may expect about 5% experimental accuracy. For less accuracy the crystal may be calibrated with a few depositions to obtain a constant

$$K = \frac{\Delta f}{\Delta T_o} . \tag{2}$$

This constant may be used to predetermine the frequency shift for a particular film thickness or deposition rate. In this manner film thickness has been controlled during the deposition process within twenty percent.

The crystal oscillator circuit is basically that developed by Dence and Goldner[15] although a few modifications were made to optimize dc operation of the output transistor stage. The circuit, shown in Fig. 6, consists of two identical crystal oscillators--one of the crystals is located in the vacuum chamber. The frequencies of the two oscillators are mixed and the difference frequency is fed to an amplifier.

The complete circuit is shown in Fig. 7. The EPUT meter (Beckman Model 7151K) and readout (Beckman Model 5915) provide for continuous monitoring of film thickness and rate. Typically the frequency is read every second. Thus for a given evaporant the deposition rate is, using equation (2),

$$R = \frac{\Delta T_o}{1 \text{ sec.}} = \frac{\Delta f}{K} . \tag{3}$$

For a given rate the predetermined frequency change is given by

$$\Delta f = RK, \tag{4}$$

for a frequency readout every second.

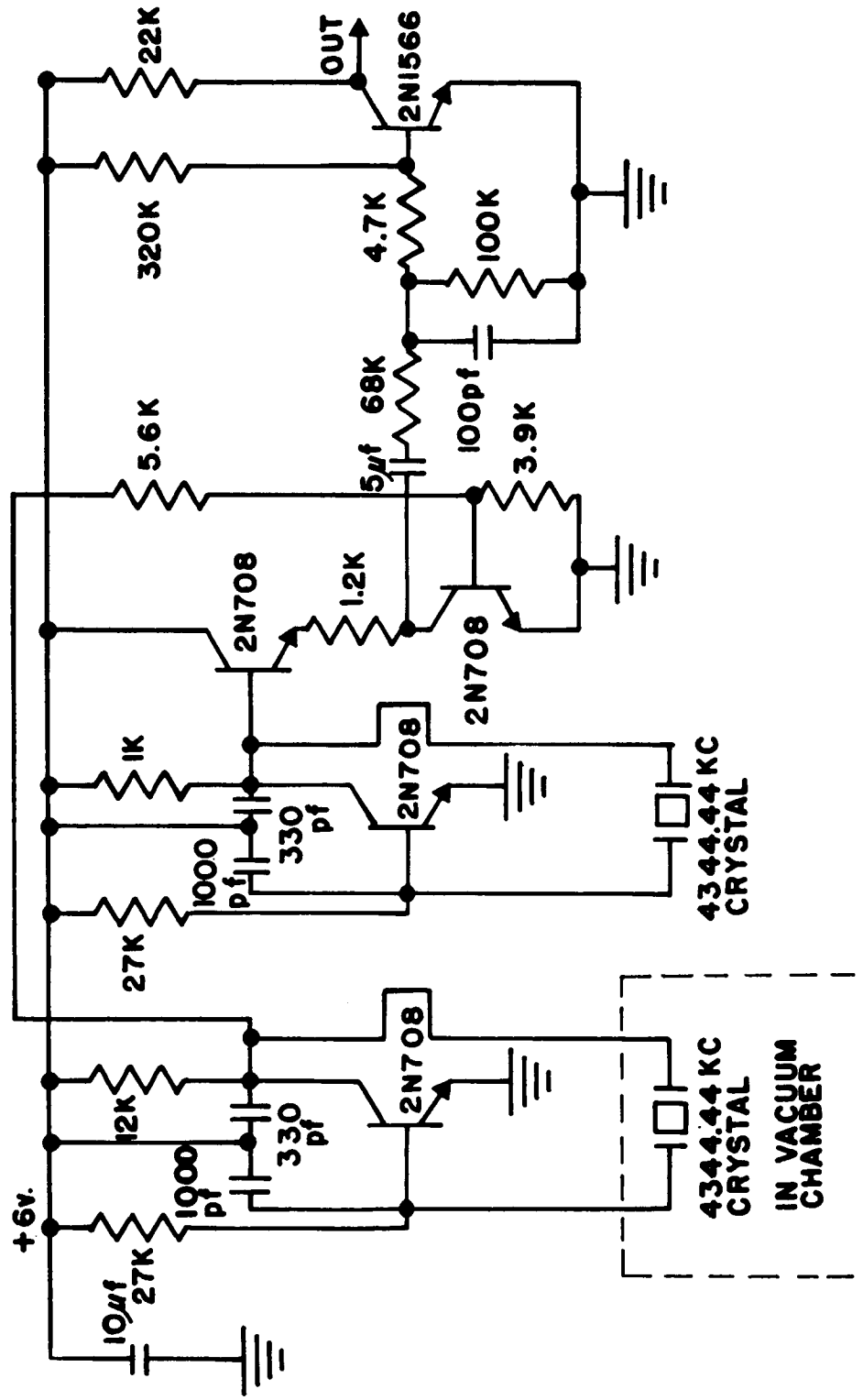

Figure 6. Schematic of crystal oscillator portion of film-thickness monitor.

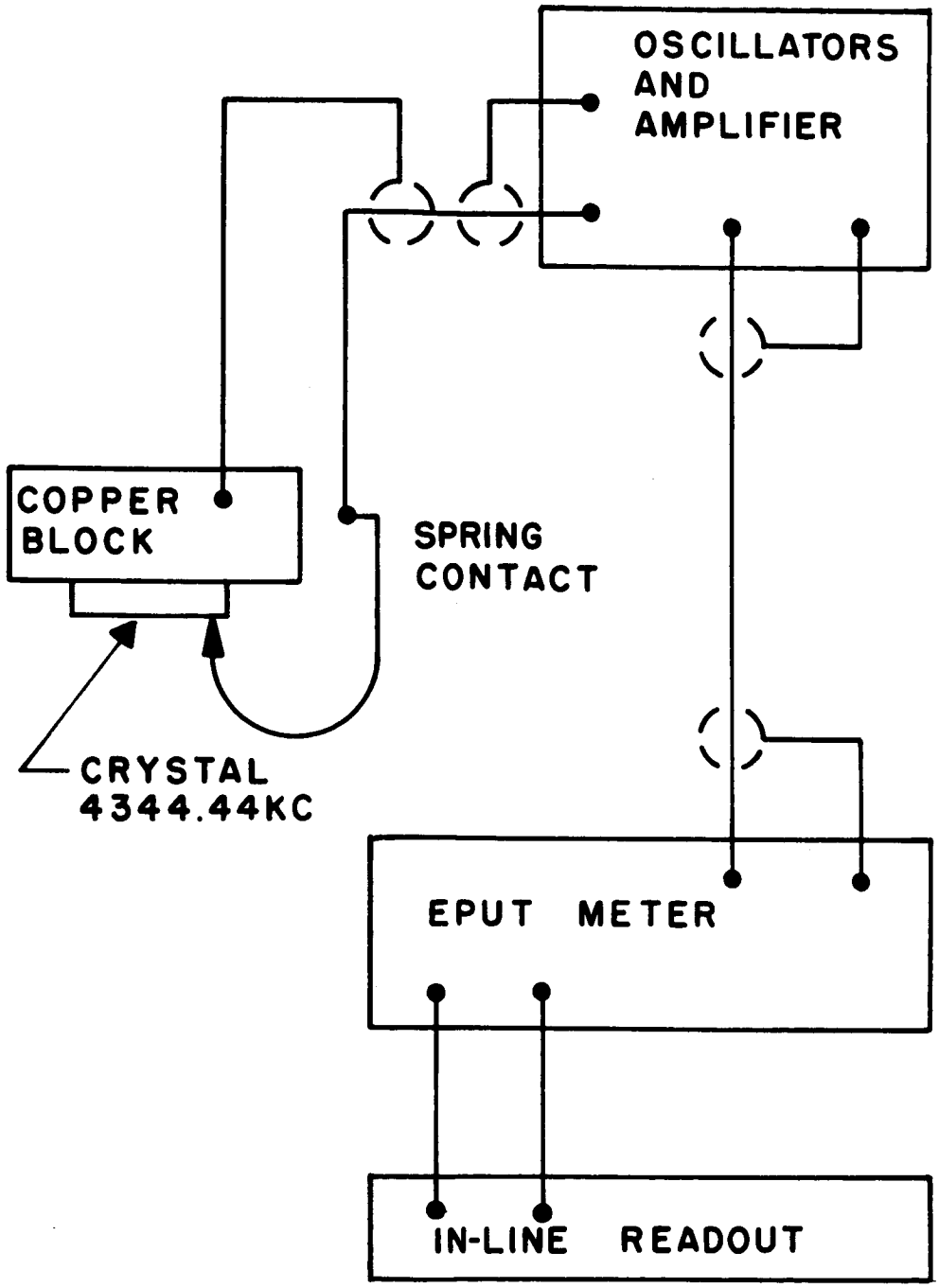

Figure 7. Block diagram of film-thickness monitor.

The crystal is calibrated by use of a Tolansky interferometer.[16] The particular instrument in this study employs a x 5 objective and a x 15 eyepiece. The silver flats are prepared by vacuum deposition and are about 200 Å thick.

Evaporation procedures

Evaporations are not begun until the pressure is below 2×10^{-6} Torr. Frequently the pressure is much lower (about 6×10^{-7}) after the system has pumped overnight. The evaporation source is outgassed for several minutes before the evaporation temperature is reached. While outgassing the pressure rises--in aluminum evaporations the pressure may be kept below 10^{-5} Torr while slowly increasing the filament current. In evaporating silicon monoxide, however, the pressure will typically rise as high as 6×10^{-5} Torr before the onset of evaporation. The shutter is opened to expose the substrate to the source after the evaporation has begun. The onset of evaporation is generally noted by a decrease in pressure due to the gettering action of the evaporating material. This pressure decrease occurs for aluminum and silicon monoxide, but not for silver. In aluminum evaporations the shutter is opened after the pressure drops below 5×10^{-6} Torr, while in silicon monoxide evaporations, the shutter is opened after the pressure drops to about 2×10^{-5} Torr. Since the pressure continues to increase after the onset of silver evaporation, the shutter is sometimes opened prior to the beginning of evaporation. Gold evaporations behave somewhat similarly to silver.

The current is manually controlled so that a predetermined increase in the crystal frequency occurs throughout the deposition. The shutter is closed when the total frequency change reaches a prescribed value corresponding to the desired film thickness.

Only one complete capacitor can be deposited in a day because the system must be opened after each evaporation so that the mask may be changed. The system has no high-vacuum valve and thus the diffusion pump must be cooled before air is admitted into the vacuum chamber. The total cycle time for one layer is three to four hours.

C. Special Techniques for Fabrication of Capacitors for Electron Microscopy

Problems in electron microscopy

There are two severe problems associated with studying the onset of capacitor breakdown in the electron microscope. One is that the thickness of the total capacitor is limited to that through which the electron beam will give an observable image. The second is that the capacitor must be removed from the glass slide and secured to a Lektromesh grid without appreciable wrinkling and tearing. The 50,000 volt electron microscope (with a 0.001 inch objective aperture) used in this study produces sufficiently intense images for total capacitor thicknesses of about 1500 Å or less. From 1500 Å to 2500 Å the image is poor, but may be worked with if one's eyes have adjusted to the dark. Above 2500 Å the image quality is too poor to be useful. Thus the capacitors should be as thin as possible. However, the thinner capacitors are more fragile and are more easily wrinkled in the stripping process. Capacitors of 1500 Å to 2000 Å total thickness form a working compromise.

The stripping procedure itself was initially a problem. It was felt desirable to use aluminum electrodes to minimize scattering of the electron beam. Williams and Bachus[17] have demonstrated that aluminum, as well as other elements which readily oxidize in air, adheres strongly to cleaned glass slides and is practically impossible to strip. Early efforts to

strip aluminum films and capacitors bore out this fact. Thus it was necessary to develop a stripping procedure so that aluminum electrodes could be used, or to revert to some heavier conductor.

Stripping procedure

Thomas[18] states that carbon may be floated off glass slides by suitable immersion in water. Thus it seemed plausible that capacitors deposited onto the glass, could be stripped with the carbon film after being coated with a collodion film. This procedure was attempted with a 50% solution of Collodion, U.S.P. in amyl acetate used to form the collodion film. Subsequently, it was found that in such a stripping procedure the carbon adhered to the glass, but an aluminum film (or capacitor) was readily stripped from the carbon. Arparently the aluminum is only weakly bound tothe carbon, in contrast with glass. The detailed stripping procedure is as follows:

1) Coat the capacitors and carbon film with a 50% solution of Collodion, U.S.P. in amyl acetate (other percentages may also be satisfactory) and allow the resulting film to dry.
2) With a razor sharp knife, cut the dried collodion to isolate the capacitors so they may be stripped individually. Care must be taken to prevent the collodion from accidentally tearing the capacitors adjacent to the line of the cut.
3) Using the same knife, scrape the edge of the collodion film so that the edge is raised and may be gripped by fine-nosed tweezers.

4) With the tweezers gripping the edge of the collodion, gently pull the collodion film off--the capacitor will come off also--and place it and the capacitor on the surface of distilled water.

5) Place a Lektromesh grid on a mesh spade under the surface of the water and bring it just beneath the capacitor. Position the capacitor over the grid with the tweezers.

6) Raise the spade, grid, and capacitor vertically out of the water and place on a paper towel which will absorb the water.

7) Before the capacitor is completely dried, place it (still on the spade) on another papertowel and, with an eye-dropper, allow drops of ethyl-methyl-ketone to slowly wash the collodion away.

With the removal of the collodion film the capacitor is ready for microscopic examination.

Carbon deposition apparatus

A carbon deposition facility was constructed for coating the glass slides. The evaporation method[19] consists of passing an alternating current through two carbon rods, thus producting sufficient temperatures at the contact point to vaporize the carbon. The contact points need not be extremely sharp. However, one of the rods must be of small diameter so that the contact resistance between rods is sufficiently high in order that the evaporation temperature will be attained. Fig. 8 shows a sketch of mating carbon rods mounted in the holder. One-eighth inch carbon rods (National Carbon Company spectrographic electrodes) were generally

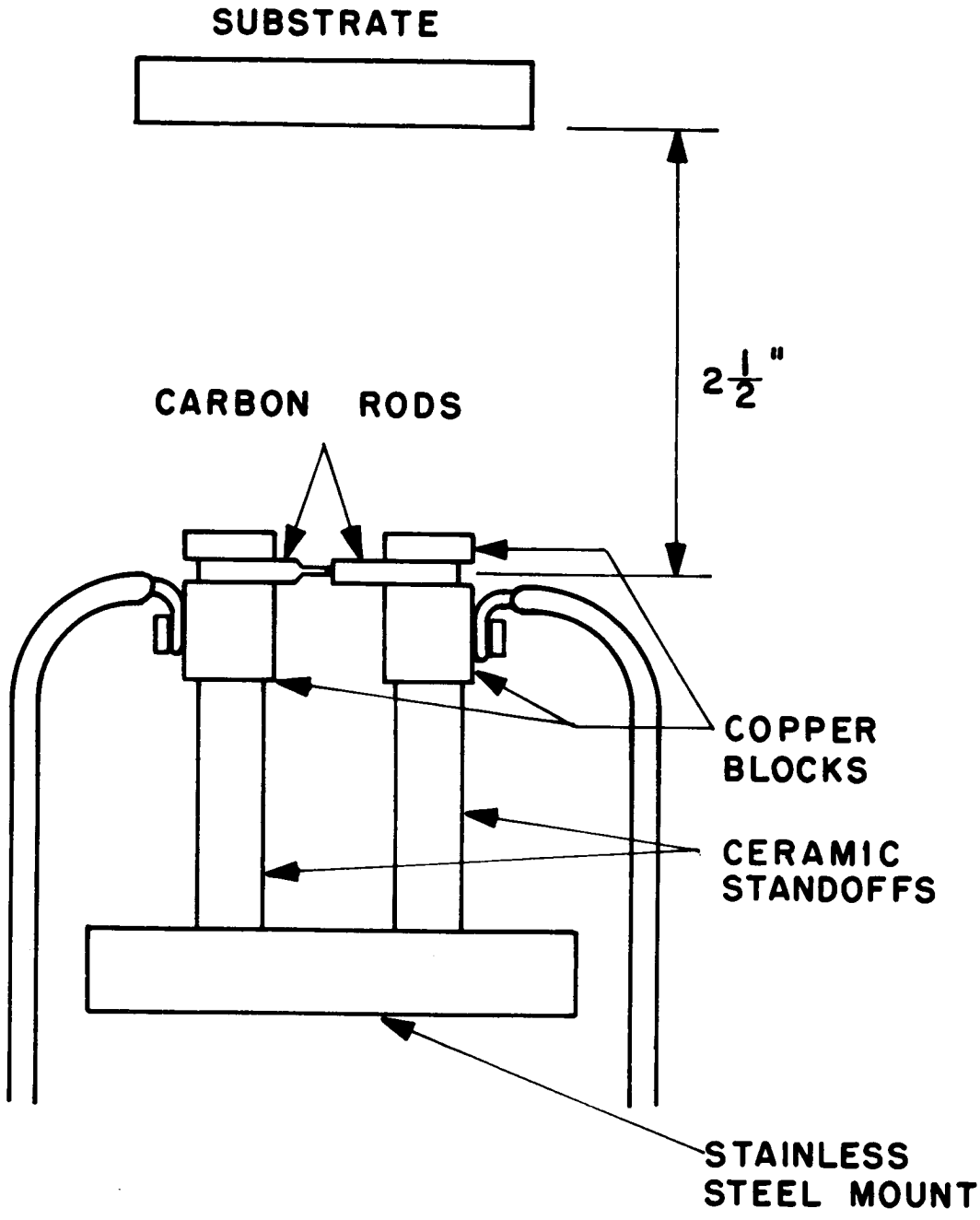

Figure 8. Substrate location for carbon deposition.

used although the holder also has slots for one-quarter inch rods. The Pyrex cross is replaced by a $2\frac{1}{2}$ foot cylindrical Pyrex pipe. The substrate is located $2\frac{1}{2}$ inches directly above the carbon arc as shown in Fig. 8.

In depositing the carbon, a current of about twenty amperes and a voltage of about fifteen volts are generally required. The 0.40 inch tip of the movable carbon rod is completely evaporated in just a few seconds. Using the Tolansky interferometer the thickness of the carbon film appears to be of the order of 200-300 Angstroms.

III. TESTING METHODS

A. Electron Microscopy

Transmission electron microscopy provides both a visual display at high magnification and structural information by selected area electron diffraction. The electron microscope used in this study allows a maximum magnification of approximately X20,000 with the standard holder.

A specially designed capacitor holder[20] provided the means for making contact to both electrodes of the thin film capacitor. Fig. 9 shows the holder with a specimen ready for observation. The main body of the holder is brass and is similar to the standard specimen holder furnished with the microscope. A teflon insulated wire is brought through the holder and soldered to a flat piece of metal which is mounted to a cylindrical teflon insulator. A 3-mil gold wire is soldered to the flat metallic insert. With the insert mounted as shown, the gold wire is bent underneath the specimen holder so that by adjusting the position of the teflon block by a screw which extends up into the body of the holder, the wire is brought into contact with the smaller electrode at the contact point. The other electrode is grounded by intimate contact with the copper grid and the specimen holder. To prevent vibrations of the capacitor and an intermittent contact the capacitor was tightly secured in the specimen holder cap with an aluminum retaining washer.

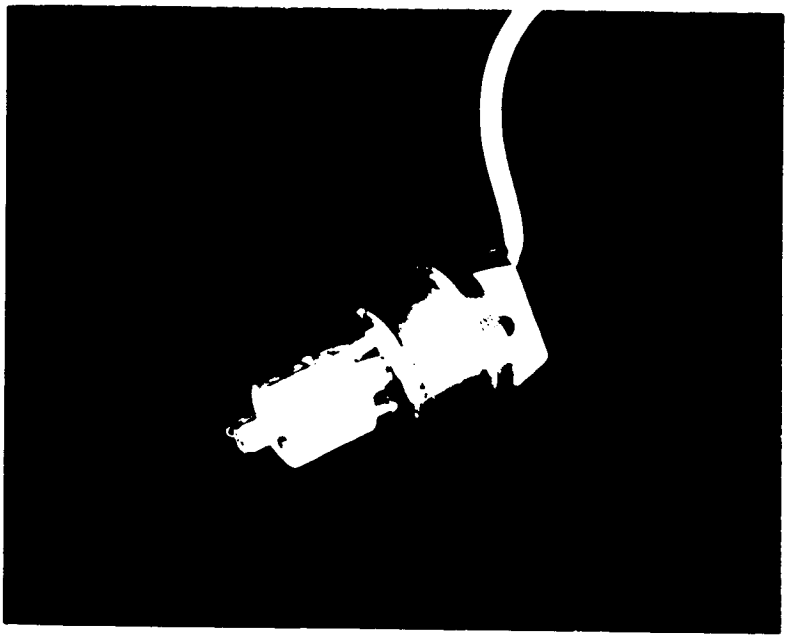

(a) actual size

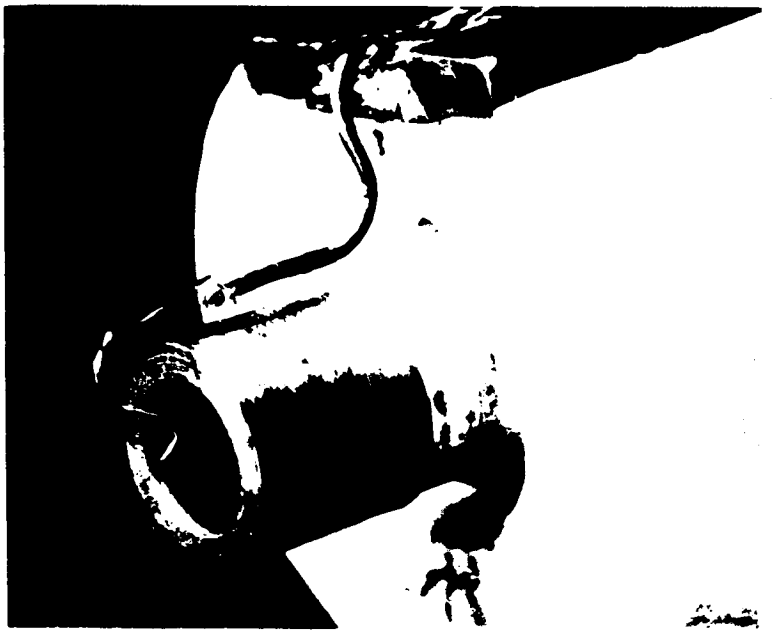

(b) x 9 magnification

Figure 9. Specimen holder for capacitor.

When placed in the capacitor holder, the specimen is located somewhat above the standard holder specimen position but below that corresponding to the stereo holder. Thus, the attainable magnification lies between the values for the standard and stereo holders. Fig. 10 shows the typical magnification settings of the instrument. Due to the size of the breakdowns and the limitation on the transmitted intensity imposed by the relatively thick specimen, the most convenient magnification for observing the occurrence of breakdown is X2000 to X9000.

The electrical testing circuit is shown in Fig. 11. It is comprised simply of a voltage source and a limiting resistor in series with the capacitor. The capacitor voltage is monitored for breakdowns with an oscilloscope. Tests made while examining the capacitors in the electron microscope have employed both dc and pulse voltages. If the dc voltage is sufficient to produce a breakdown, then usually many breakdowns and relatively large areas of destruction suddenly occur in a completely uncontrolled fashion. Pulse voltages, on the other hand, may be made to have pulse widths short enough to limit the capacitor to a single breakdown. Thus the bulk of the electron microscope study has employed pulse voltages. Either voltage polarity can be pre-selected with the pulser (Tektronix Type 161), thus one side of the capacitor may remain conveniently at ground potential.

Light microscopy has shown the breakdown sites to be randomly distributed over the area of the capacitor. However, it is impossible to view the capacitor with visible light and predict the location of the next breakdown. This is not the case in the electron microscope. Because the total thickness of the capacitor (1500 Å to 2500 Å) is near

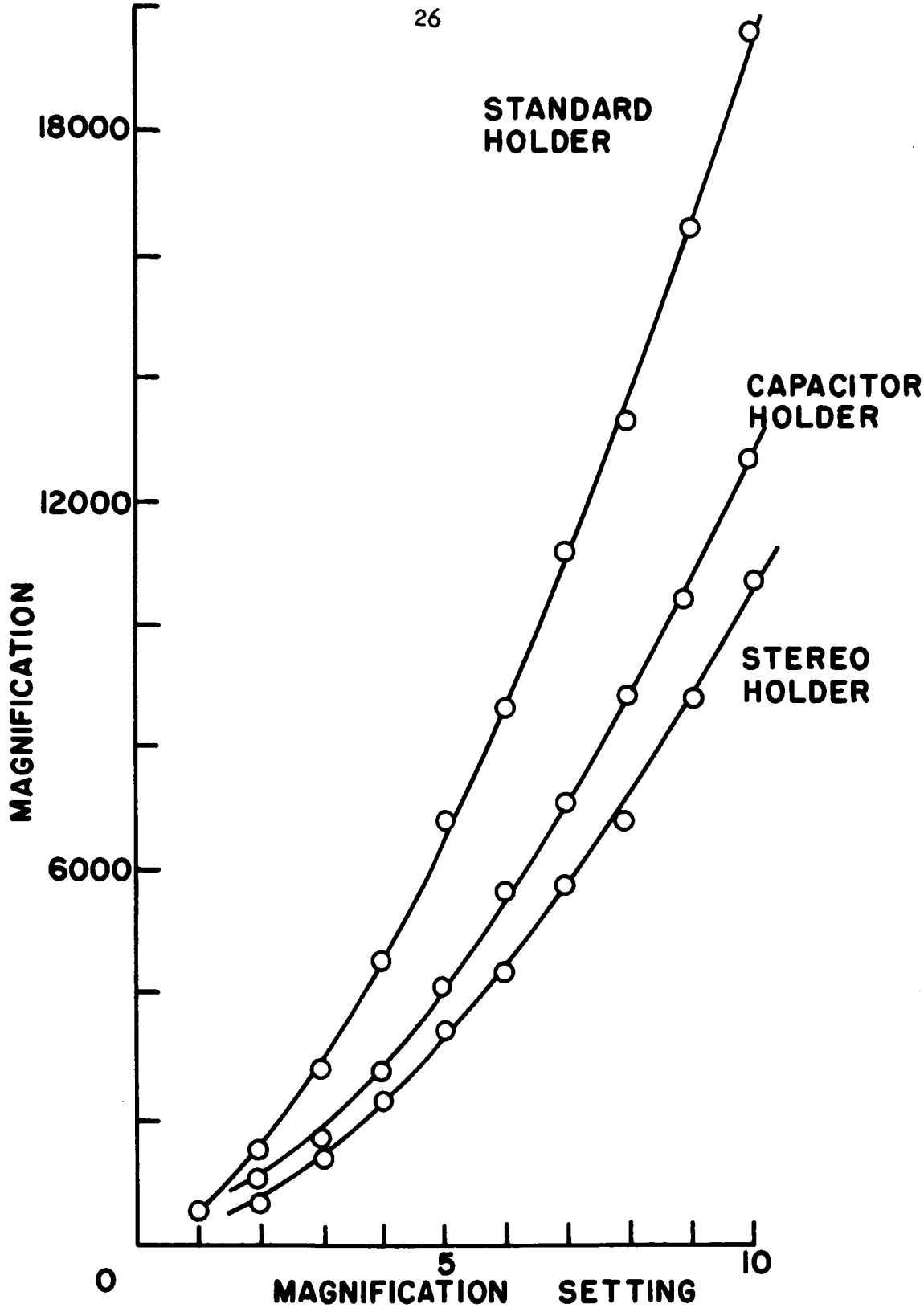

Figure 10. Typical magnification of the RCA-EMU 2D electron microscope.

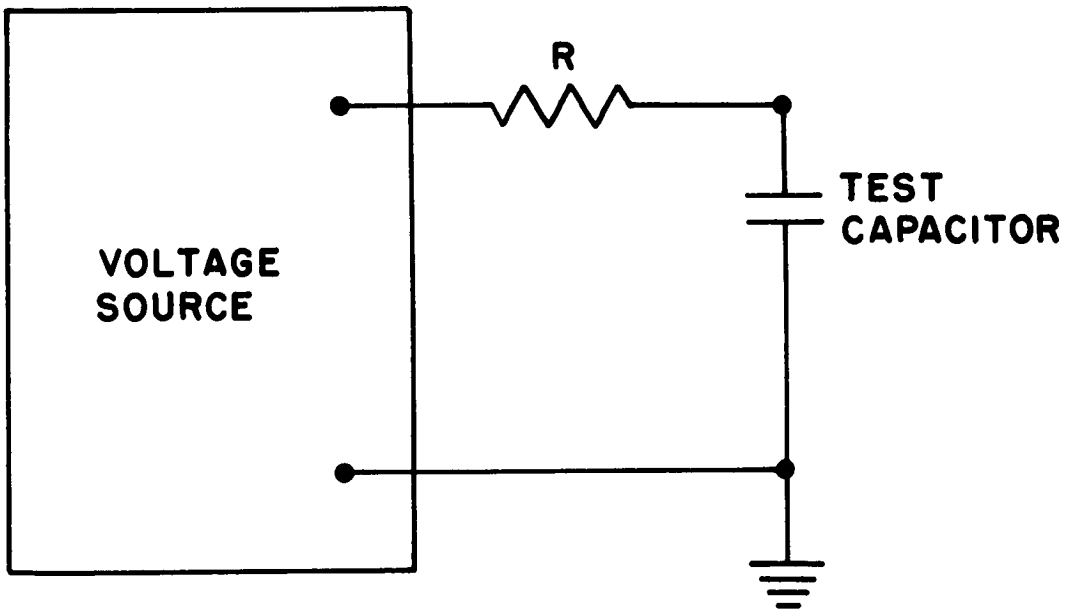

Figure 11. Electrical testing circuit.

the maximum for sufficient transmission of a 50,000 volt beam, it is necessary to focus the beam near crossover to obtain reasonable transmission for visual examination of the image. With this arrangement the electron beam promotes the occurrence of breakdown in the field of view in preference to other parts of the capacitor not illuminated so strongly. The breakdown voltage is practically unchanged but the randomness of breakdowns is eliminated. This feature of the electron microscope makes it a useful tool for studying breakdown.

The thickness of the capacitors has severely limited the use of the 50,000 volt microscope in selected area diffraction. The patterns obtained contain so much background illumination that generally no lines of any crystalline material can be seen. This area of study has been supplemented by access to 100,000 volt electron microscopes[21,22].

B. Pulse Voltage Tests

Capacitance measurements

Prior to any breakdown tests a rough measurement of capacitance was made using the circuit of Fig. 11. The resistance R was 22,000 ohms and a pulse voltage supply (General Radio Type No. 1217-B) was used. The capacitance was evaluated from the time t' for the voltage across the capacitor to reach one-half of its final value. The instantaneous voltage V_{CAP} across the capacitor (neglecting any leakage resistance) is given by

$$V_{CAP} = E_{MAX} (1 - e^{-t/RC_T}), \qquad (5)$$

where E_{MAX} is the applied pulse voltage and C_T is the total capacitance composed of the test capacitor C and the cable capacitance C_C. With the oscilloscope it is convenient to measure the time t' at which V_{CAP} is

one-half E_{MAX}. Thus, for these values of V_{CAP} and R, equation (5) yields

$$C = 66\ t'\ pf - C_C \qquad (6)$$

where t' is measured in microseconds. The cable capacitance, typically 60 pf, is not negligible for the capacitors made for the electron microscope where the capacitances are about 400-500 pf. However, the capacitance of the larger capacitors may be found by neglecting the cable capacitance in equation (6).

Breakdown tests

Pulse voltages of sufficient amplitude to produce breakdowns are applied in the circuit of Fig. 11. Only the negative voltage output of the pulser was used with larger capacitors tested outside the electron microscope. The positive output uses a negative voltage as reference while the negative output uses ground as a reference. A double-pole, double-throw switch was placed in the circuit to facilitate polarity reversals.

The output capability of both of these supplies is fifty volts. The resistor R was generally small (typically 100 ohms) so that the full voltage could be impressed on the capacitor. Pulse repetition rate was no more than three pulses per second and frequently was much less. Pulse width was 50-300 milliseconds for the larger capacitors and 10-70 microseconds for the smaller capacitors in the electron microscope.

An oscilloscope is used to monitor the pulse. With a fixed pulse width and repetition rate the pulse is increased until breakdowns occur. The pulse height at which the first breakdowns are seen is assumed to be that corresponding to the breakdown strength--V_{MAX}.

By increasing the pulse height well above the breakdown strength many breakdowns occur. With many breakdowns a measurement of V_{MIN}, the minimum voltage to which the capacitor drops during a breakdown, may be made. Further discussion of both V_{MAX} and V_{MIN} is given in Chapter IV.

Pulse voltages are useful in controlling the number of breakdowns in the capacitors during observations with the electron microscope. The pulse width can be made short enough to limit the capacitor to a single breakdown. This limitation on the number of breakdowns is necessary for correlating the electrical breakdown pulse with the breakdown's appearance.

By triggering an oscilloscope on the opposite polarity of the applied pulse, it is possible to observe closely the electrical characteristics of the breakdown pulse. Such observations were made on several capacitors. However, this aspect has not been thoroughly investigated because of the difficulty of simultaneously manipulating the electron microscope, pulser, and oscilloscope in a darkened room.

C. Ramp Voltage Tests - Capacitors on Glass Slides

Breakdown strength

The breakdown strength is the maximum electric field which the capacitor can withstand before breakdown occurs. It may be measured by applying a linearly increasing voltage and observing the first breakdown by any of a number of methods. If the voltage is allowed to increase above the breakdown strength the breakdown rate increases rapidly. Thus to prevent destruction of the capacitor the voltage should be removed by the occurrence of the first breakdown.

The circuit shown in Fig. 12 has been constructed for just this purpose. After application of the ramp voltage the circuitry will

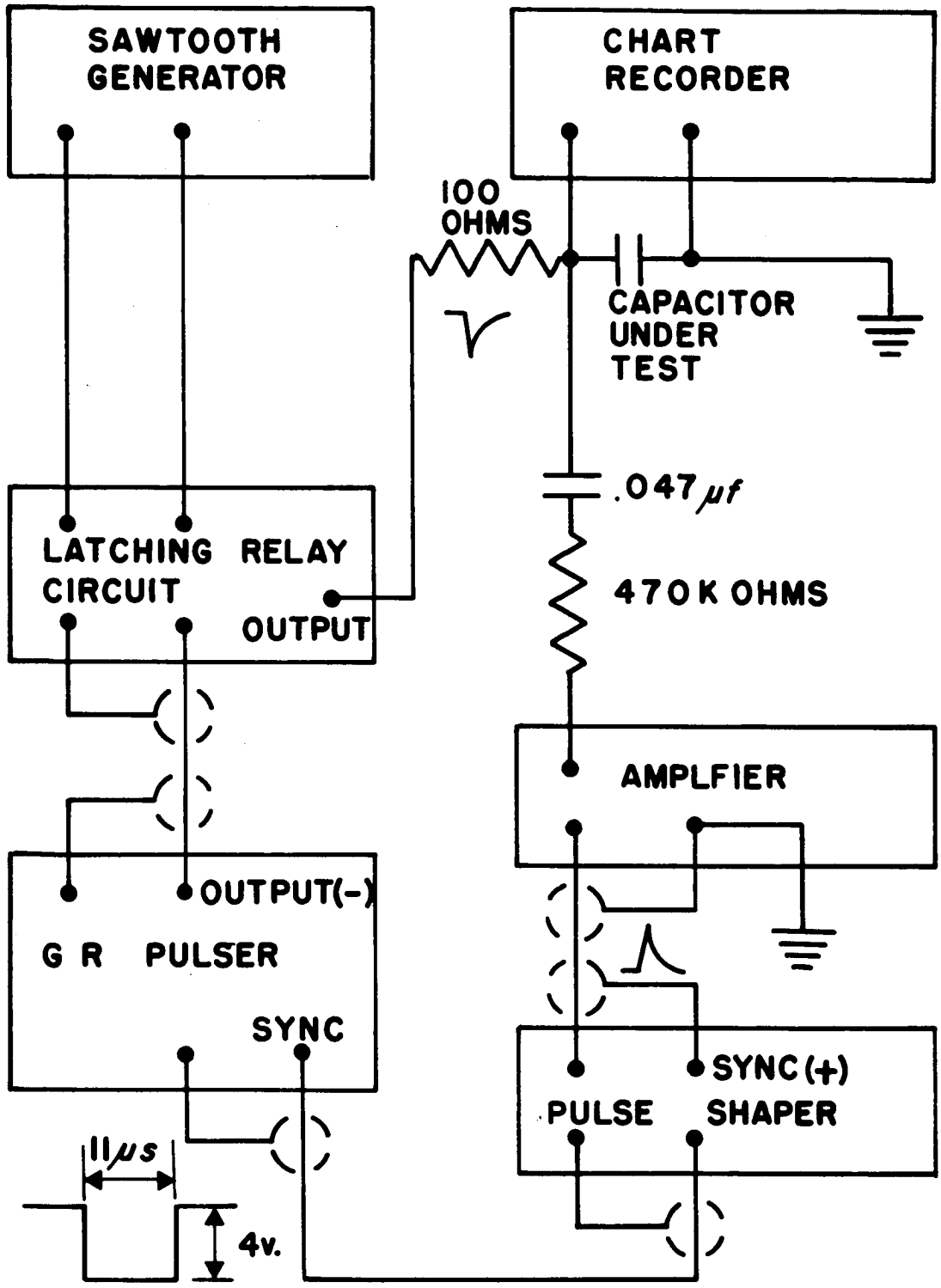

Figure 12. Block diagram for measurement of breakdown strength.

disconnect the voltage from the capacitor test circuit at the occurrence of the first pulse of amplitude greater than two volts. The ramp is made sufficiently slow so that it may be monitored by a strip chart recorder (Bausch & Lomb, VOM 7). Typically, the one second per centimeter sweep of the oscilloscope was used. The sawtooth output of the oscilloscope extends only to 150 volts. A sawtooth generator was constructed (see Appendix A) to provide higher ramp voltages and used whenever the breakdown voltage exceeded about 100 volts.

The breakdown pulse (Fig. 12) is amplified 20 times by a three stage transistorized amplifier (see Appendix B for the amplifier circuit) and emerges inverted. The amplified pulse drives a pulse shaper (Hewlett-Packard Model 212a Pulse Generator) whose output triggers a second pulser which in turn triggers the latching relay circuit. The GATE output of the oscilloscope provides the holding voltage for the latching relay circuit. The circuit free runs with the oscilloscope in the automatic sweep mode.

The breakdown strength measurements have been made typically from room temperature down to near liquid-nitrogen temperatures. The range was extended to 90°C on a few capacitors. For these tests the capacitors were mounted in a vacuum chamber and the chamber evacuated to a pressure of about 350 microns. Thus no water vapor condensed on the capacitors, yet the system could still be cooled fairly rapidly.

Rate-of-breakdown

To investigate the probability of breakdown occurrence a circuit was constructed to measure the breakdown rate as a function of voltage. The circuit, shown in Fig. 13, is a modification of the circuit used to

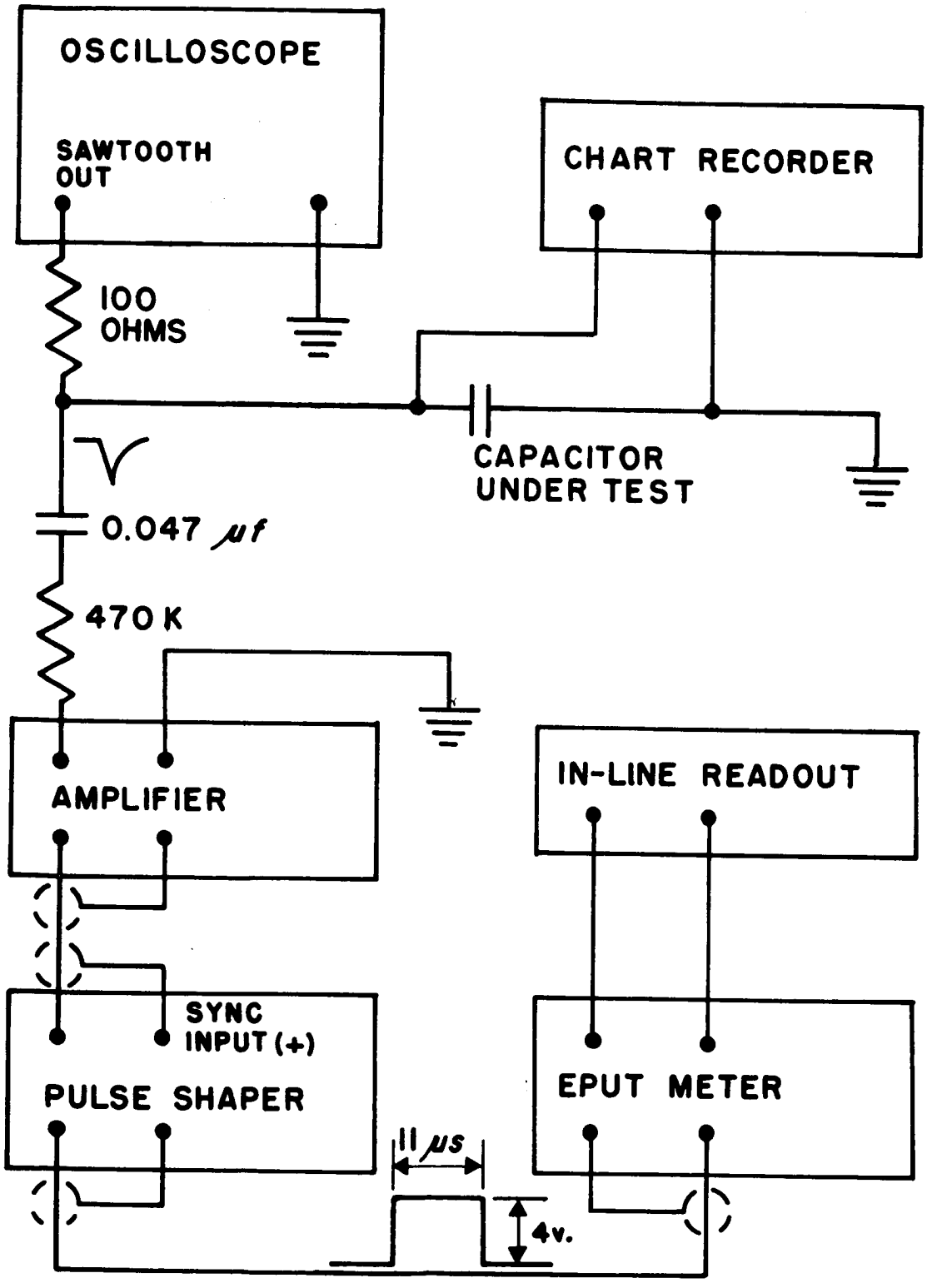

Figure 13. Block diagram of breakdown rate counting circuit.

measure breakdown strength. The breakdown pulse is amplified and shaped the same as in the breakdown strength circuit with the shaped pulse going to a Beckman EPUT meter capable of automatic in-line readout. The ramp voltage is not cut off after the first breakdown, but is maintained until an appreciable overvoltage is reached.

The capacitor voltage is continuously recorded on the strip chart recorder as the number of breakdowns per second is recorded manually. Typically the ramp time is twenty seconds and breakdown rate is recorded every 1.5 seconds. The readout generates a pulse which triggers a marker on the strip recorder. Thus a given breakdown count is correlated with the voltage at readout.

These breakdown rate tests have been made only at room temperature.

IV. RESULTS AND INTERPRETATION

A. Electron Microscopy

Effect of beam on capacitor

Prior to performing an experiment it was an open question as to the effect of the 50 kv electron beam on the structure and electrical behavior of a capacitor in its path. One might expect two effects to influence the capacitor electrically: creation of carriers by collision interactions and heating by absorption of energy from the beam. However, the majority of capacitors tested, and practically all of those which were considered to be good capacitors after having been stripped, exhibited negligible electrical changes due to the beam. With a small dc voltage (a few volts) across the capacitor, the dc leakage current increases slightly when the electron beam is activated. Larger increases occur when the beam is not focused directly on the capacitor, i.e., when the whole capacitor is irradiated fairly evenly. With the beam focused sharply on a local area (at crossover) of the capacitor, the current is practically the same as when the beam is off.

These observations indicate that the effect of the beam is to cause a significant increase in current only if a rather large area (about 3.6×10^{-3} cm^2) is illuminated by the beam. If a small area (about 5×10^{-5} cm^2) is illuminated the total increase in current is negligible even though the beam density is somewhat higher. Similar increases in current are observed in the larger capacitors when temperature is increased.[23]

The breakdown strength of silicon monoxide capacitors is only very slightly temperature dependent as shown below (Chapter IV), but this slight dependence may be enough to cause the observed elimination of the randomness of breakdowns when the beam is focused near crossover. Perhaps this loss of randomness is related to carrier production by beam collisions. The breakdown voltage is so slightly affected when the beam is turned on that it is practically unchanged. With the beam off, any of the "susceptible breakdown sites" may result in a breakdown and predetermination of the site at which the next breakdown will occur is impossible. However, when the beam is on and focused near crossover on a susceptible breakdown site, and the applied voltage is sufficient, breakdown will occur in the highly illuminated portion of the capacitor. This feature makes the electron microscope unique for studying the onset of breakdown and its relation to the capacitor structure.

In general the beam does not cause the capacitor to buckle and wrinkle. However, problems of this nature are occasionally encountered in capacitors which are exceptionally thin.

In summary, the electron beam does not appear to cause appreciable degradation in the quality of capacitors.

Breakdown-center defects

It was found that single breakdowns occur at opaque spots in the capacitor. These dark spots vary in size, but are generally about one-half micron to one micron in diameter. A number of these dark spots are seen in Fig. 14. More often than not they are irregularly shaped and have regions of transparency around the edges as shown in Fig. 15 at higher magnification. Fig. 16 shows a large irregular spot A and also

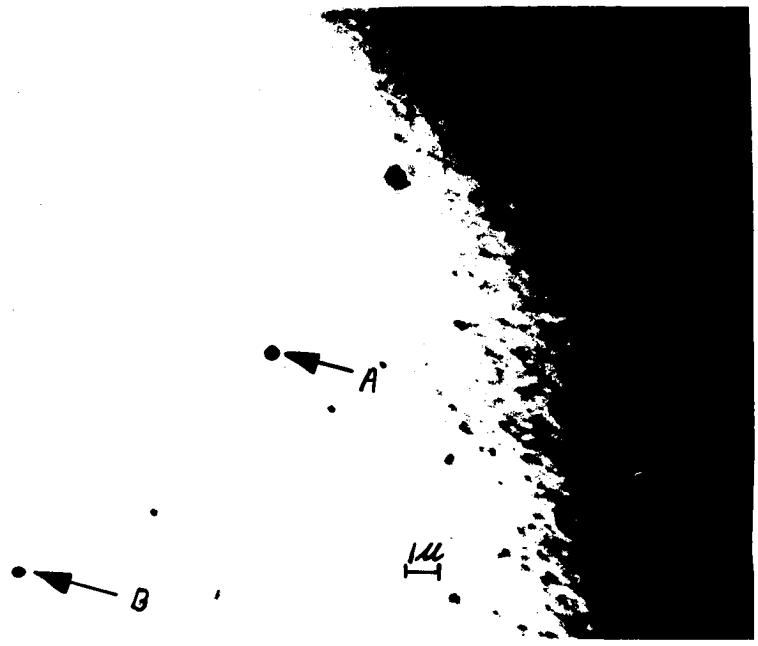

Figure 14. Defects in capacitor 1033-1.

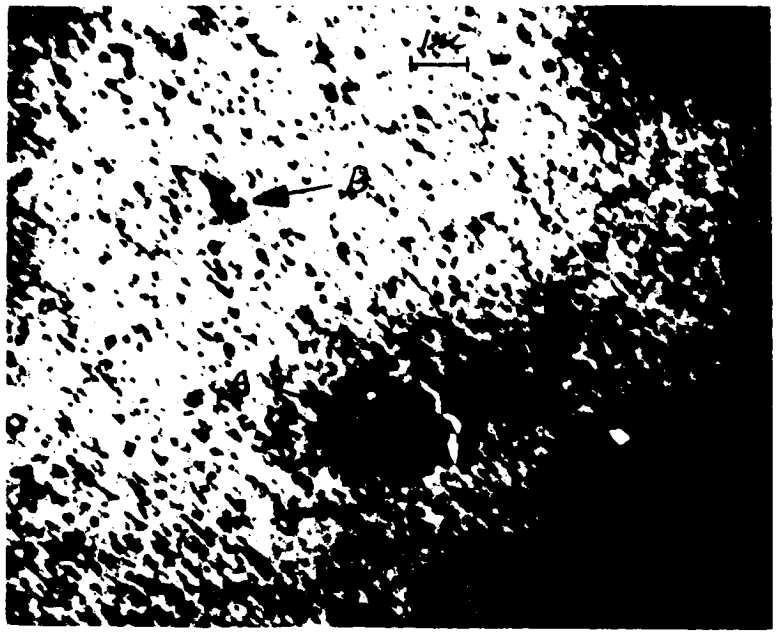

Figure 15. Defects in capacitor 1011-13.

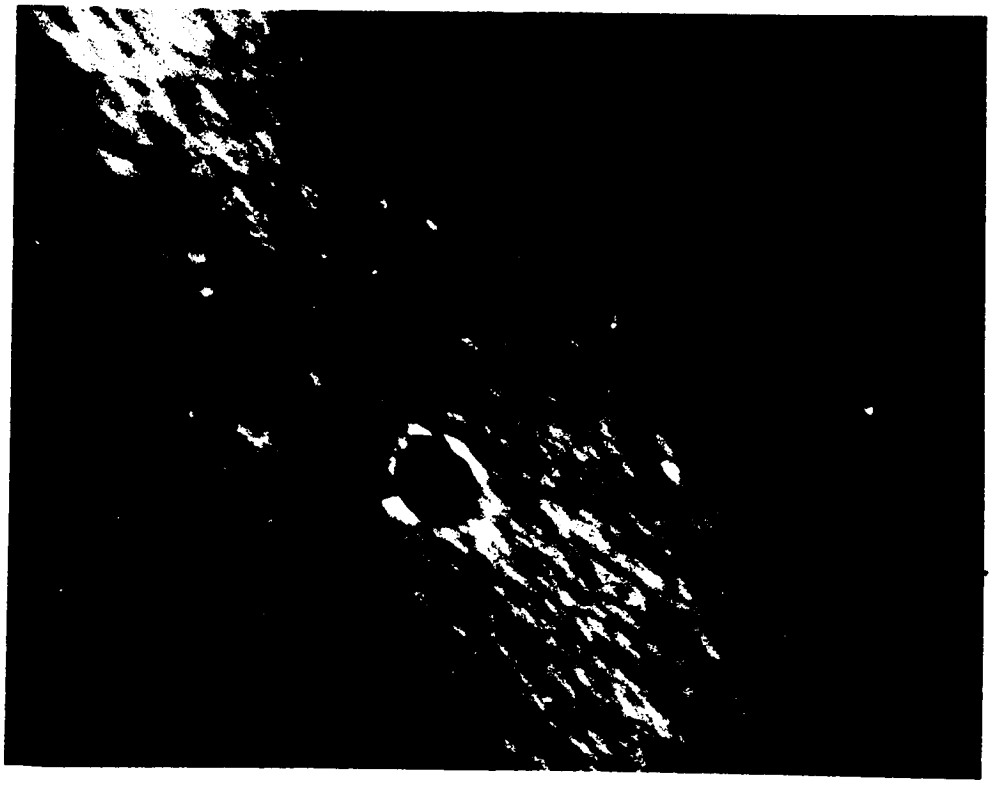

Figure 16. Defects in capacitor 1015-5.

several smaller spots B, C, and D which appear to be more intimately secured within the capacitor. Occasionally these spots are nearly spherical with much smaller spots seemingly attached as is the case with spot B. The tiny irregularities scattered uniformly throughout the capacitor are typical for single layers of aluminum or silicon monoxide. Only the larger, more prominent spots are the susceptible breakdown sites. In fact, when the electron beam is focused on an area where none of these "large" dark spots are present and the capacitor is subsequently pulsed to generate breakdown, the breakdowns do not occur in the area being viewed. The exact location of such breakdowns cannot always be determined, but they are presumed to be at dark spots located elsewhere in the capacitor.

Efforts to identify the material producing these dark spots, or defects, have not been successful. Selected area diffraction is severely limited in the 50,000 volt electron microscope because of the rather large thickness of the capacitors. Any diffraction rings which might be present are typically hidden in the incoherent background resulting from the amorphous silicon monoxide. It is even difficult to detect the diffraction pattern of the aluminum electrode metal. In spite of extensive effort, no diffraction pattern of a dark spot has been obtained. The lack of a well-defined diffraction pattern could imply that the dark spots are amorphous in nature and hence, most likely, silicon monoxide.

Siddall[24] detected an irregular structure of about one-half micron diameter in surface replicas of silicon monoxide films which were deposited at 15 $\mathring{A}$ per second on glass. This structure was thought to be an agglomeration of the shadowing metal used in preparing the replica. However, this may be evidence that the dark spots originate from the silicon monoxide

deposition. Such a possibility cannot yet be eliminated, but, as seen in Fig. 17, similar dark spots occur in aluminum films.

The defects could be attributed to electrode depositions. Since no two evaporations are exactly alike, the number, size, and detailed structural arrangement of the dark spots within the capacitor may vary from one electrode deposition to the next. One would expect that if relatively large lumps were produced by the bottom electrode evaporation they would penetrate deeply into the dielectric and possible produce areas of thin, strained dielectric where there could be field concentrations. However, if they were produced in the top electrode deposition the dielectric penetration should be very slight. This is consistent with the electron micrographs wherein some of the dark spots have an associated transparent region.

The surface condition of the silicon monoxide, after deposition, may contribute to polarity effects. If the surface is very irregular, protrusions of the upper electrode would be expected.

It might be speculated that the dark spots may be an aluminum compound, carbon, or a carbon compound (since the films are deposited onto carbon). X-ray patterns of portions of capacitors scraped off glass slides have shown no aluminum compounds.[25] There are two observations which indicate that the spots are not carbon or any other products which might be derived from the special prodecure used in preparing capacitors for electron microscopy:

1) The breakdown strength is the same as that for a larger capacitor deposited simultaneously, but onto a glass substrate.

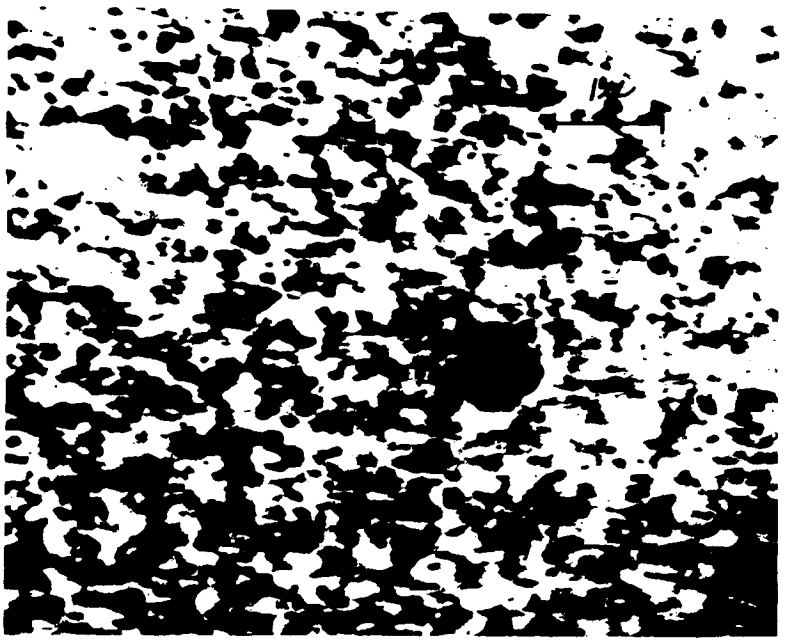

Figure 17. Dark spots in aluminum films.

Figure 18. Dark spots in aluminum-silicon monoxide films - no heat treatment.

2) The carbon film left on the glass substrate after stripping the capacitor is generally very smooth and no irregularities are seen at X 600 magnification.

The spots do not seem to be dust particles for, as stated above, they appear to be "grown into" the film.

A batch of twenty-two aluminum-silicon monoxide "partial capacitors" was deposited so that some could be heat treated to determine if the dark spots would change. The heat treatment was done at atmospheric pressure in a closed furnace. Figs. 18, 19, and 20 show, respectively, dark spots in the untreated films, films heated to 450°C, and films heated to 580°C. The pictures are of three different specimens, but are typical of each heat treatment. The films heated to 450°C do not appear to be significantly different from those not heated. However, the films heated to 580°C exhibit much larger dark spots as well as a random smearing of the smaller spots. The large spot in Fig. 20 seems to have grown out of the film since it is out of focus relative to the structure within the film. It may possibly be a product of oxidation and not a basic change in the structure of the film. It should be noted that with or without an applied voltage the dark spots show no change upon irradiation with the electron beam until the breakdown occurs. Thus the beam does not cause the defect to grow.

Breakdown patterns

An extensive electron micrographic study was made of the breakdown areas of many capacitors. A summary of these follows.

Breakdown center defects. Two sets of pictures (Figs. 14 and 21 and Figs. 22 and 23) illustrate the relationship of the dark spots (defects)

Figure 19. Dark spots in aluminum-silicon monoxide films after being heated to 450°C.

Figure 20. Dark spots in aluminum-silicon monoxide films after being heated to 580°C.

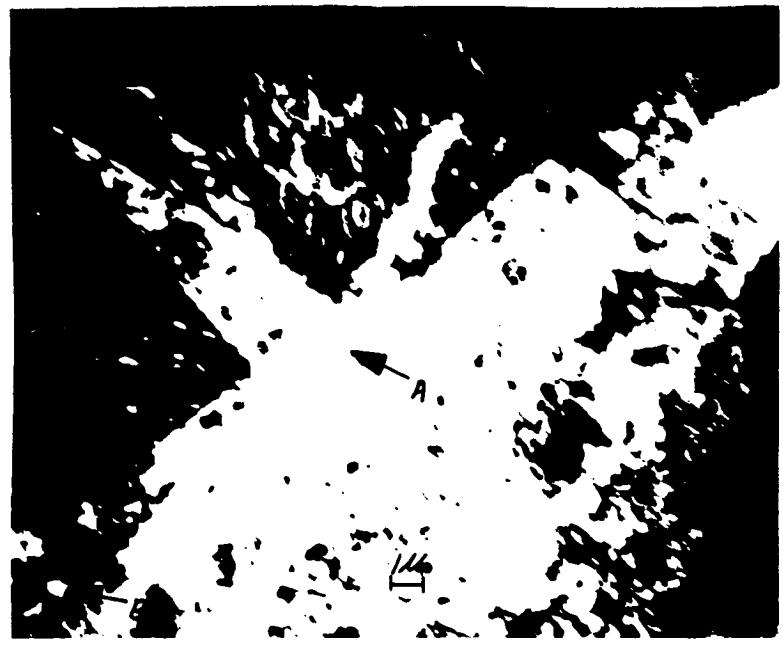

Figure 21. Breakdown formed around the site of a defect - capacitor 1033-1.

Figure 22. Dark spots and a breakdown in capacitor 1033-1.

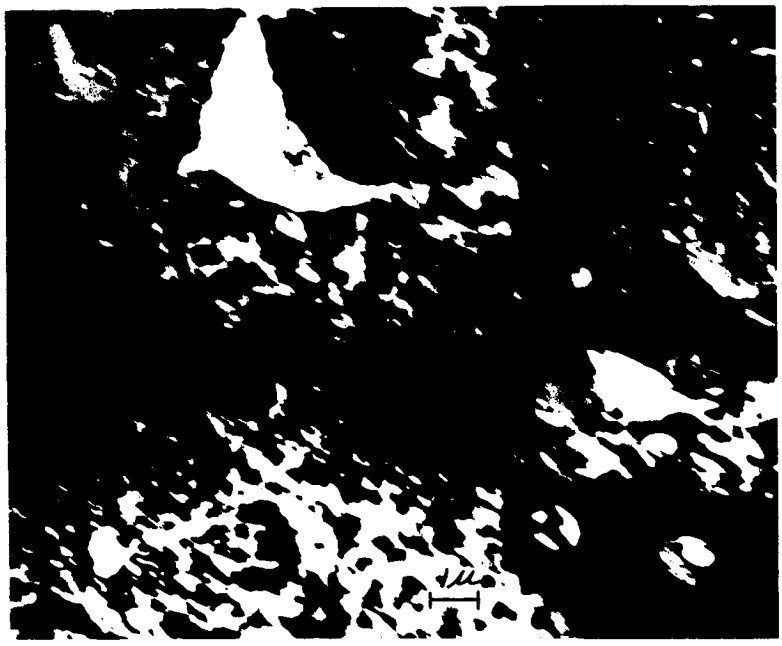

Figure 23. Breakdowns which occurred at dark spots shown in Fig. 22 - capacitor 1033-1.

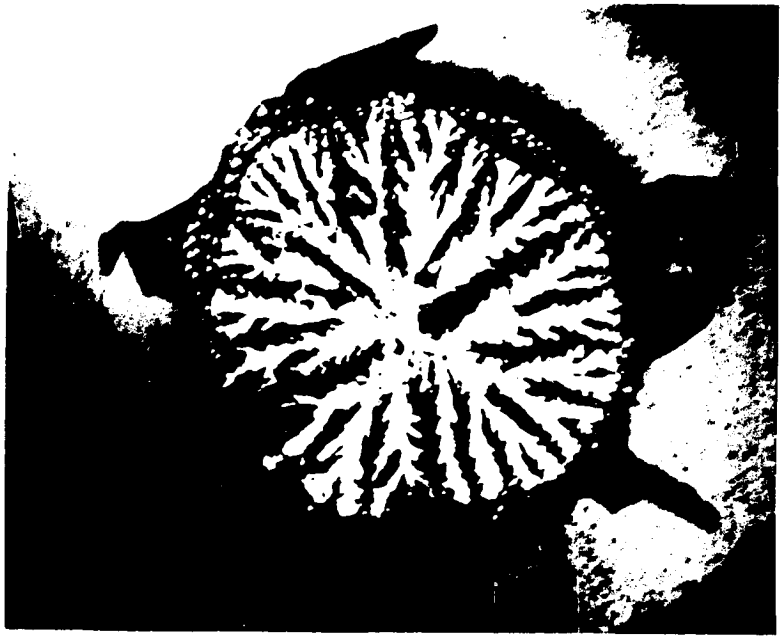

Figure 24. Lichtenberg breakdown in capacitor 1015-1.

prior to voltage application and after breakdowns have occurred. In both cases pulse voltages were used with negative polarity on the counter (last deposited) electrode. These and all other breakdowns are completed in about one-half microsecond and thus the detailed progression of the breakdown patterns is not observable. Fig. 21 may be compared with Fig. 14. The breakdown center coincides with the spot marked A . Several other spots are marked to facilitate their identification near the breakdown. Spot B was also removed during the breakdown. The diameter of the breakdown region is about thirty microns and the capacitor thickness is approximately 880 $\mathring{A}$. The energy dissipated in the breakdown was about 5×10^{-7} joules.

The radial streaks (seen in Fig. 21) characteristic of a Lichtenberg pattern are typical of isolated breakdowns which occur with the counter electrode negative. As shown below, Lichtenberg breakdown patterns are not observed with the counter electrode positive. Merrill and von Hippel[26] have discussed the generation of Lichtenberg patterns in gaseous discharges between a plane and a rounded electrode ($\frac{1}{2}$inch rod with a rounded tip). They showed that the form of the breakdown pattern depends on the polarity of the applied voltage. With the point electrode positive a Lichtenberg pattern with radial branches was formed. However, application of a negative voltage on the point electrode yielded a different pattern which did not exhibit random radial branches. In silicon monoxide capacitors studied in the electron microscope, Lichtenberg breakdowns are formed when the top electrode is negative but only a central hole is formed with the opposite polarity. In analogy with the above discussion of gaseous discharges, this indicates that the defect is a conductive protrusion from the bottom electrode which serves as a point electrode.

The broad light areas shown by the arrow (Fig. 21) are regions where the electrode(s) have been blown off the dielectric. The dark lumps in the inner section of the breakdown are described in connection with later pictures.

Fig. 22 shows another region of the same capacitor just described after one breakdown had already been formed as a result of a pulse voltage with negative polarity again on the counter electrode. A second pulse of the same polarity was then applied, resulting in two separate breakdowns as indicated on the monitor oscilloscope and in Fig. 23. The details of the breakdowns are similar to those in Fig. 21.

Lichtenberg breakdowns. Fig. 24 shows a typical Lichtenberg breakdown resulting from a pulse voltage with the counter electrode negative. The dielectric here is about 2000 Å as compared with 880 Å for that shown in Figs. 21, 22, and 23. The center of the Lichtenberg pattern is a hole of about the size and shape of the dark spot which was present before voltage application. A number of radial streaks extend outward. Each streak appears to be a rather broad region of dielectric destruction near the center of breakdown. Near the periphery of the breakdown the streaks become a series of smaller holes which may be tiny local breakdowns in the dielectric. One of the electrodes has been folded back around the edge of the breakdown. A possible interpretation of this pattern is that upon initiation of the breakdown there results a large transfer of electronic charge from the volume of the cathode into the region surrounding the breakdown center defect (a funneling effect). The density of carriers most likely would be greatest near the defect and along random paths which correspond to the branches of the Lichtenberg pattern. Because of the additional available carriers in the

localized regions near the defect, the funneling effect may cease with the occurrence of many tiny breakdowns through the dielectric.

Fig. 25 shows a Lichtenberg pattern resulting from a dc voltage application. This pattern is similar in size and structure to that in Fig. 24, but shows more detail in the radial streaks. Most of the streaks are not holes, but are regions reduced to a more transparent material, possibly one of the electrodes. A circular pattern is also seen in this breakdown. The dark balls scattered throughout the breakdown are common in almost all breakdowns. Evidence that these are clusters of silicon is given in connection with a later picture and the diffraction work.

Breakdowns with a large central hole. Fig. 26 shows a breakdown which occurred during application of a pulse voltage with the counter electrode positive. The capacitor under test is the same as that shown in Fig. 24 for identical conditions, but opposite polarity. As shown, with the counter electrode positive a much larger hole results and the radial streaks are missing. The thicker portion near the periphery of the breakdown is one of the electrodes which has been wrinkled. Pieces of the electrode are also seen folded back.

Fig. 27 shows another breakdown which occurred similarly to that in Fig. 26, but in a thinner capacitor. Several circles of what appears to be electrode material surround the center hole. In region A it appears that one of the electrodes has been removed. In region B both electrodes appear to be missing. Evidence that the rings are electrode material is borne out by the presence of interference colors within the breakdowns, which occur in the larger capacitors on glass slides and is presented in Chapter IV below.

Figure 25. Lichtenberg breakdown and ball formation in capacitor 1011-3.

Figure 26. Breakdown with a large central hole - capacitor 1015-5.

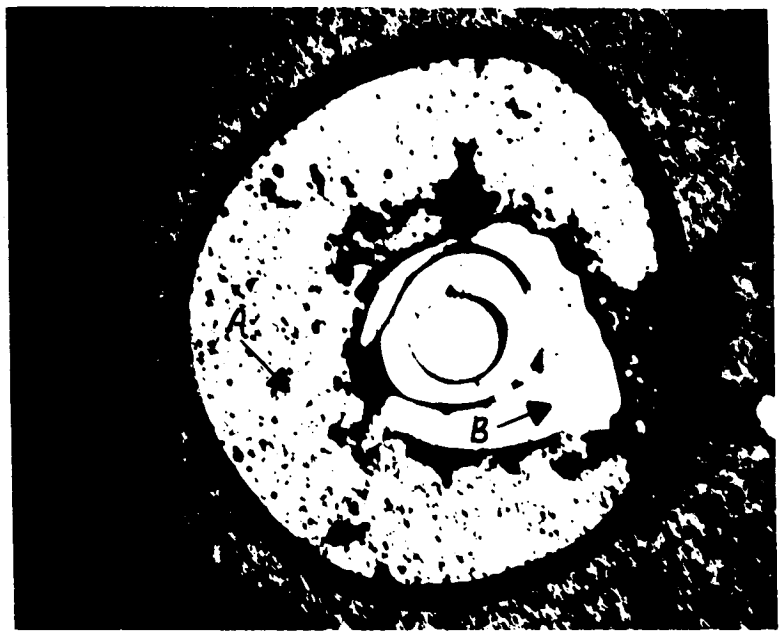

Figure 27. Breakdown with ring pattern in capacitor 1011-12.

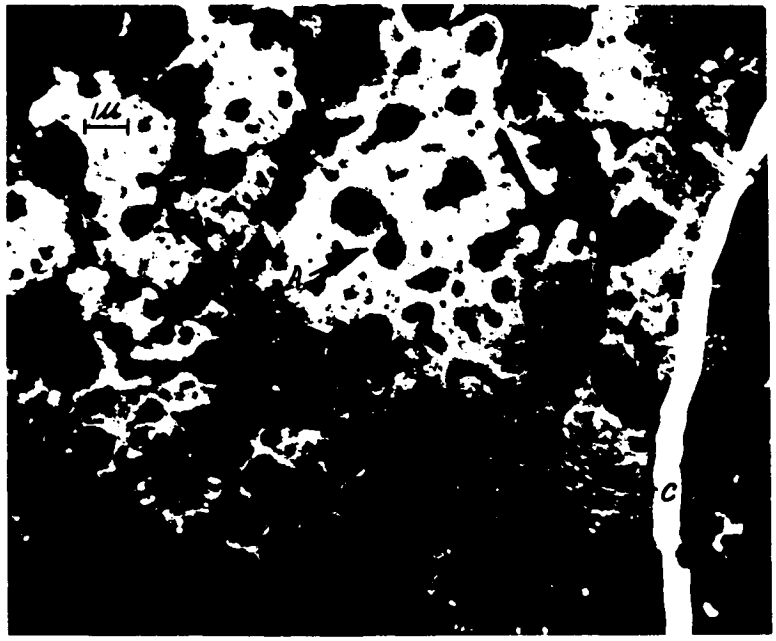

Figure 28. Large regions of destruction and ball formation in capacitor 1011-13.

Broad regions of destruction and silicon balls. Figs. 28 and 29 show large breakdown regions in two different capacitors. Such large areas of breakdown frequently result when the capacitor is subjected to a dc voltage. The onset of breakdown is frequently characterized by many successive breakdowns which collectively produce these large areas of destruction. As mentioned above, the dark balls and clusters are typical of almost all breakdowns. In fact they have been found in the breakdowns of all but a few of the thick capacitors, where their detection is probably limited by poor contrast. In Fig. 28 the semicircular patterns such as in region B are interpreted as an indication of stresses within the films during the breakdown. The opaque material labeled C is thought to be aluminum. Fig. 29 shows balls of less than one tenth micron diameter as well as the large clusters.

Fig. 30 is a view of region A in Fig. 28 and reveals the balls and clusters at higher magnification. Contrary to expectations, selected area diffraction in the vicinity of these balls (over an area about the size of that shown in Fig. 30) shows practically no aluminum; rather, very definite diffraction rings of silicon are observed. Fig. 31 is a diffraction pattern of the capacitor before breakdown. After breakdown the pattern is typically that shown in Fig. 32. The balls in the Lichtenberg pattern of Fig. 25 are interpreted as silicon because of their similarity with those of Fig. 30. Frequently the balls occur in a somewhat orderly fashion as seen in Fig. 33. Fig. 34 is a low magnification (optical microscope) view of a large destroyed region such as that of Figs. 28 and 29. The circular area with small isolated breakdowns is the silver contact point. The breakdowns in the silver area are isolated holes because of

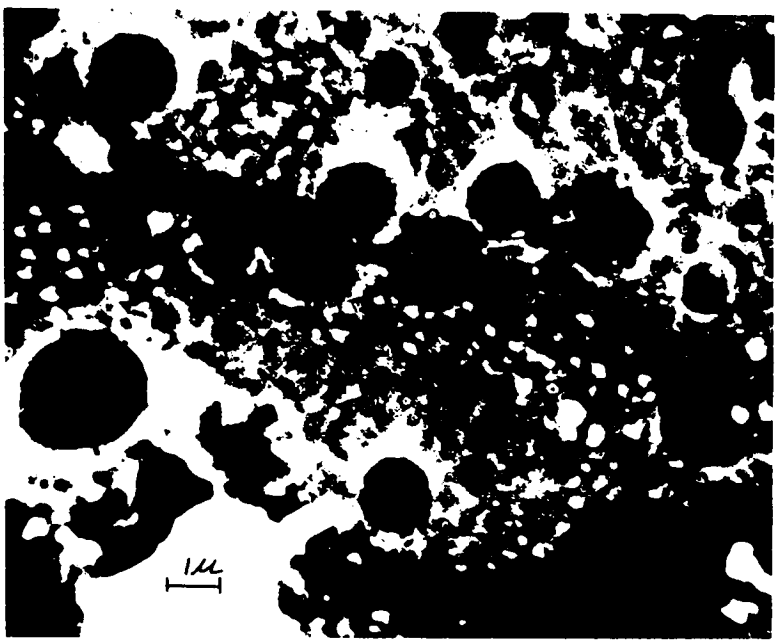

Figure 29. Ball formation on capacitor 1014-1.

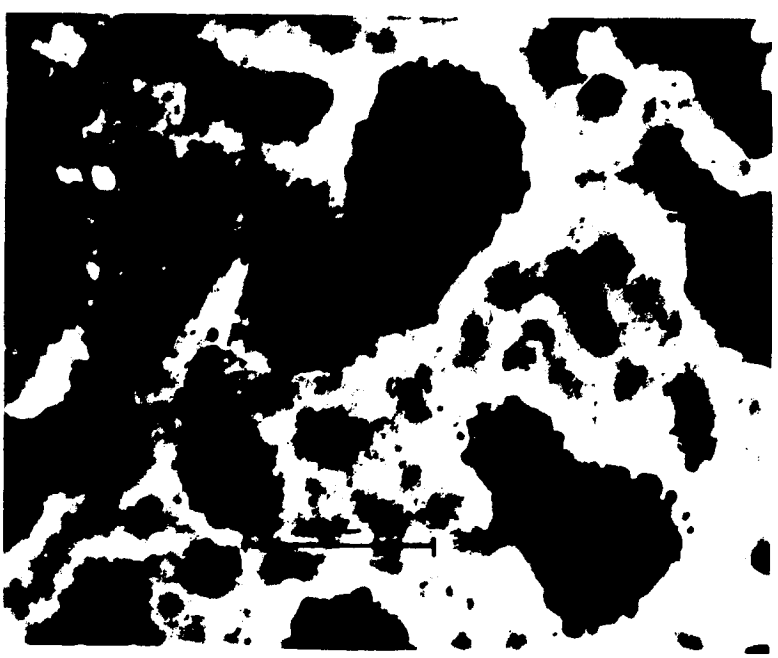

Figure 30. Balls and clusters identified as silicon-from region A of Fig. 28.

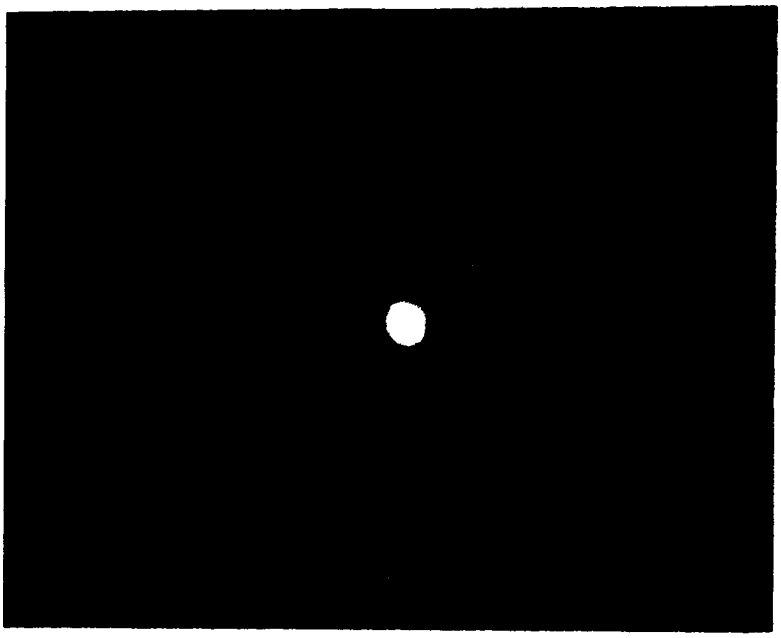

Figure 31. Diffraction pattern from capacitor prior to breakdown.

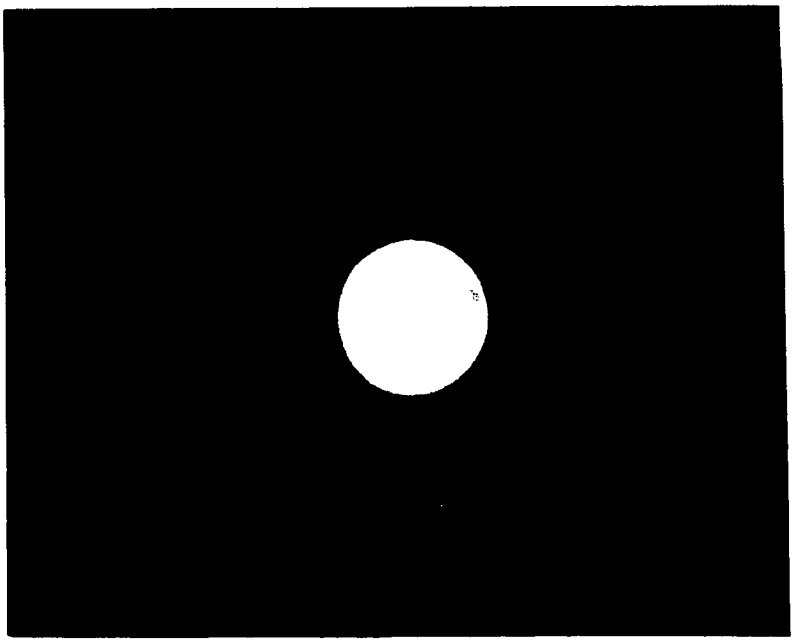

Figure 32. Diffraction pattern in breakdown area such as that shown in Fig. 30.

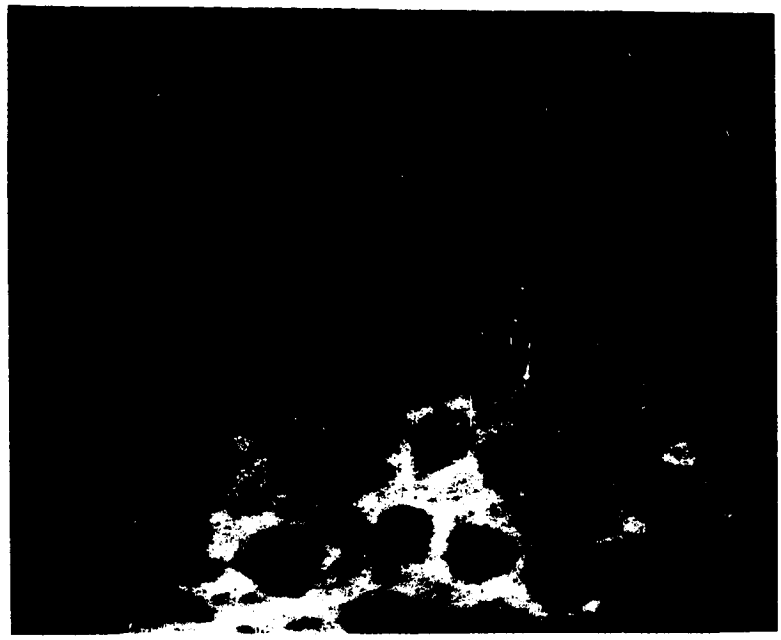

Figure 33. Orderly array of balls in a breakdown region of capacitor 1011-13.

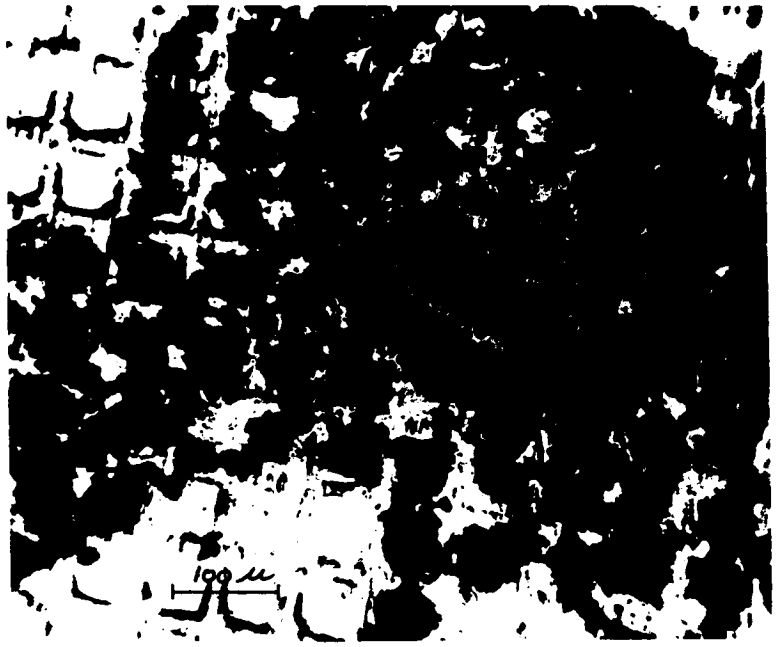

Figure 34. Optical photomicrograph of a large region of destruction in capacitor 1012-7.

the very great thickness of the silver which severely limits the area of the breakdown. Surrounding the silver contact point is a large area of destruction where both electrodes are relatively thin.

Stereo views. A stereo set, Fig. 35, was taken to observe the relative height of the balls with respect to the surface of the film. The balls appear to be "grown" into the film and not merely resting on the surface. The vertical protrusion of the large balls above the film surface appears to be about half their diameter or less. Another stereo set in Fig. 36 shows rings of balls about a large central hole--buckling of the film has occurred either before or during the breakdown.

Patterns in larger capacitors. Portions of a few of the larger capacitors were stripped, after breakdown, by a collodion overcoat and examined in the electron microscope. In general the breakdowns are larger than those discussed above because of the much larger capacitance and correspondingly larger energy release for a similar voltage drop during breakdown. Exceptions to the larger breakdowns occur when the capacitor voltage does not drop to the minimum voltage discussed in Chapter IV below. Fig. 37 shows a micrograph of the edge of a large breakdown such as that shown in Fig. 123 below. The streaks cover a rather broad area of the capacitor and consist of a very large number of separate holes. However, each hole is not a separate breakdown, but the entire pattern is formed simultaneously with the appearance of one breakdown pulse. The thinner regions such as those indicated by the arrows are places where one of the electrodes has been removed. With only a few exceptions the holes indicating dielectric damage do not occur in these regions. In the few exceptions the holes must have occurred prior to removal of the

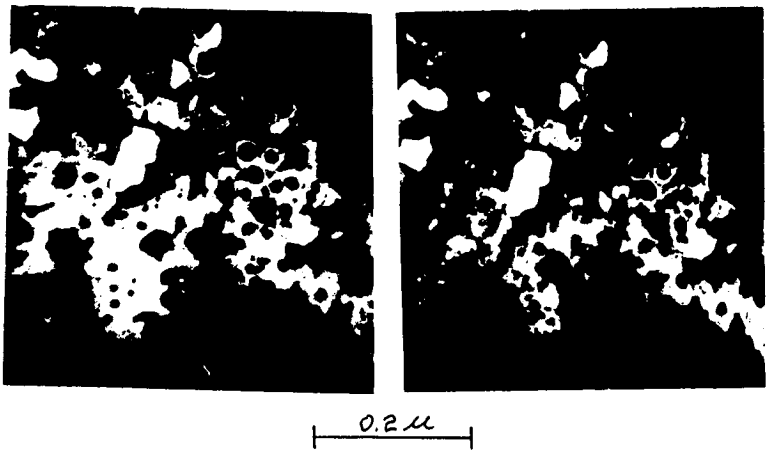

Figure 35. Stereo view of breakdown area in capacitor 1009-8.

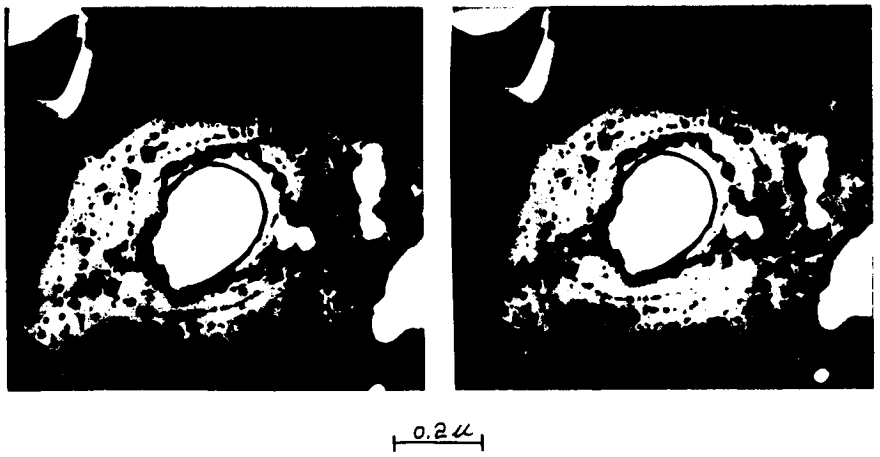

Figure 36. Stereo view of breakdown area in capacitor 1009-8.

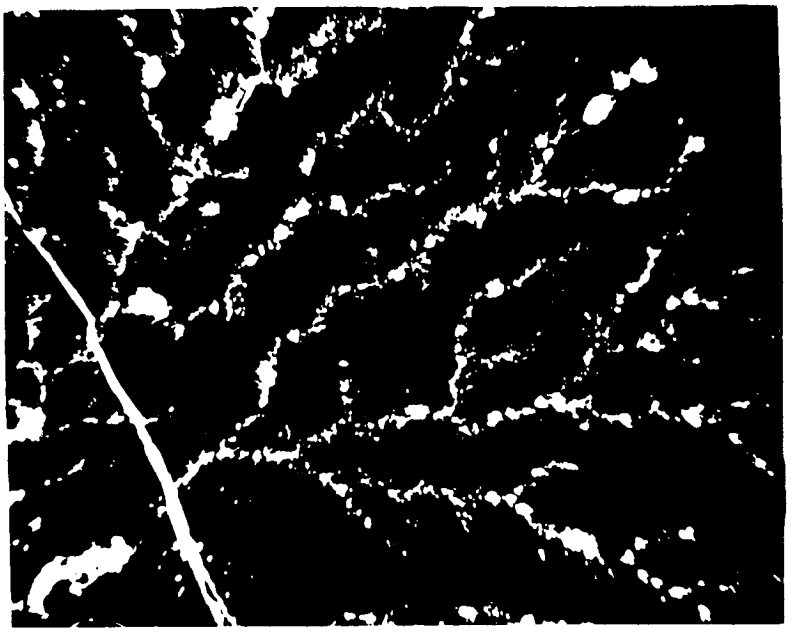

Figure 37. Streaks in capacitor 1015-T which was broken down on a glass substrate.

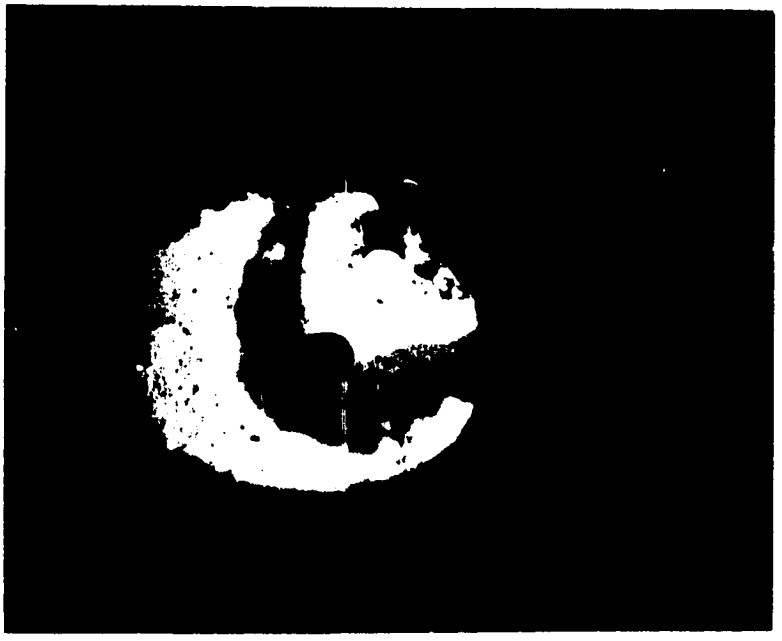

Figure 38. Small breakdown in capacitor 1015-T.

electrode. The crack in the film resulted in the stripping process as indicated by the continuation of the path of the streaks on both sides.

The small breakdowns of Fig. 123 below were also examined in the electron microscope. Fig. 38 depicts such a breakdown. A portion of the blown-out center of the breakdown is seen lying on the surface. The electrode rings resemble those seen above in Fig. 27. Buckling of the capacitor is also evident around the perimeter of the breakdown. The light "tear-drop" area results from the stripping procedure. That portion of the bottom electrode adhered to the glass.

Fig. 39 shows another small breakdown from the same capacitor. Many rings of what is thought to be electrode material encircle the central hole. Again the blown-out center lies on the surface.

In Fig. 40 is shown, at higher magnification, another small breakdown. It appears that the electrode material has gathered at the center of the breakdown, but that the center has not been completely removed.

In general the balls identified above as silicon have also been found in the larger capacitors on glass. The range of sizes includes the one micron diameter, but extends somewhat higher as will be discussed with the optical photomicrophy work below.

It should be pointed out that breakdowns do not have a tendency to occur at cracks or pin-holes which occasionally are present in the capacitor. Nor are they concentrated near the capacitor edge. Futhermore, no change in the capacitor has been observed just prior to breakdown. The one clue to a susceptible breakdown site is the presence of the dark spot or defect of about one-half micron diameter.

Figure 39. Breakdown in capacitor 1015-T.

Figure 40. Breakdown in capacitor 1015-T.

B. Breakdown Strength Observations and Discussion

Breakdown characteristics and definitions

The breakdown strength of the larger capacitors fabricated on glass slides has been investigated with both pulse and ramp voltages. Many of these capacitors were made in a Consolidated Vacuum CV-18 system arranged so that all layers could be deposited without opening the system to the atmosphere. At the outset of this study several observations were made concerning the details of breakdown. One of the most significant was the observation that after the onset of breakdown the voltage across a capacitor did not drop quite to zero but rather to a level V_{MIN}. It was also found that the occurrence of breakdown was of a statistical nature. These features are discussed in connection with breakdown strength prior to the presentation of data. References to polarity will refer to the top (counter) electrode and the bottom electrode will always be denoted as ground.

With the application of an applied pulse of sufficient amplitude, breakdowns may be observed on an oscilloscope as shown in Fig. 41. The pulse amplitude is labeled V_{CAP} and is the voltage across the capacitor. Generally this voltage is the same as the applied voltage since the resistor R in the test circuit (Fig. 11) is one hundred ohms and is negligible compared to the capacitor leakage resistance. After the initiation of breakdown the voltage across the capacitor V_{CAP} drops within approximately one-half microsecond to V_{MIN} or to a voltage between V_{CAP} and V_{MIN}. The C breakdowns are only occasional whereas the A and B breakdowns are typical. After termination of the breakdown the capacitor again recharges along a curve depending on the circuit time constant. Fig. 42 is an oscillogram of a negative pulse application; V_{MIN} is approximately twenty

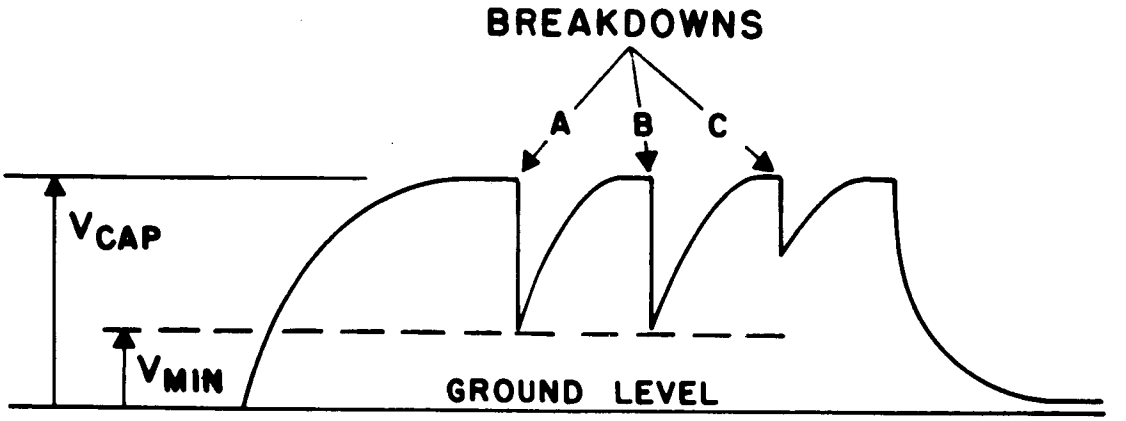

Figure 41. Application of a pulse voltage and subsequent breakdowns.

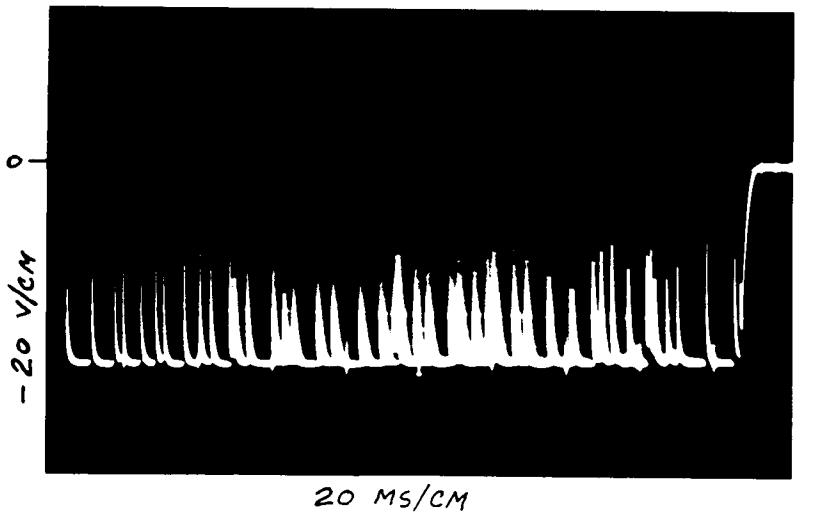

Figure 42. Oscillogram of a negative pulse.

volts. The pulse amplitude substantially exceeds that capacitor's V_{MAX} and its duration is considerably greater than the pulse in Fig. 41 so that a large number of breakdowns may be shown. Should V_{CAP} be increased to large values relative to V_{MIN} the quantity and size of the breakdowns increase, but still they terminate at V_{MIN}. Thus, with variations in V_{CAP}, the energy release of the breakdown is varied. This might be expected to yield a variety of breakdown sizes in a given capacitor.

V_{MIN} must be recognized as an important parameter since it is the minimum voltage at which the breakdown process can either be initiated or continued. No breakdowns have ever been observed with an applied voltage less than the value of V_{MIN}! An accurate measurement of V_{MIN} may be made if a sufficient number of breakdowns occur. This is accomplished either by using a pulse voltage which sufficiently exceeds V_{MAX} or by using a ramp voltage which increases above V_{MAX}. Fig. 43 is an illustration of the effect to be expected from a ramp voltage. Figs. 44 through 49 show ramp applications to several capacitors. After a large number of breakdowns the capacitors open-circuit and the breakdowns cease. In most capacitors the leakage resistance at voltages near and above the breakdown strength becomes low enough to load the ramp voltage supply thus causing the applied voltage curve to deviate from a linear increase. As the capacitor breaks down and begins to open circuit the leakage resistance begins to increase. Accordingly the applied voltage curve again approaches a straight line. This open-circuit effect is very sharp in Figs. 46, 47, and 48, but not so sharp in Fig. 49.

Measurements of V_{MIN} by either pulse or ramp voltages yield identical results. V_{MIN} is unaffected by humidity changes and is constant over the temperature range of the tests which was about 80°K to 363°K.

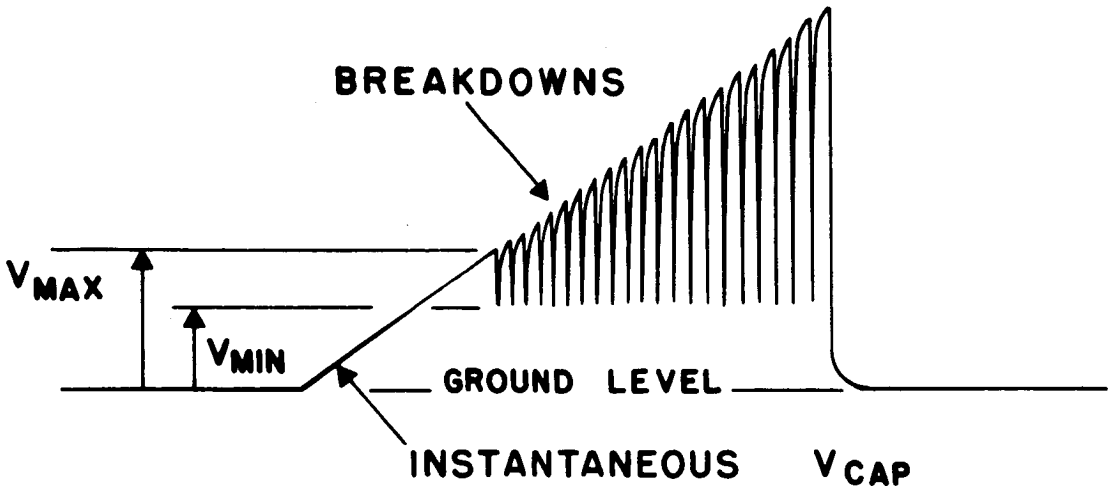

Figure 43. Sketch of a ramp voltage which exceeds the breakdown strength.

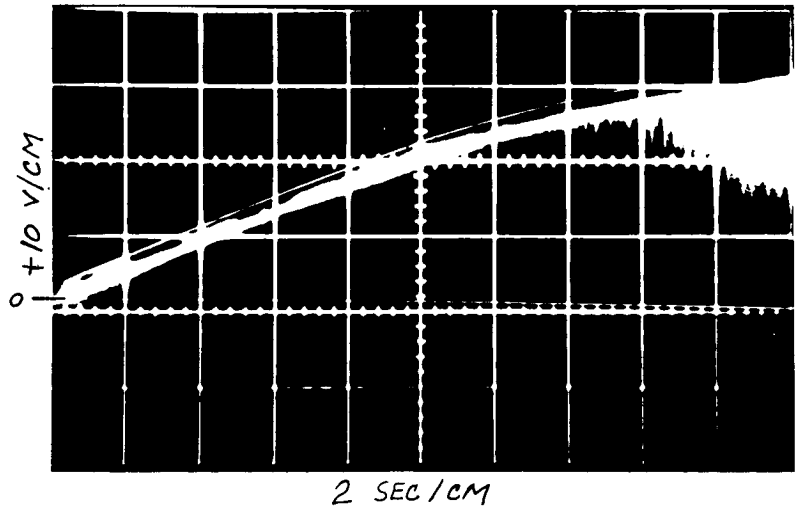

Figure 44. Oscillogram of a ramp voltage applied to capacitor 1027-T. (positive ramp voltage; low intensity does not reveal the first few breakdowns)

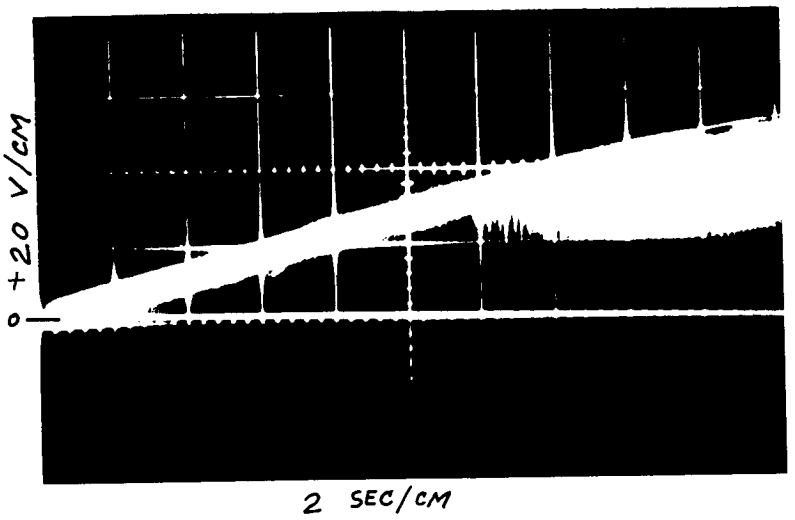

Figure 45. Oscillogram of a ramp voltage applied to capacitor 102b.

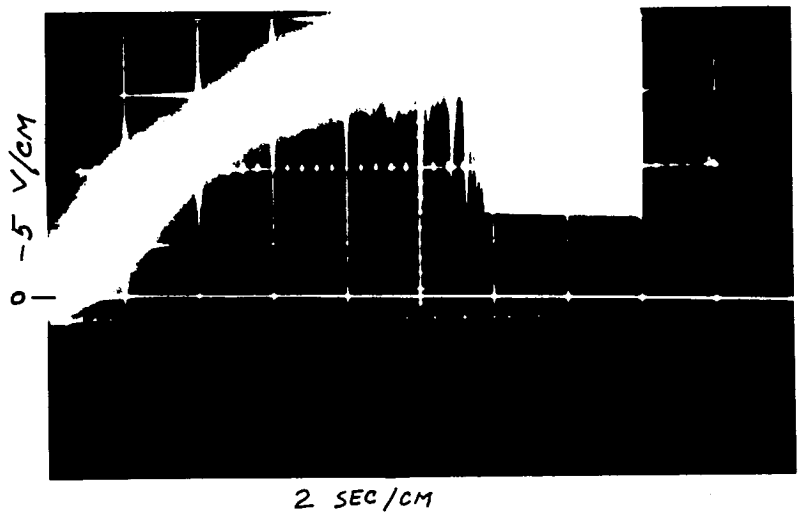

Figure 46. Oscillogram of a ramp voltage applied to capacitor 1022-T. (High intensity first few breakdowns shows many breakdowns as a continuous sheet)

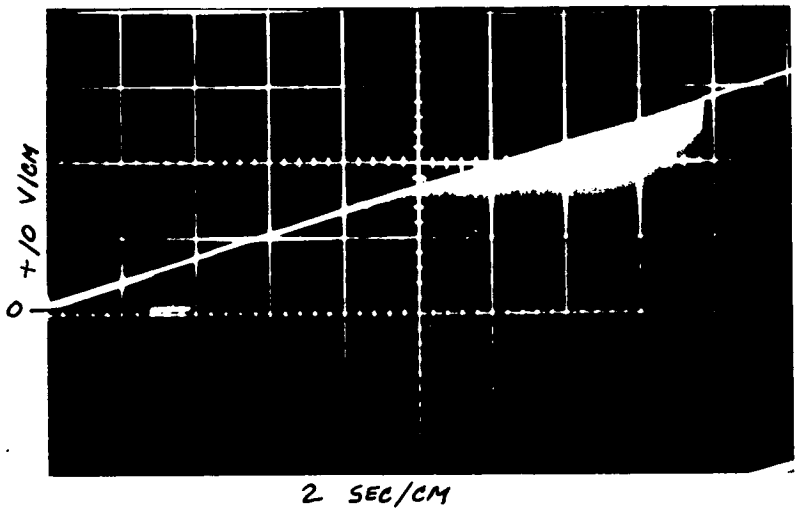

Figure 47. Oscillogram of a ramp voltage applied to capacitor 1017-T.

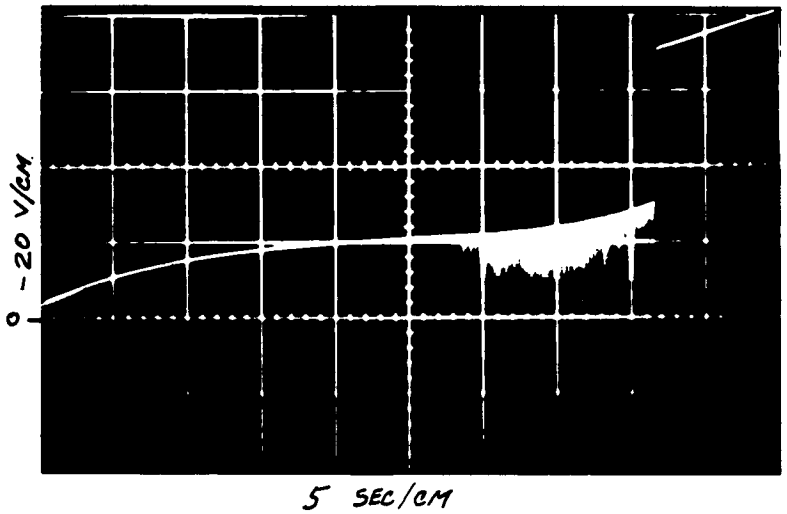

Figure 48. Oscillogram of a ramp voltage applied to capacitor 1020-T.

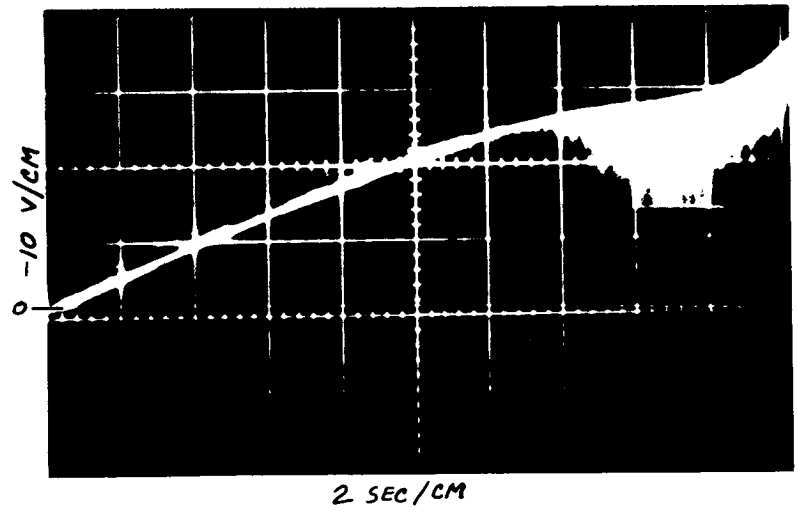

Figure 49. Oscillogram of a ramp voltage applied to capacitor 1027-T. (Negative ramp voltage; low intensity does not reveal first few breakdowns)

V_{MAX} has been measured in two fashions, one in which the amplitude of a pulse of fixed duration and repetition rate was slowly increased until breakdown(s) were observed to occur (pulse method). The second method employed a slowly increasing voltage which was repetitively applied and, by appropriate circuitry, removed from the capacitor by the occurrence of the first breakdown of greater than two volts amplitude (ramp method).

As mentioned above the occurrence of breakdowns is of a statistical nature. The factors which have been found to influence the statistics are humidity and humidity changes, past history, and, of course, voltage. Humidity has been controlled by the use of drierite chambers and vacuum chambers. However, the effects are illustrated in the measurement of V_{MAX} by the pulse method. After the pulse amplitude has been increased to V_{MAX} as indicated by the occurrence of breakdown pulses, successive pulses of the same amplitude do not always produce breakdown. Frequently the amplitude must be increased again to a "new" V_{MAX} before more breakdowns occur. Such increases may be as much as fifty percent of the initial measurement. In the data presented below the initial voltage at which breakdowns occurred is assumed to be the breakdown voltage V_{MAX}.

One might speculate that there is a voltage-sensitive distribution of local defects within the capacitor and that those corresponding to the initial V_{MAX} are removed by the initial breakdowns, thus leading to cessation of breakdown occurrences. More breakdowns cannot be generated until V_{CAP} is increased to a "new" V_{MAX}. This sort of explanation is not very acceptable because either of two effects, polarity reversal or temporary removal of the applied voltage, will again result in more breakdowns at the same voltage. Thus the pulse measurement of F_{MAX} most likely yields

a low value of the breakdown strength because of this tendency for the breakdowns to cease.

In the ramp voltage method a number of successive measurements of V_{MAX} (at least ten) were used in determining a statistical mean. Breakdowns of less than two volts were few. Typical ramps were 15 volts/sec. Variations in the ramp speed from 150 volts/sec to 3 volts/sec generally showed no measurable change in V_{MAX}. The recorder was operated at one inch per minute so that with a ramp of 15 volts/sec there were about six ramps per inch. This gives a series of peaks each of which is a measurement of V_{MAX}. Fig. 50 depicts a representative chart recording and gives the appearance of a breakdown threshold voltage.

Observed data

Fig. 51 is a summary of the breakdown strength (F_{MAX}) measurements made by the pulse technique for positive voltages. F_{MIN}, as measured by either the pulse or ramp method, is also shown there for comparison. Similar data for negative polarity are shown in Fig. 52. Figs. 53 and 54 give, respectively, positive and negative voltage measurements of F_{MAX} using the ramp voltage method. The pulse voltages were measured to within five percent accuracy using the oscilloscope. The spread of a ramp voltage measurement is the standard deviation of the voltages at which the first breakdown occurred during successive ramp applications. The breakdown voltage V_{MAX} is included for the ramp voltage tests. Figs. 55 and 56 give the V_{MAX} data which correspond, respectively, to the F_{MAX} data in Figs. 53 and 54.

In some of the thicker capacitors the voltage corresponding to the first breakdown increased with successive ramps from an initial value to

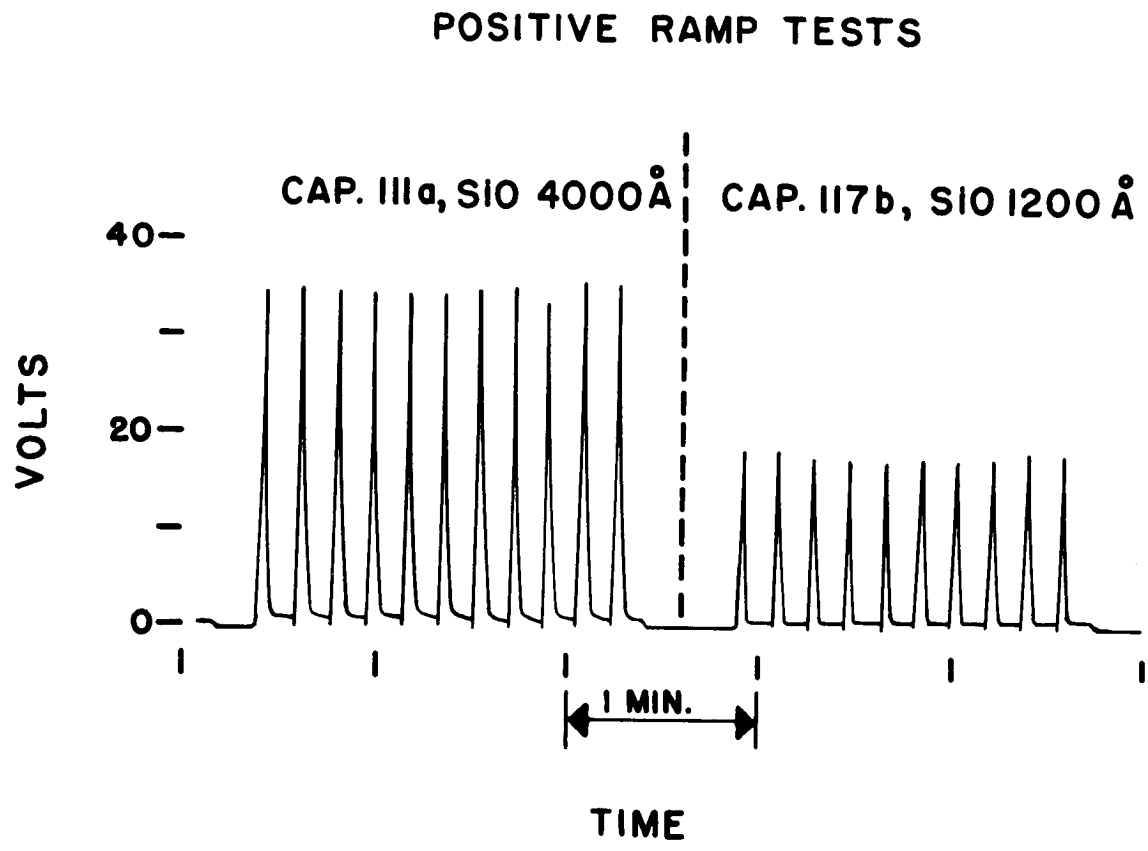

Figure 50. A duplication of a typical recording illustrating peaks which are a measurement of V_{MAX}.

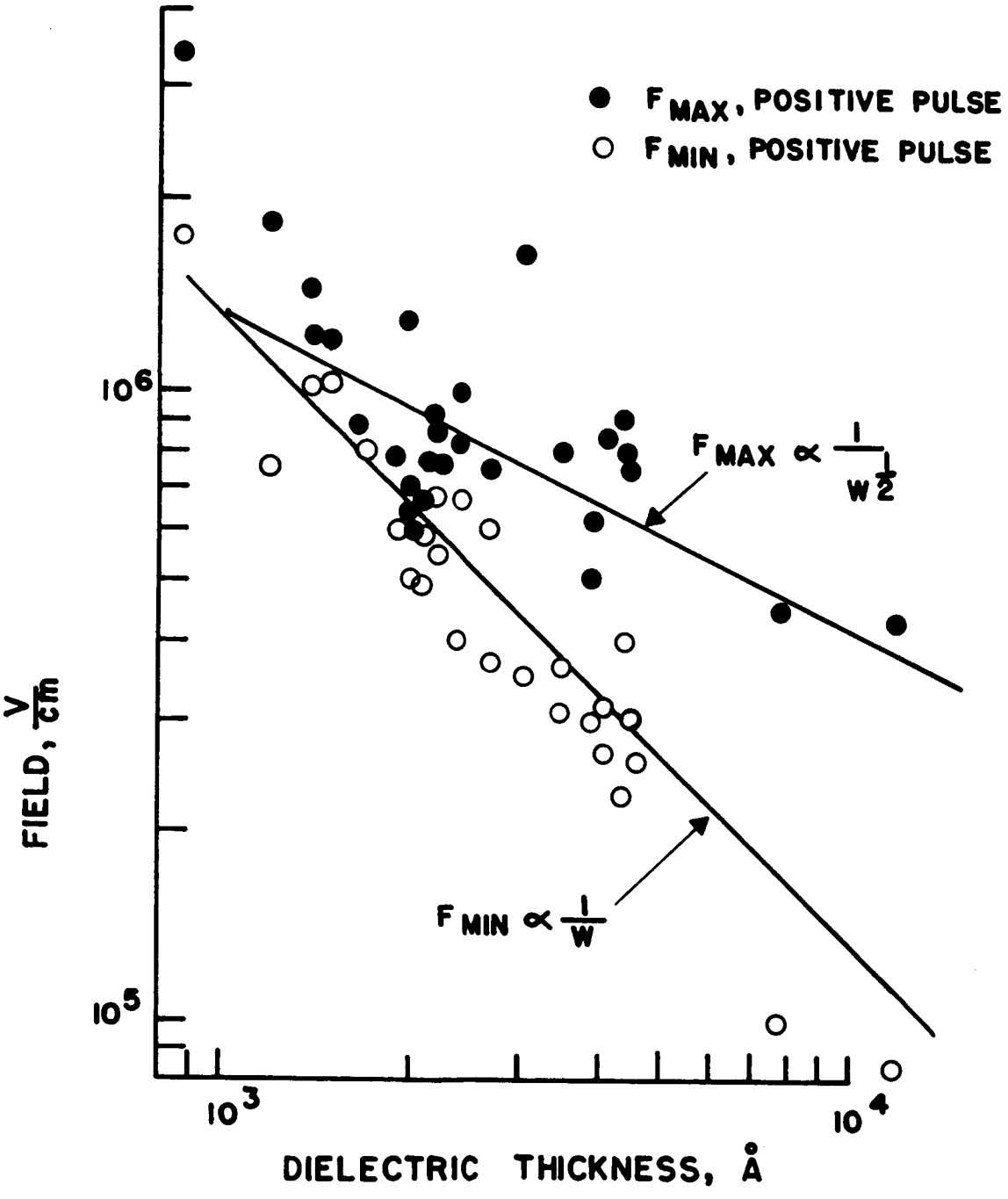

Figure 51. F_{MAX} and F_{MIN} versus silicon monoxide thickness for positive pulse voltage measurements.

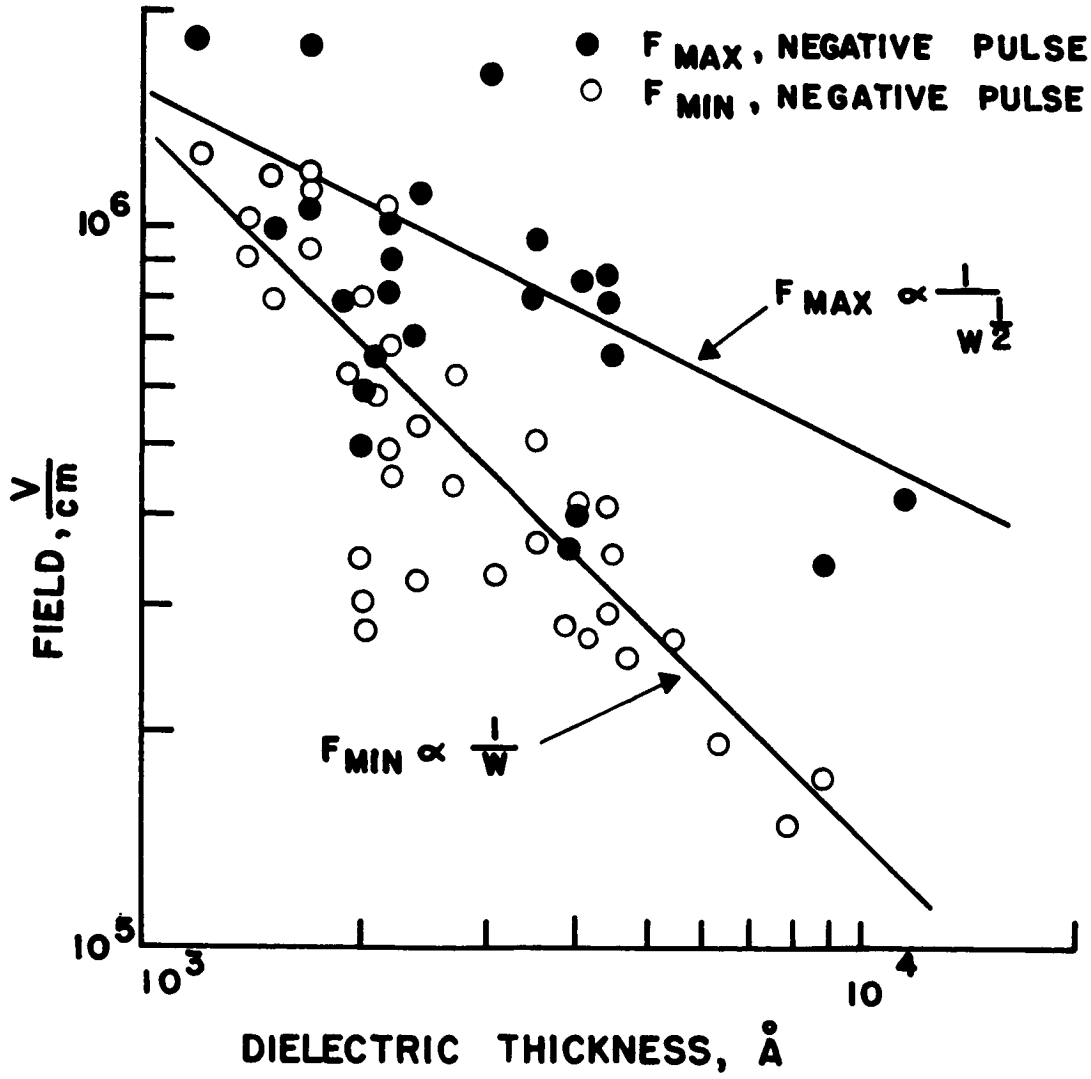

Figure 52. F_{MAX} and F_{MIN} versus silicon monoxide thickness for negative pulse voltage measurements.

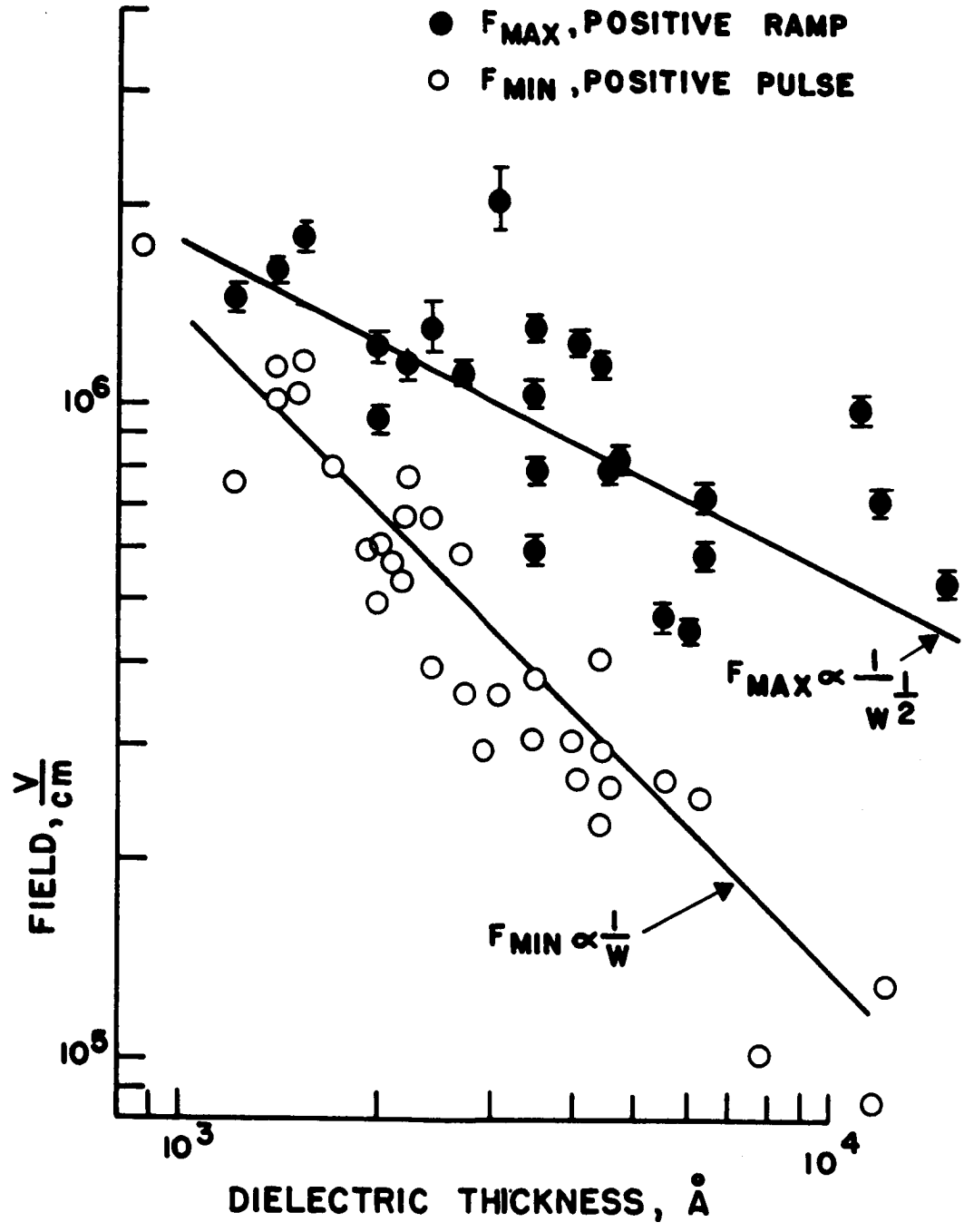

Figure 53. F_{MAX} and F_{MIN} versus silicon monoxide thickness for positive ramp voltage measurements.

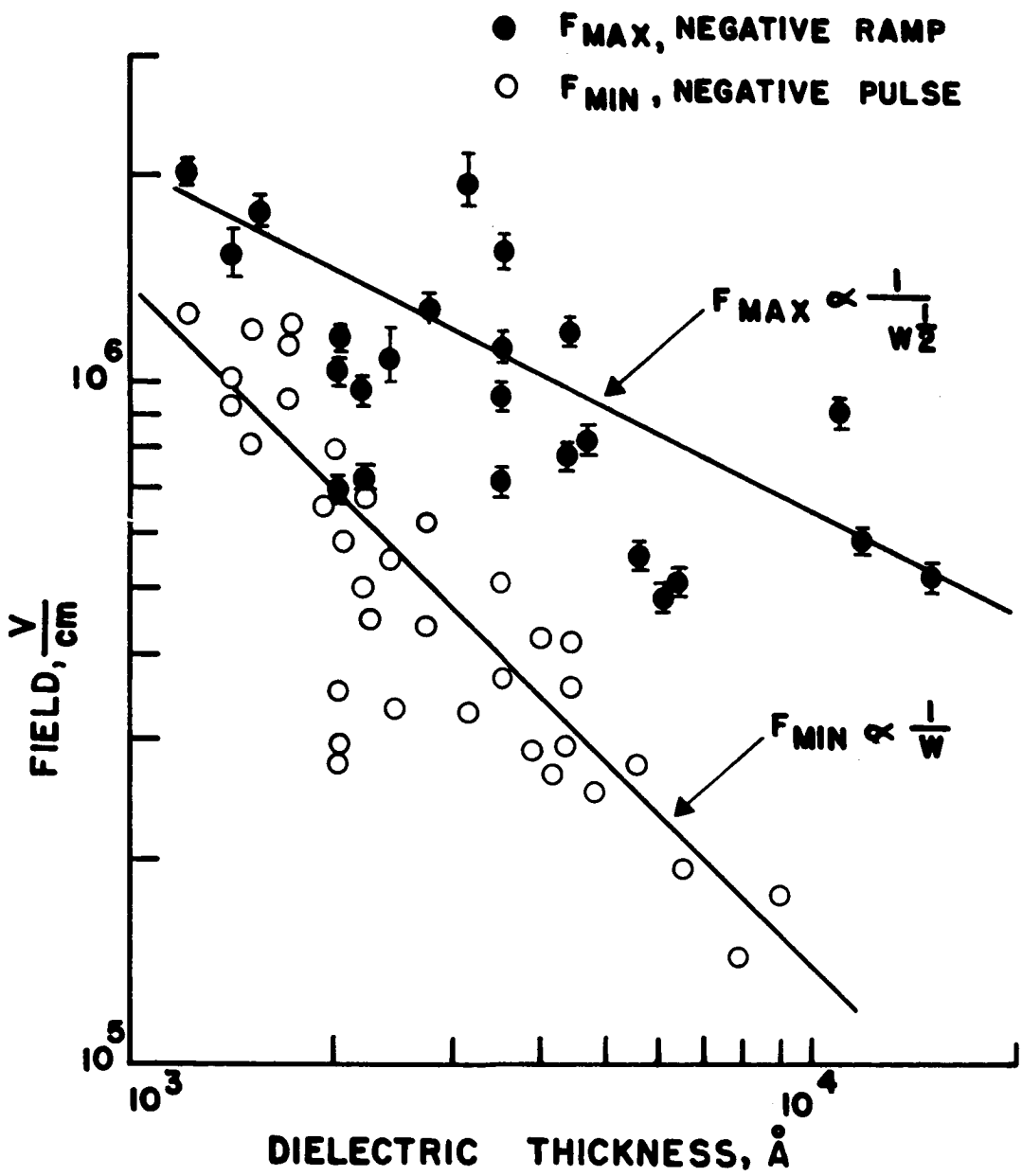

Figure 54. F_{MAX} and F_{MIN} versus silicon monoxide thickness for negative ramp voltage measurements.

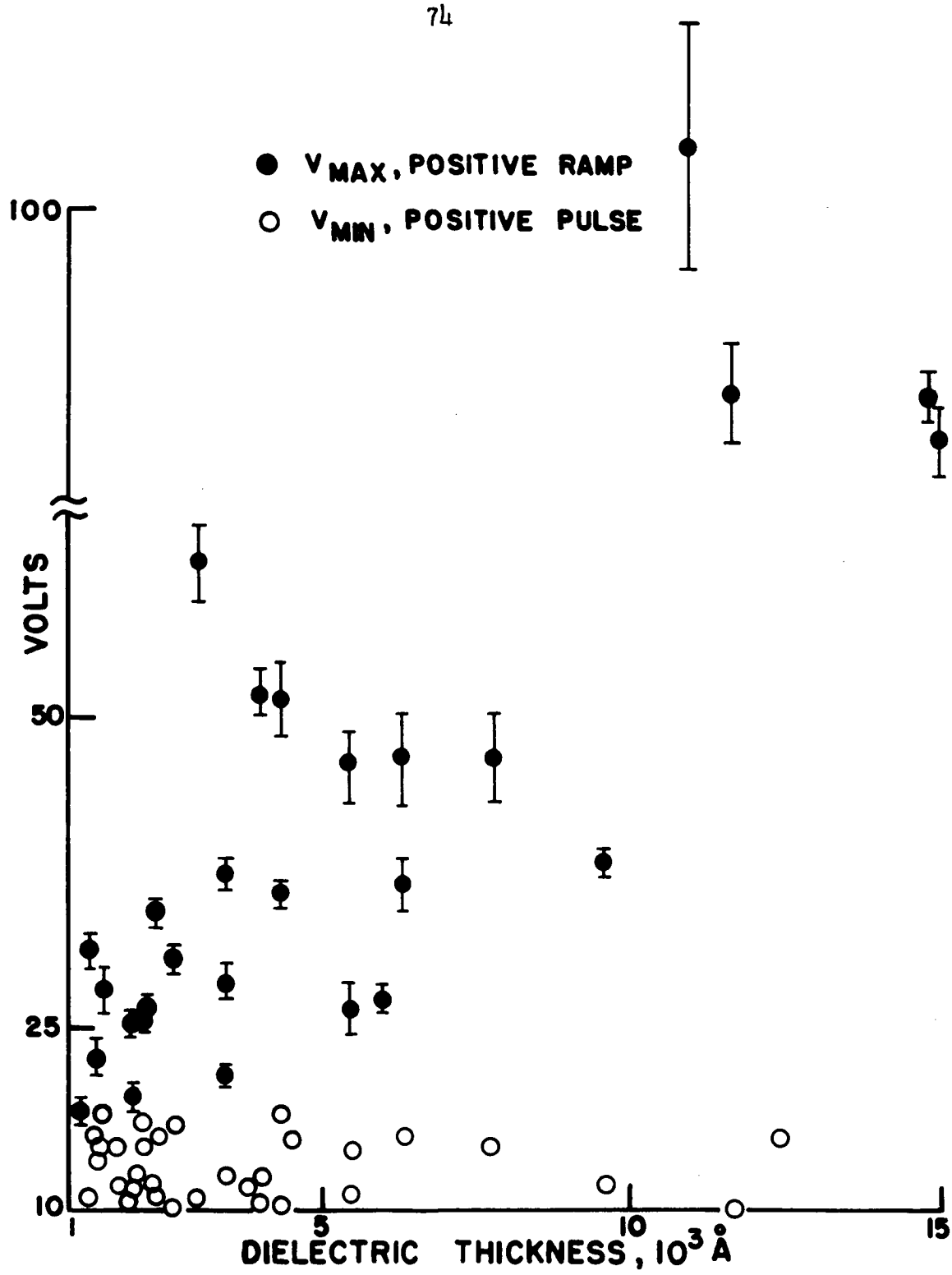

Figure 55. Voltages V_{MAX} and V_{MIN} corresponding to Fig. 53 (positive ramp voltages).

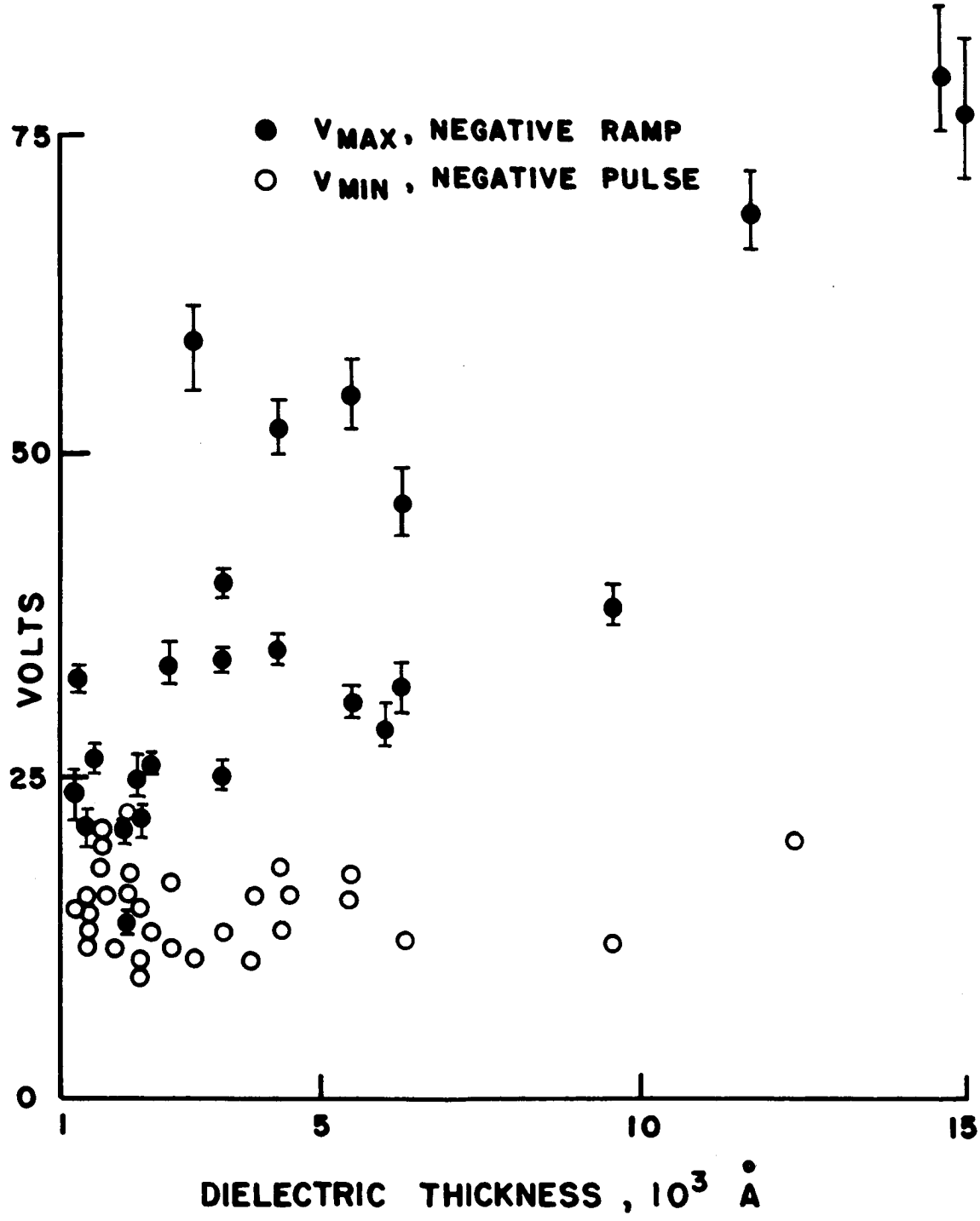

Figure 56. Voltages V_{MAX} and V_{MIN} corresponding to Fig. 54 (negative ramp voltages).

a higher and more nearly constant value as shown in Fig. 57. In such cases the upper level was used as a measurement of V_{MAX}.

Comparison of the F_{MAX} data for the two polarities of a given test method indicates no basic difference in the breakdown strength. This is somewhat misleading because $F_{MAX}(+)$ and $F_{MAX}(-)$ are well defined for a single capacitor. The difference in the positive and negative breakdown strengths $\left[F_{MAX}(+) - F_{MAX}(-)\right]$ is neither constant in sign nor in magnitude as shown in Fig. 58. Perhaps this randomness can be interpreted as further evidence for the random distribution of defects such as was observed in the electron microscopy. Fig. 59 shows the difference in the minimum fields for different polarities. Again the somewhat erratic variation seems to indicate random defects.

A number of capacitors were subjected to the ramp voltage breakdown strength tests over a range of temperatures varying from about $80^{o}K$ to $303^{o}K$ (near liquid nitrogen to room temperature). Figs. 60 through 65 present the V_{MAX} and F_{MAX} data of several capacitors. The value of V_{MIN} for a given capacitor and polarity was never observed to change and thus a temperature plot is unnecessary. These temperature plots show only a very slight decrease in breakdown strength as the temperature is increased from near-liquid nitrogen temperature to room temperature. In some cases the tests were begun at room temperature and in others they were begun at liquid-nitrogen temperature. As mentioned above this slight decrease in breakdown voltage with increasing temperature could account for the elimination of the randomness of breakdowns with no measurable change in V_{MAX} in a capacitor while under electron microscopic examination. Further discussion of these data is given in connection with the various theories of dielectric breakdown.

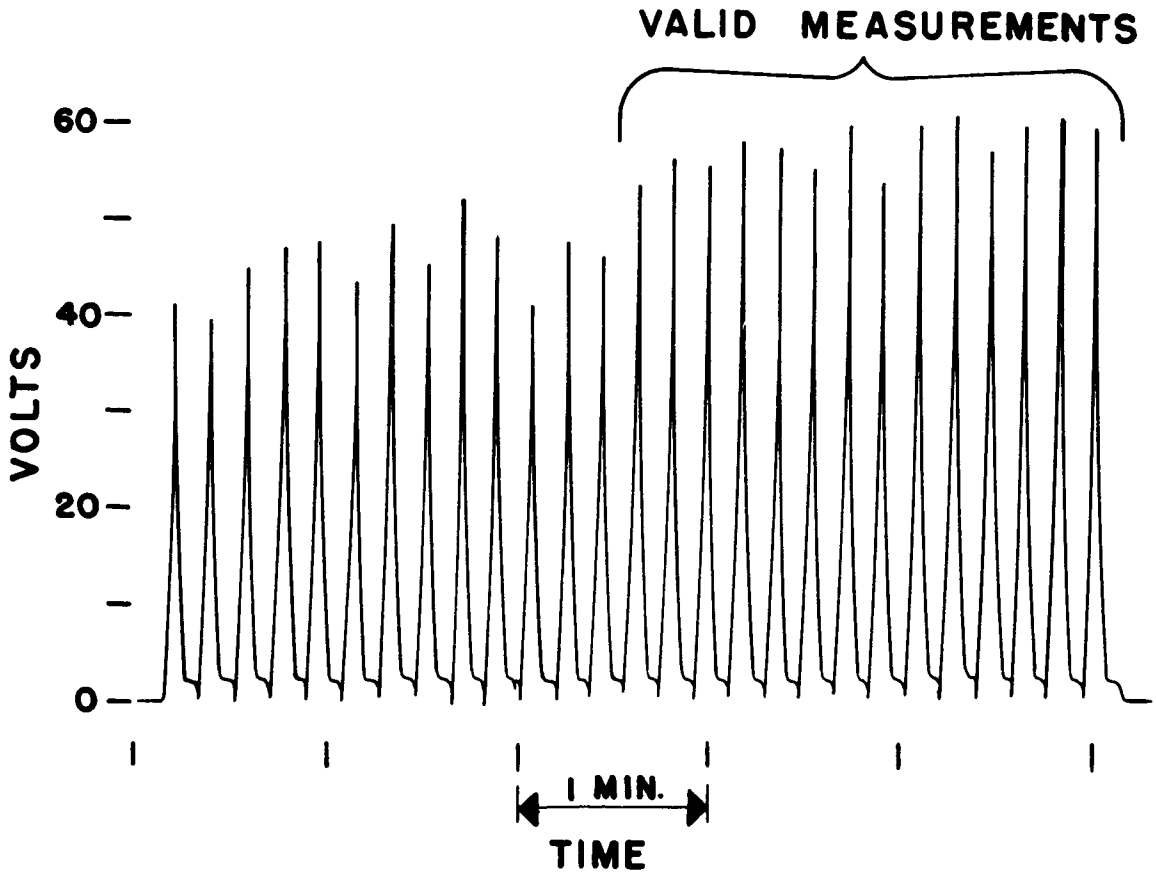

Figure 57. Changing of breakdown voltage in a thick capacitor.

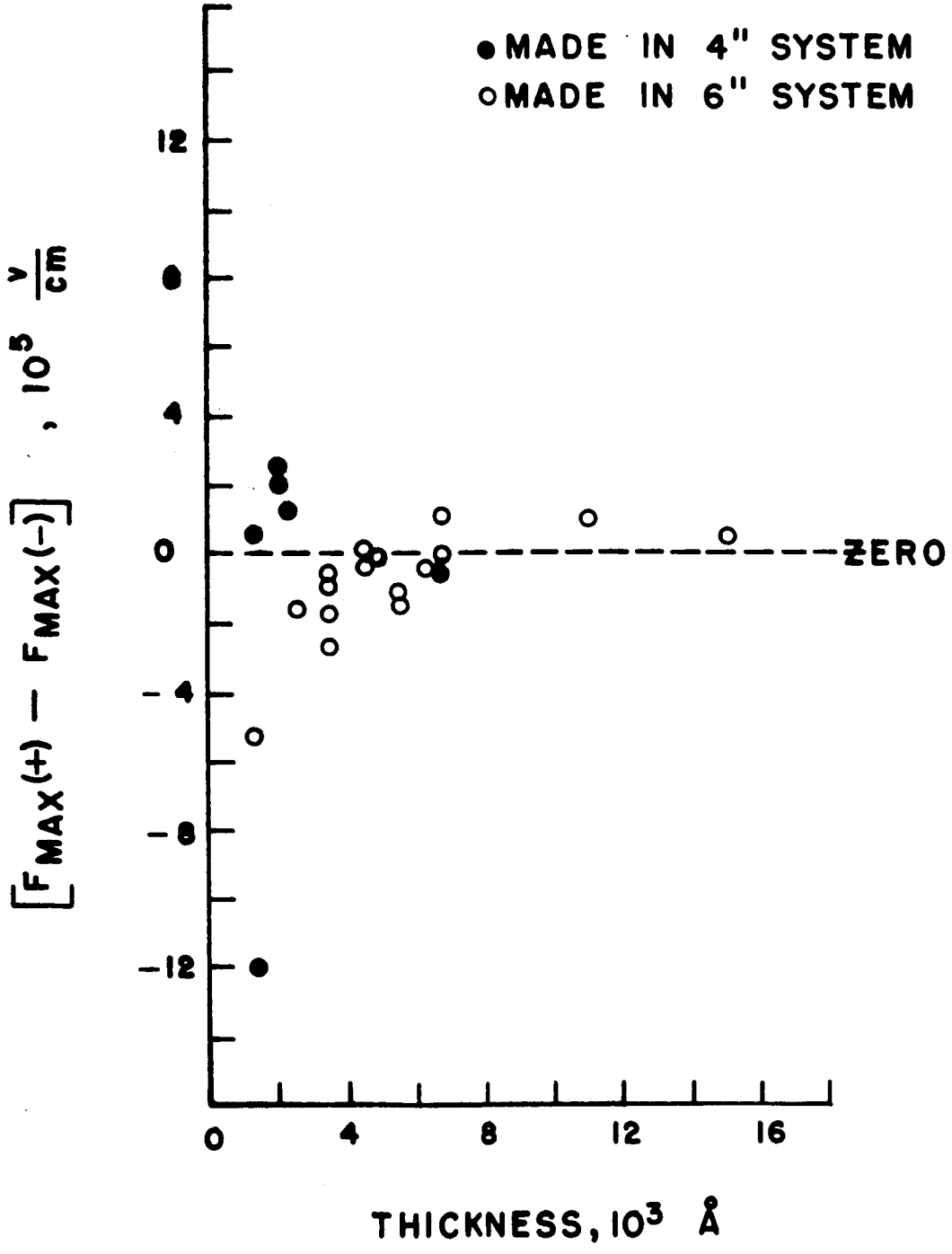

Figure 58. $\left[F_{MAX\ (+)} - F_{MAX\ (-)}\right]$ for ramp voltage test.

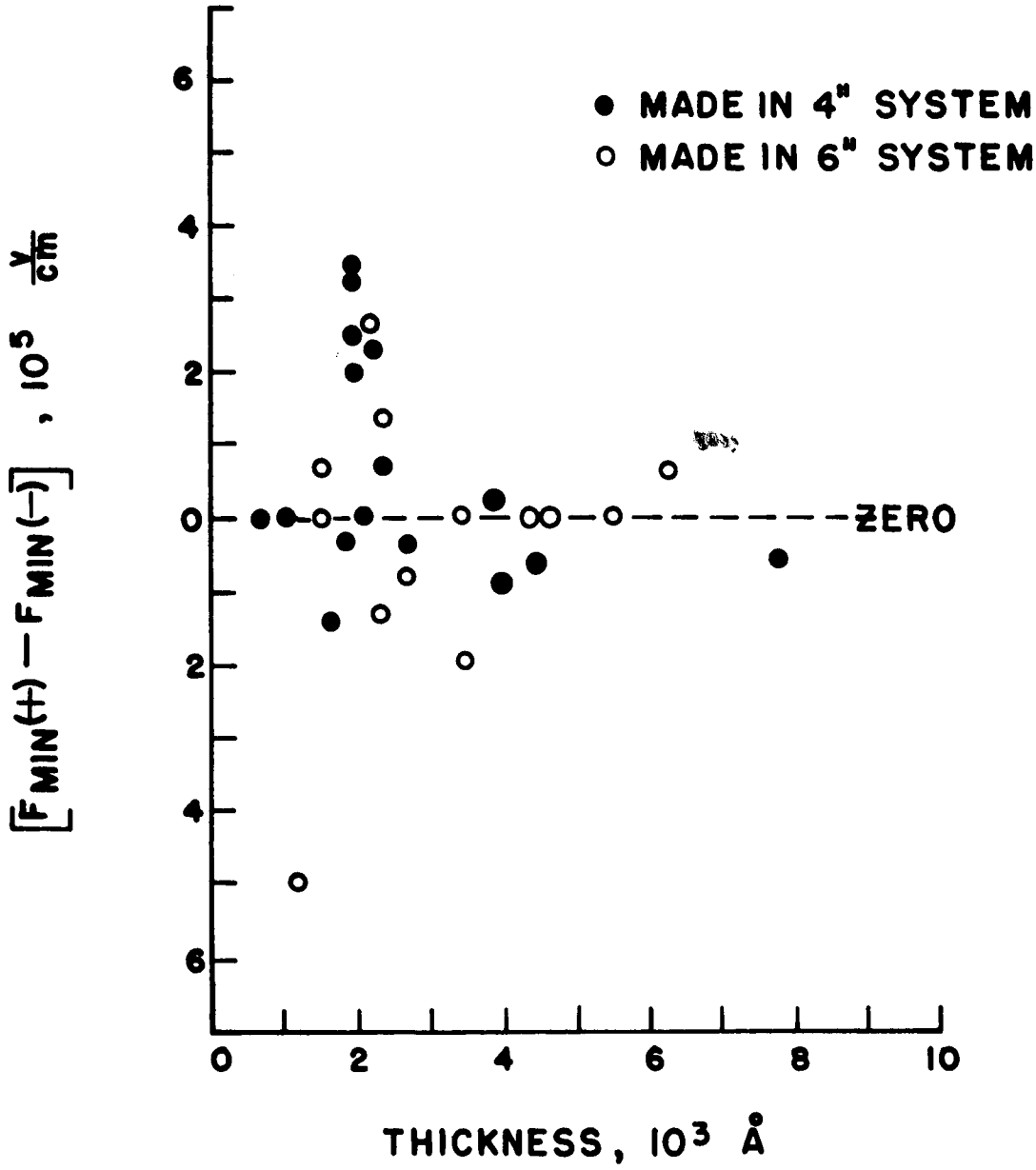

Figure 59. $\left[F_{MIN\ (+)} - F_{MIN\ (-)}\right]$ for pulse voltage test.

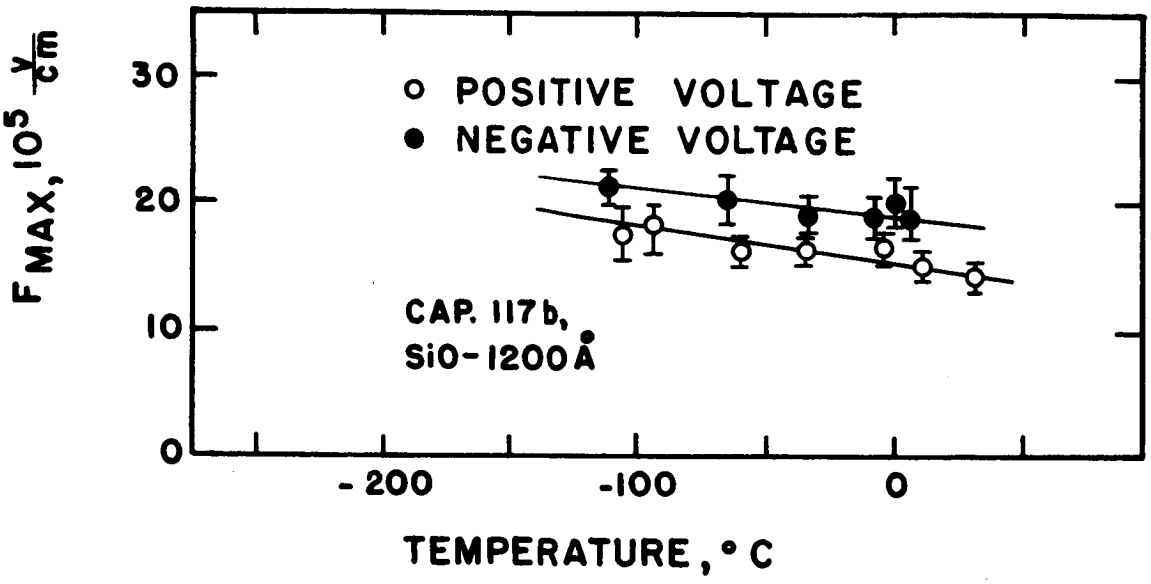

Figure 60. Breakdown strength of capacitor 117b versus temperature.

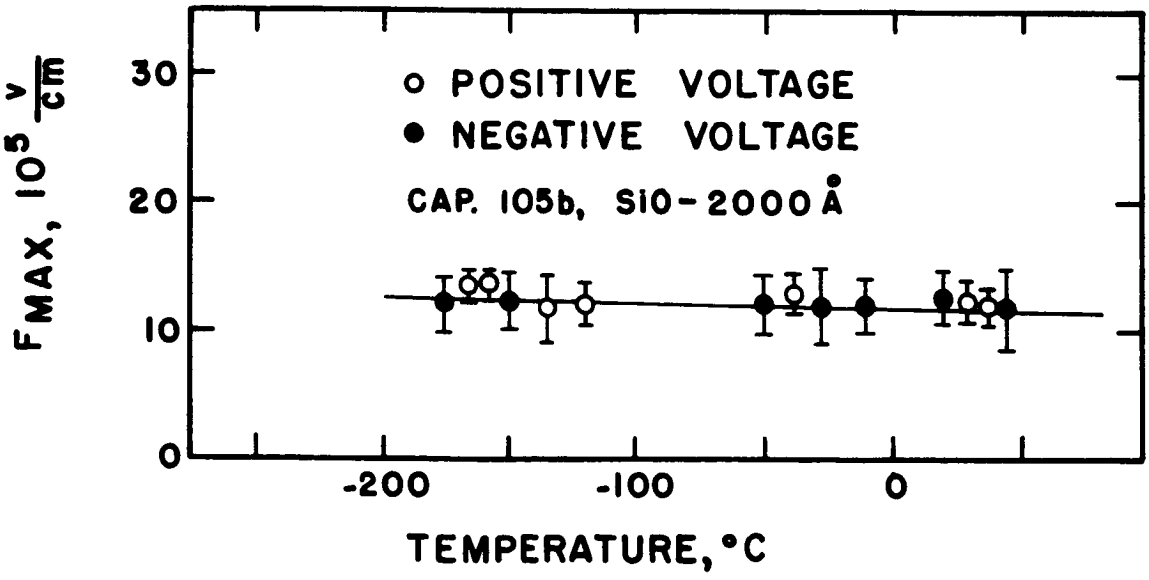

Figure 61. Breakdown strength of capacitor 105b versus temperature.

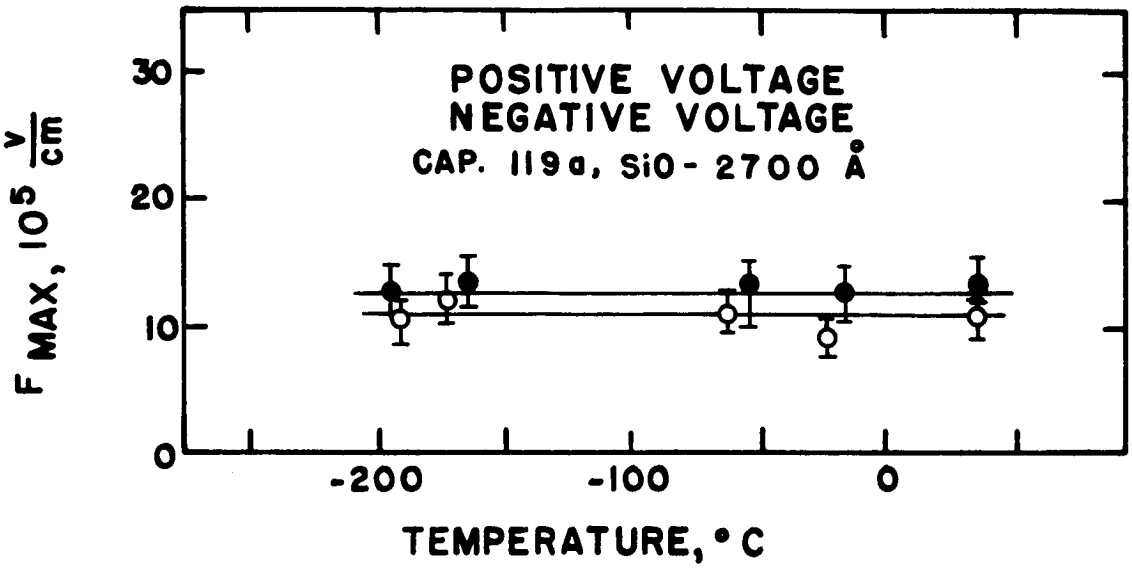

Figure 62. Breakdown strength of capacitor 119a versus temperature.

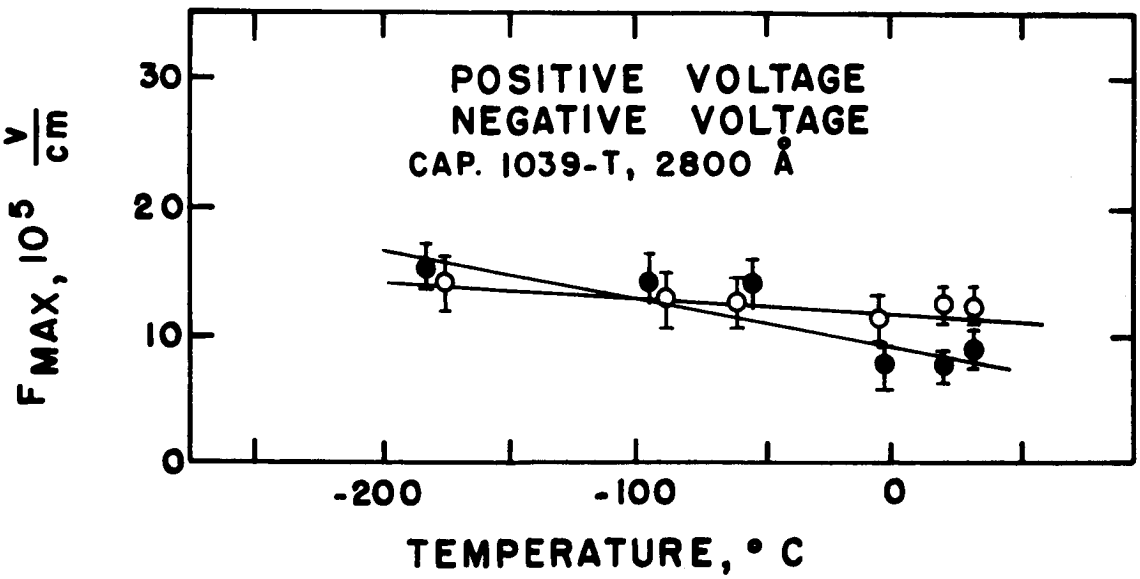

Figure 63. Breakdown strength of capacitor 1039-T versus temperature.

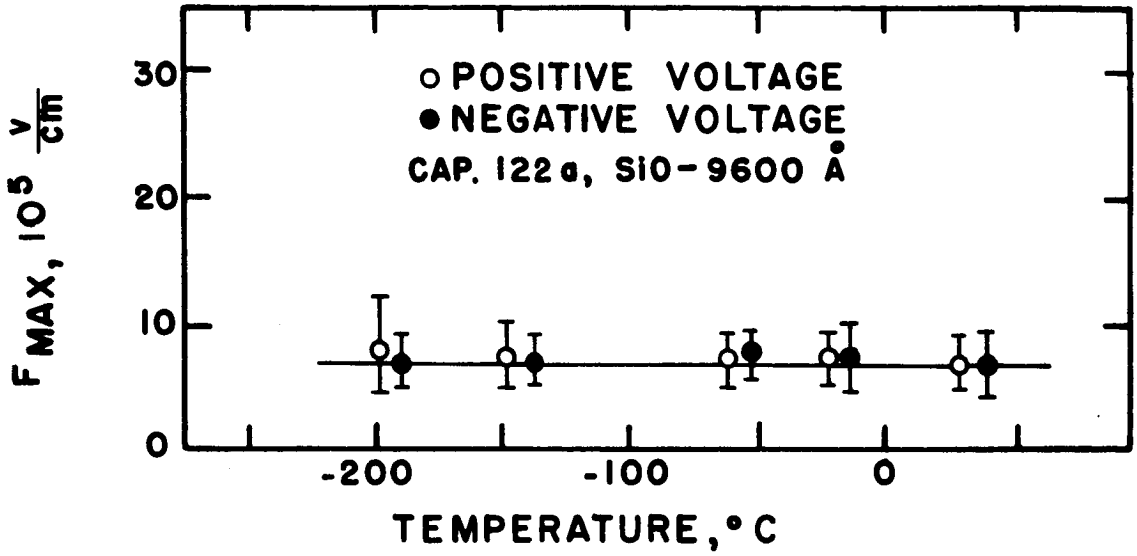

Figure 64. Breakdown strength of capacitor 122a versus temperature.

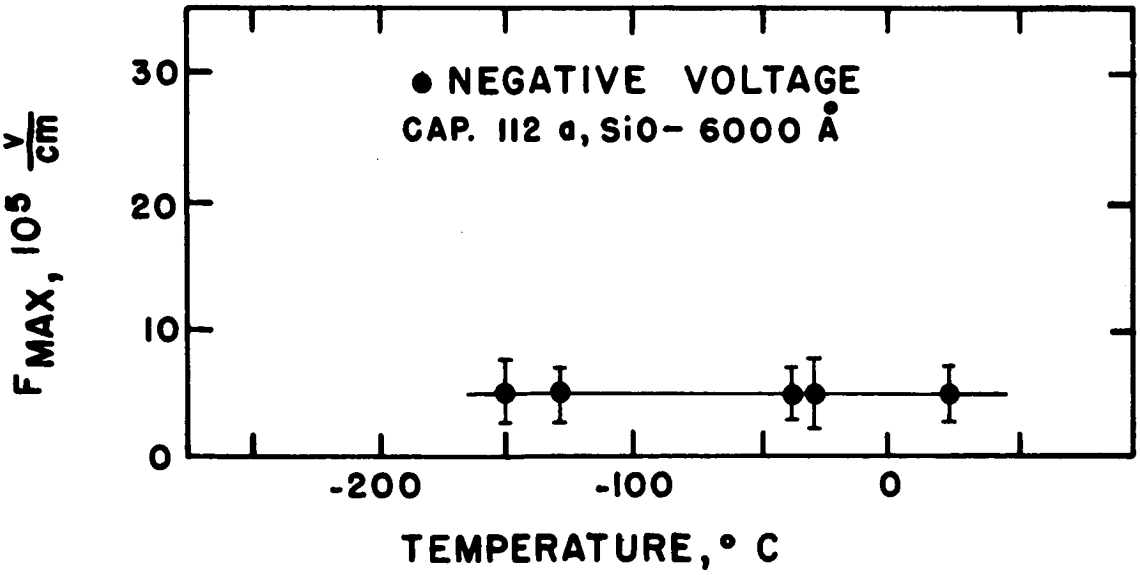

Figure 65. Breakdown strength of capacitor 112a versus temperature.

Comparison with theory

Theories on dielectric breakdown usually distinguish four aspects: intrinsic breakdown, thermal breakdown, avalanche breakdown and electrochemical breakdown. Experimentally, one or more of these may be effective at once. Intrinsic breakdown is a bulk property of an infinite dielectric immersed in a uniform electric field of such strength that field ionization occurs catastrophically. The magnitude of the critical field is a function of the ambient temperature, i.e., the temperature prior to application of the critical field. Once the critical field is reached, breakdown is virtually instantaneous.

Thermal breakdown assumes a gradual heating of the dielectric due to field-produced currents. At the critical field electrical energy is converted to thermal energy fast enough to cause a continuing temperature rise and eventual destruction. The macroscopic equation of heat conduction with a volume distribution of currents is the basic equation.

Avalanche breakdown is descriptive of a mechanism wherein carriers absorb from the electric field sufficient energy to generate other carriers which in turn generate others, etc. Thus this type alludes to a mechanism, while the two above refer to macroscopic manifestations.

Electrochemical breakdown is a mechanism whereby a critical electric field causes a chemical decomposition of the dielectric. This definition is somewhat different from electrochemical deterioration discussed by Whitehead.[27]

The data presented above give breakdown strength as a function of thickness and of temperature and thus are suitable for comparison with the various breakdown theories. The purpose of the following discussion

is not to give a derivation of the various theories, but to determine which theory best explains breakdown in thin film silicon monoxide capacitors.

Electron ionization avalanche. A theoretical development is given by Forlani and Minnaja.[28] Their physical hypotheses are that the dielectric is an ionic crystal and that electrons in the conduction band are free. The avalanche process includes tunnel-emission of electrons at the cathode into the conduction band of the dielectric and leads to a field dependent current density which reaches a value sufficient to produce breakdown. The breakdown threshold is given by

$$F_{MAX} = \frac{A}{W^{\frac{1}{2}}}, \tag{7}$$

where A is a constant which depends on the forbidden gap of the dielectric and W is the dielectric thickness. It is pointed out that electron injection by tunneling at the cathode is a key mechanism in producing breakdown and that if the electrons have a high affinity for the dielectric the breakdown strength is approximately

$$F_{MAX} = \frac{B}{W^{\frac{1}{4}}} \tag{8}$$

where B is a constant.

With reference to Figs. 51 through 54, the range of F_{MAX} for a given thickness is fairly large, but there is a trend toward a decreasing value as thickness increases. A straight line corresponding to equation (7) is drawn through the data. The $1/W^{\frac{1}{2}}$ relationship seems to fit better than the $1/W^{\frac{1}{4}}$. However, the spread in data for the minimum field F_{MIN} is not so great and reasonably follows the relationship

$$F_{MIN} \propto \frac{1}{W} \tag{9}$$

The theory has no explicit development of a field F_{MIN}, however such a condition is implied in that the probability for an electron to reach an "unstable equilibrium energy" (necessary for breakdown) goes to zero at a given value of the field. The experimental F_{MAX} data referenced by Forlani and Minnaja for Al_2O_3 thin film dielectrics are about an order of magnitude greater than the silicon monoxide data contained herein.

To compare the minimum and maximum fields a computation of F_{MAX}/F_{MIN} is made for each capacitor using the experimental data. Comparison of equations (7) and (9) shows that F_{MAX}/F_{MIN} should depend on $W^{\frac{1}{2}}$. Figs. 66 and 67 are plots of F_{MAX}/F_{MIN} for positive and negative voltages respectively. For positive voltages this quantity does not appear to depend on $W^{\frac{1}{2}}$; however, the dependence on $W^{\frac{1}{2}}$ is better for the negative voltage data.

Of all the breakdown theories considered, this one gives the closest agreement with the experimental breakdown strength data.

If, as indicated by electron microscopy, breakdown is intimately connected with random defects, then the wide range of breakdown fields observed is expected. Thus the tendency for F_{MAX} to follow the $1/W^{\frac{1}{2}}$ relationship and also its weak temperature dependence seems to be strong evidence for concluding that the breakdown mechanism, at least over the thickness range of 1000 Å to 15,000 Å, is consistent with the electron ionization avalanche theory.

Franz breakdown field theory. Forlani and Minnaja make reference to a theoretical development of breakdown strength by Franz.[29] This theory

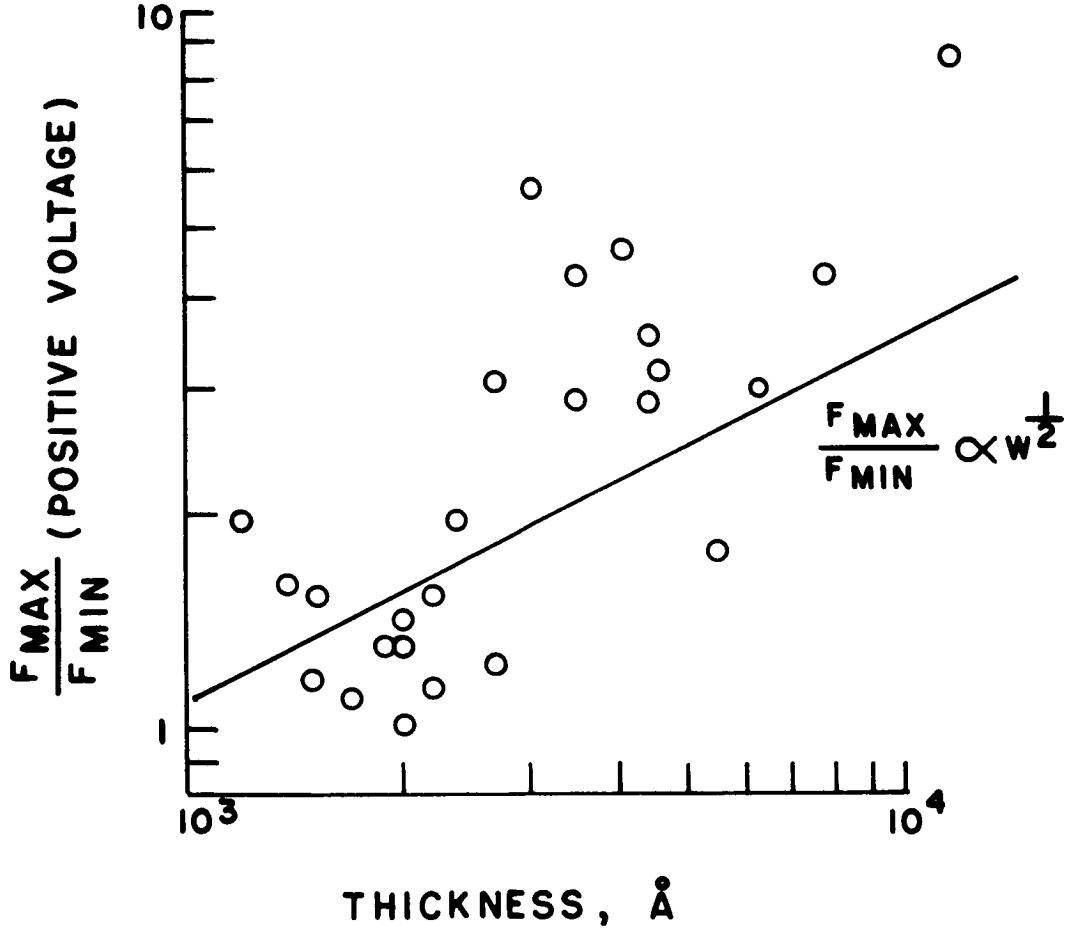

Figure 66. F_{MAX}/F_{MIN} versus dielectric thickness for positive ramp voltage.

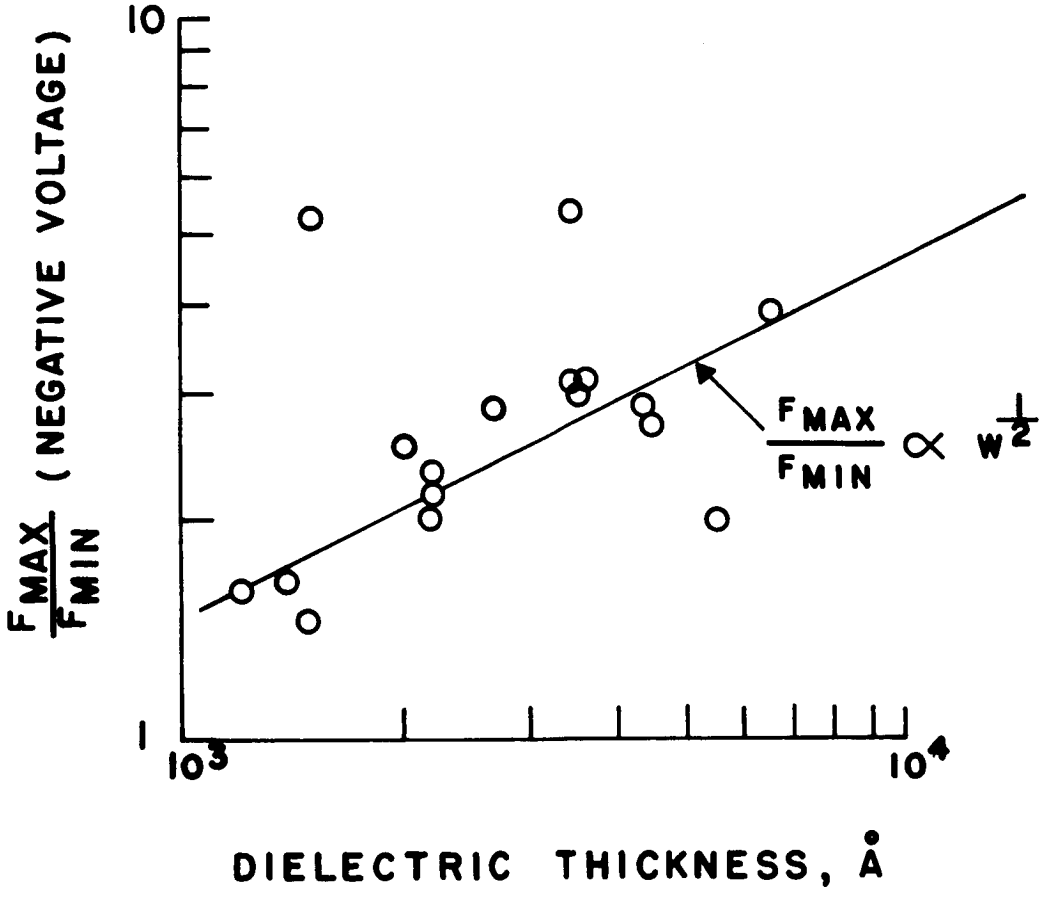

Figure 67. F_{MAX}/F_{MIN} versus dielectric thickness for negative ramp voltage.

also attributes breakdown to avalanche effects, but the final result is given by

$$F_{MAX} \propto \frac{1}{\ln\left[\frac{x_o}{W}\right]}, \tag{10}$$

where x_o is a recombination length. Since the experimental data for silicon monoxide roughly follows the $1/W^{\frac{1}{2}}$ relationship, they do not agree with this theory because of the inverse thickness in the denominator. The fact that the experimental data for F_{MAX} is not satisfied by this theory is shown by the positive slope in Fig. 68. Therefore, it can be concluded that this avalanche theory does not explain breakdown in silicon monoxide capacitors.

Field emission breakdown. This theory attributes breakdown to an uncontrolled emission of electrons from the valence band of the dielectric to the conduction band. The theory is summarized by O'Dwyer.[30] For a linearly increasing field it is found that

$$F_{MAX} = \frac{\beta}{\ln\left[\frac{e\alpha\mu F_{MAX}^{22/3} N_v t_c^2}{\beta^2 C_v (T_M - T)}\right]}, \tag{11}$$

where α and β are constants peculiar to the dielectric, μ is the electron mobility, t_c is the time of application of F_{MAX}, N_v is the density of valence electrons, T_M is the temperature of the center of the dielectric, T is the ambient temperature, C_v is the specific heat per unit volume, and e is the electronic charge. Incorporated within this theory is the impulse thermal breakdown criterion which essentially means that the temperature is increased much faster than it can be dissipated and thus the effects of

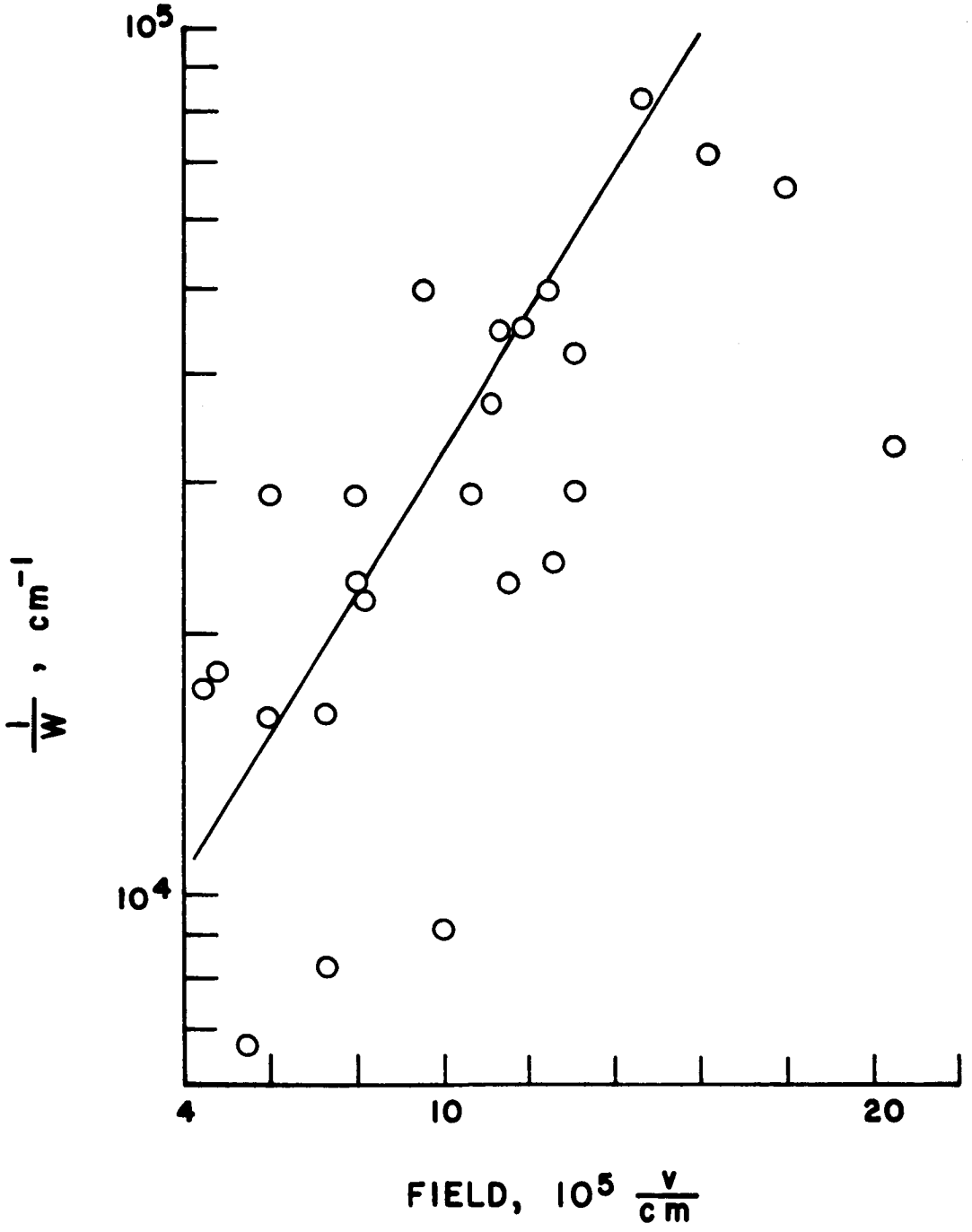

Figure 68. Comparison of data with Franz breakdown theory.

heat loss may be neglected. By defining

$$A = \frac{e\alpha\mu N_v t c^2}{\beta^2 C_v}, \tag{12}$$

equation (11) may be expressed as

$$F_{MAX} = \frac{\beta}{\ln\left[\frac{F_{MAX}^{22/3}}{T_M - T}\right] + \ln A}, \tag{13}$$

The experimental breakdown strength of silicon monoxide capacitors may then be checked for agreement with this theory. One can see that if equation (13) is to be satisfied by the experimental data (which shows that F_{MAX} increases as T decreases) then the quantity

$$\frac{F_{MAX}^{22/3}}{T_M - T}$$

must increase as T increases, i.e., a plot of $F_{MAX}^{22/3}/(T_M - T)$ versus T should exhibit a positive slope. Using the experimental data this plot is made in Fig. 69 for three separate values of T_M which might be expected to cause destruction of the capacitor. The curves have a negative slope and thus it must be concluded that equation (13) does not hold true and the breakdown field is not thermal breakdown initiated by volume field emission.

Intrinsic breakdown-the Frohlich high energy criterion. This theory is also summarized by O'Dwyer[31] and is derived from consideration of the average behavior of a single conduction electron under the influence of a strong electric field. It is assumed that the number of conduction electrons is small and hence electron interactions are negligible. Breakdown results when the electron-lattice interactions generate more energy

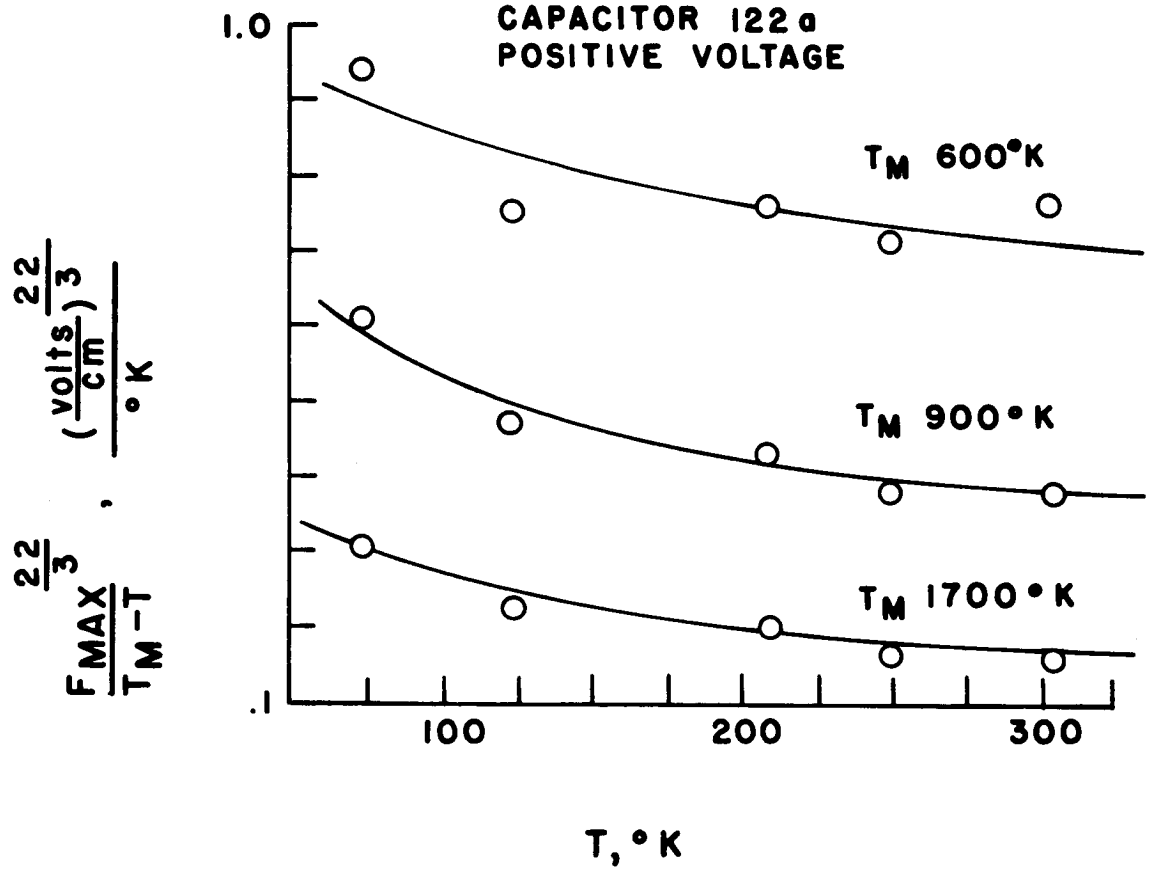

Figure 69. Comparison of a typical set of data with the field emission breakdown theory.

than can be dissipated by the system. Also incorporated within this theory is the idea that electron-lattice collisions lead to conduction electron multiplication which, in turn, leads to destruction of the dielectric. The breakdown strength is found to be related to the temperature through the relation

$$F_{MAX} \propto \left[1 + \frac{2}{e^{A/T} - 1}\right]^{\frac{1}{2}}, \qquad (14)$$

where A is a constant peculiar to the dielectric and T is the ambient temperature.

A comparison of the experimental data for silicon monoxide with this theory requires a plot of equation (14) for various chosen values of A. Such a plot is shown in Fig. 70 for three values of the constant A. The experimental data plot is that of a single capacitor, but is typical. It can be seen that the theoretical curves always have a positive slope whereas the slope of the experimental curve is negative. Thus it is concluded that this intrinsic breakdown theory cannot explain the breakdown of silicon monoxide thin film capacitors.

Intrinsic breakdown in amorphous dielectrics. O'Dwyer[32] presents this theory which was proposed by Frohlich. The model provides for a number of isolated traps located within the energy span ΔV immediately below the conduction band of the dielectric. The lowest traps are an energy distance W above the valence band. The process for transferring energy from the field to the lattice is by phonon emission resulting from electron transitions within the "band", ΔV, of trap levels. The result of this theory is given by

$$V_{MAX} \propto e^{\frac{\Delta V}{2kT}}, \qquad (15)$$

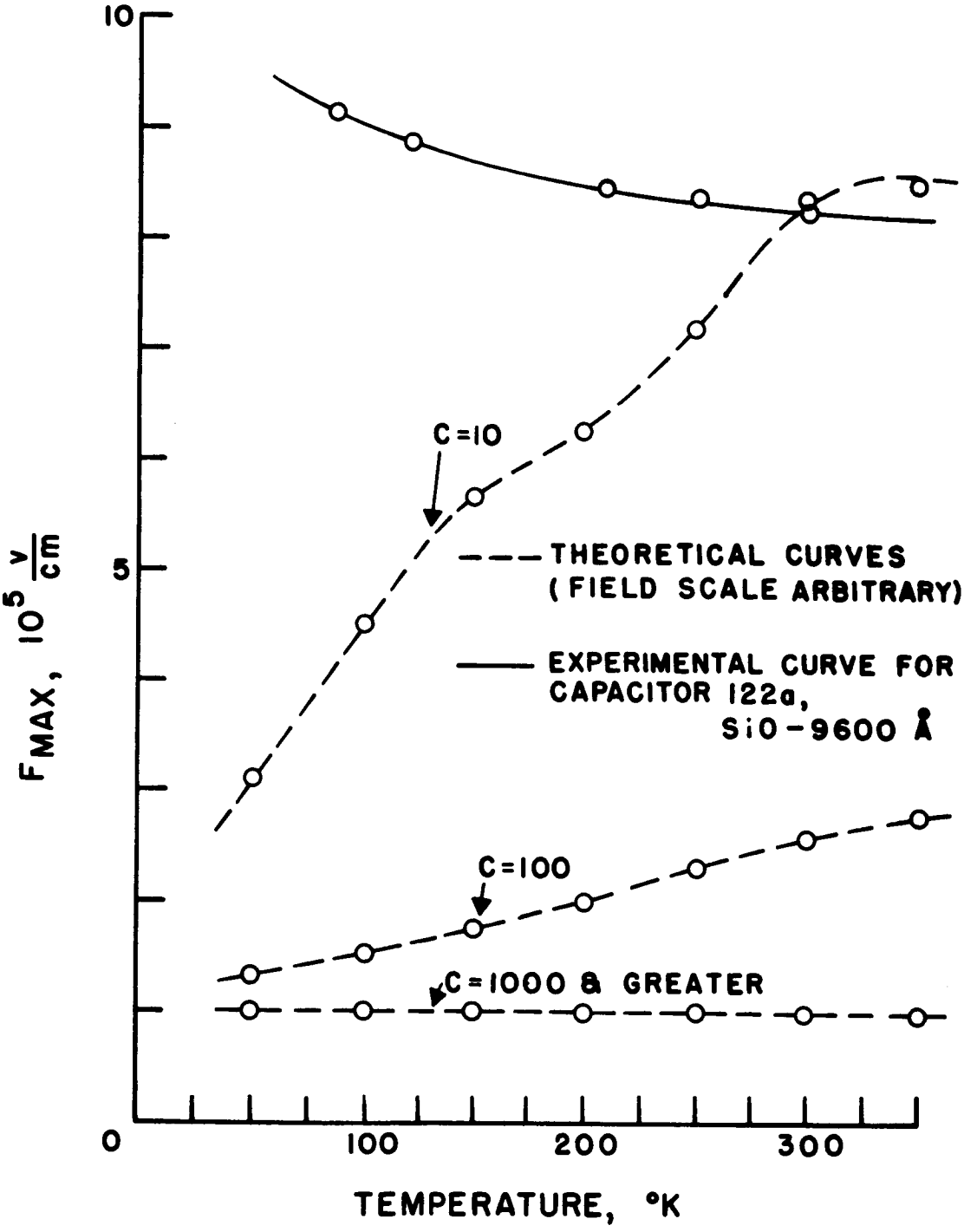

Figure 70. Comparison of a typical set of data with the intrinsic breakdown theory.

where T is again the ambient temperature and k is Boltzmann's constant.

The logarithm of the experimental breakdown voltage for a typical capacitor is plotted against the reciprocal of temperature in Fig. 71. The straight line relationship is fair, but a calculation of the slope gives

$$\Delta V/2k = 62$$

and thus $\Delta V = 0.01$ electron volt. This spread of trapping levels seems to be unreasonably low and is interpreted as an indication that this theory of amorphous silicon monoxide dielectric capacitors. In fact, this value of ΔV is an order of magnitude less than similar values found for NaCl and KCl[33] and the values there were thought to be much too low to represent point defects.

Thermal breakdown. A simple glance at the breakdown strength - temperature data seems to preclude any possibility of the breakdown being classified as thermal. This indication is further substantiated by comparison with the theory of thermal breakdown. An impulse thermal breakdown theory for a linearly increasing field is given by O'Dwyer.[34] The breakdown voltage is expressed as

$$V_{MAX} \propto Te^{\frac{\phi}{2kT}}, \qquad (16)$$

where ϕ is the activation energy for a conductivity of the form

$$\sigma \propto e^{-\phi/kT}. \qquad (17)$$

The conductivity measurements of Budenstein[35] on many of these silicon monoxide capacitors show that ϕ/k is of the order of $5000^{\circ}K$.

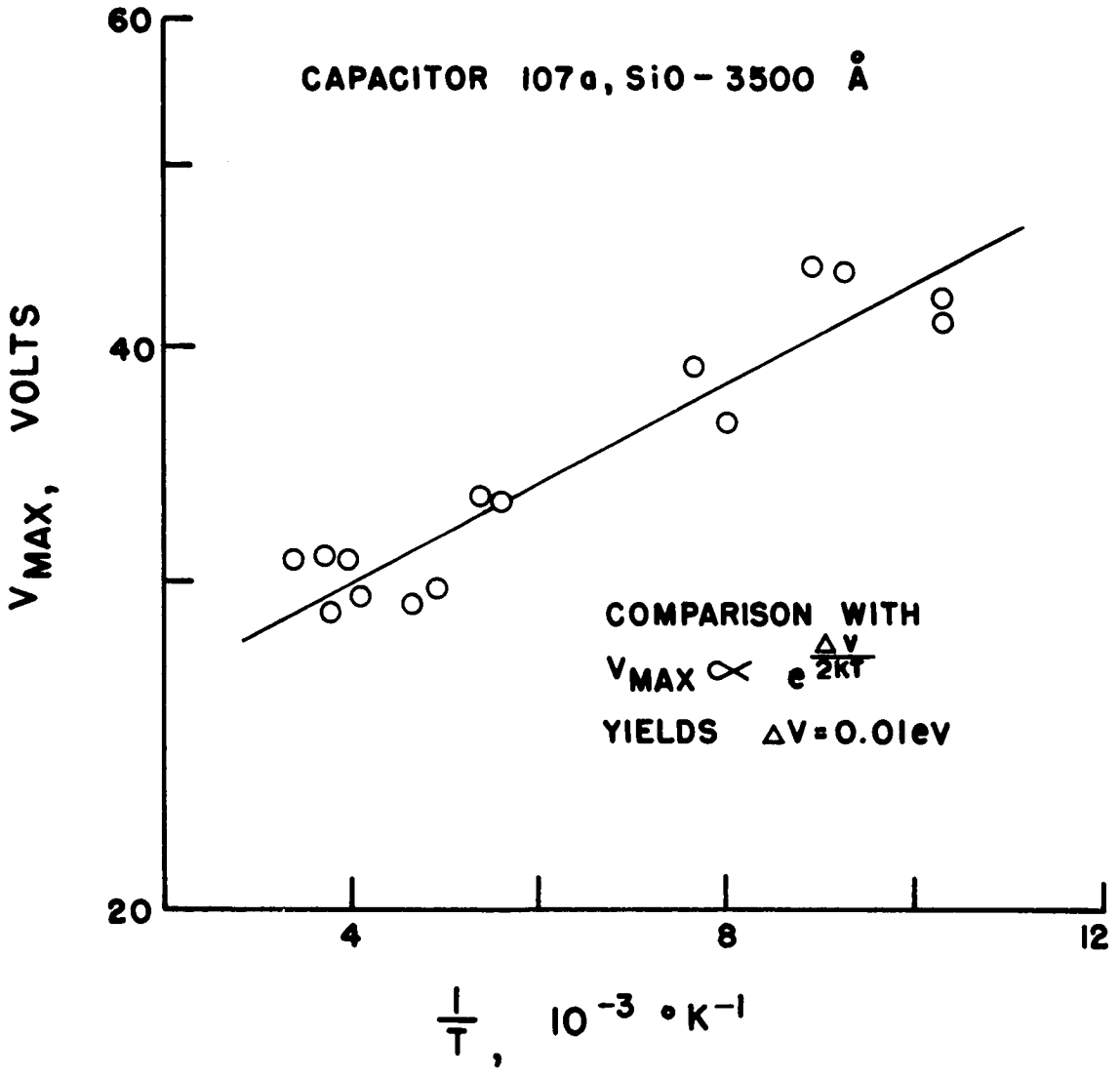

Figure 71. Comparison of a typical set of data with the theory of intrinsic breakdown in amorphous dielectrics.

A semi-logarithmic plot of the experimental data from a typical capacitor in suitable form for comparison with equation (16) is given in Fig. 72. A calculation of the slope of the line representing the best fit yields a value

$$\phi/k = 460^{\circ}K$$

which is more than an order of magnitude below that determined from the conductivity measurements. This result illustrates clearly that the breakdown is not explained as thermal breakdown.

The aspect of electrochemical breakdown.[36] The formation of crystalline silicon during breakdown indicates that the breakdown process is accompanied by important chemical changes. It is tempting to try to connect these with the existence of the fairly well-defined V_{MIN}. Recall that V_{MIN} shows no systematic dependence on dielectric thickness or on temperature. Fig. 73 (a) shows a schematic diagram of an SiO molecule and a nearby Si atom. It is assumed that the latter does not have four tightly bound nearest neighbors. Fig. 73 (b) is a qualitative potential diagram for the bonding electron of silicon atom A. A one-dimensional representation is assumed for simplicity. If, due to the action of the applied field, the electron can acquire an energy ϕ in a distance ΔX, then the oxygen bond will be broken. Further, if this process is to be connected with the limitation of breakdown, it must provide carriers or otherwise modify the system. It is assumed that the silicon-silicon bond is so strong that the system Si-Si is left excited with an electron available for conduction and that highly doped crystalline silicon is created. It is instructive to compute ϕ from V_{MIN} and a plausible value of ΔX. Thus $\phi = eF_{MIN}\Delta X = 10^{6}\ (5 \times 10^{-8})eV = .05eV$. This is an order of magnitude

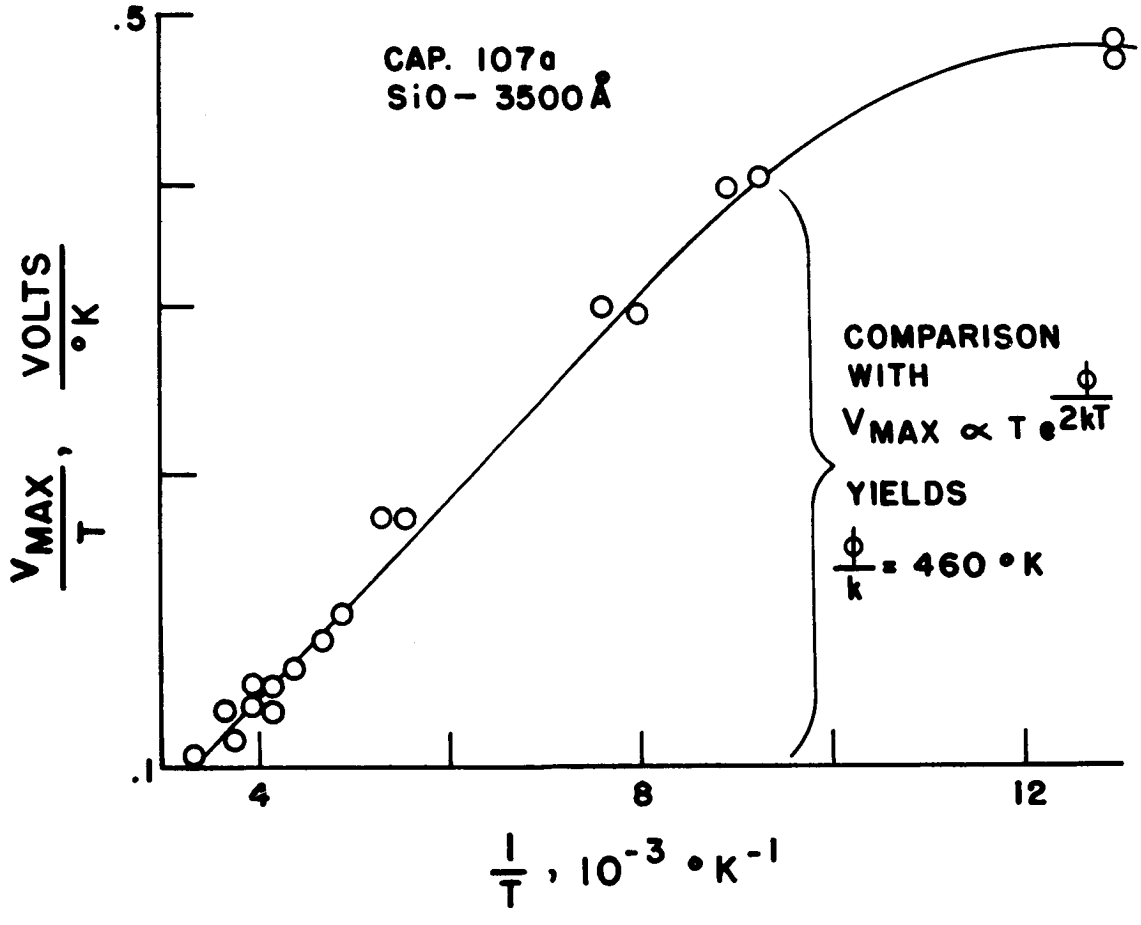

Figure 72. Comparison of a typical set of data with thermal breakdown theory.

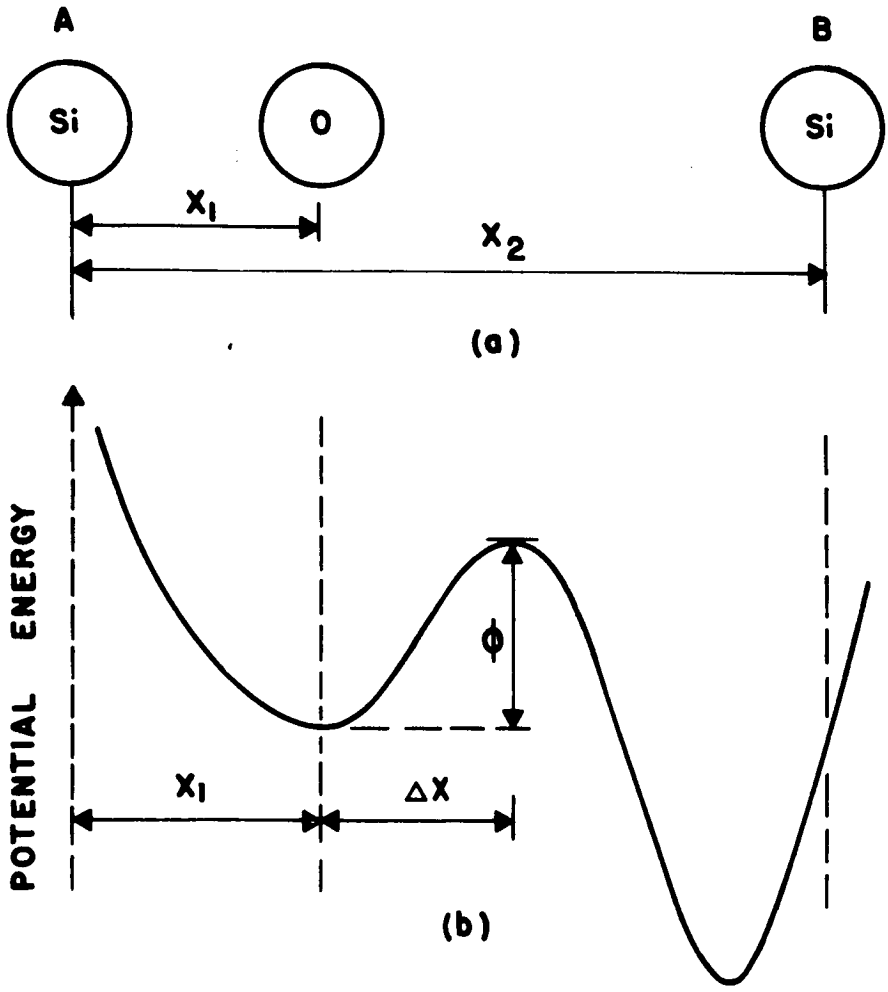

Figure 73. A model for electrochemical breakdown. a) SiO molecule near a loosely bound silicon atom B. b) Schematic potential diagram of electron in silicon atom A showing barrier ϕ that must be crossed if SiO bond is to rupture and the Si-Si bond is to form.

small. It predicts a very strong thermal dependence of V_{MIN} at low temperatures which is not observed.

An alternate process is that of tunneling through the barrier. The exponential field dependence in tunneling makes the probability of a transition strongly field dependent, which can then account for a threshold field. However, experiment shows a threshold voltage V_{MIN} that is constant. Hence it is necessary to assume a non-uniform field distribution, perhaps similar to that in a gaseous discharge where almost the entire voltage drop occurs close to the cathode. Thus the picture that emerges is chemical decomposition and crystal growth initiated by tunneling with a concurrent emission of an electron, the entire process taking place at an active interface of high field intensity.

This discussion also sheds light on V_{MAX}. Prior to breakdown the applied field produces a dc current that is not connected with chemical transformation. (This was demonstrated by maintaining a capacitor under 7 volts and drawing 10 ua for 106 hours. No change occurred either in appearance or in electrical properties. Further, x-ray diffraction showed no diffraction lines except those of the aluminum electrode materials.) The internal field is probably relatively uniform except at local imperfections, such as the dark spots seen in electron microscopy. At some such place the field reaches the value required to cause the SiC bond to exchange for the excited Si-Si bond. The electron produced presumably catalyzes the reaction so that the complete breakdown follows.

Comparison with other parameters

Although the breakdown theories do not incorporate many capacitor parameters it was thought that the possibility of any correlation should be investigated.

Fig. 74 shows that there is little correlation between either F_{MAX} or F_{MIN} and a figure of merit value (leakage resistance at ten volts and room temperature).

As shown in Figs. 75 and 76, there is no correlation of F_{MAX} (or F_{MIN}) with either the temperature dependent fractional change in capacitance or the rate of deposition of the dielectric respectively.

The experimental values of F_{MAX} and F_{MIN} do not seem to depend on which vacuum system the capacitor was fabricated. Thus, it may be concluded that the breakdown strength of a capacitor fabricated without breaking the vacuum does not seem to differ significantly from that of a capacitor fabricated at an order of magnitude higher pressure and with a vacuum-break between each layer. Fig. 77 is a plot of the same data shown in Fig. 53, but with the vacuum systems designated. Budenstein[37] has demonstrated that minor surface irregularities in the substrate have no profound effect on F_{MAX}. Further, there has been no indication that breakdowns are concentrated at dust particles on the substrate.

A number of capacitors of approximately 2000 Å dielectric thickness were fabricated with varied electrode materials and thicknesses in an effort to determine their effect on F_{MIN}. A summary of this work is presented in Table I. During this investigation the lowest values of V_{MIN} were observed. As shown in Table I there were several measurements of V_{MIN} of about five to eight volts. This group of data indicates that the negative value of V_{MIN} is significantly lower than the positive value when aluminum is the top electrode. Such low values of V_{MIN} could not always be duplicated. There seems to be no dependence on electrode thickness, at least for aluminum.

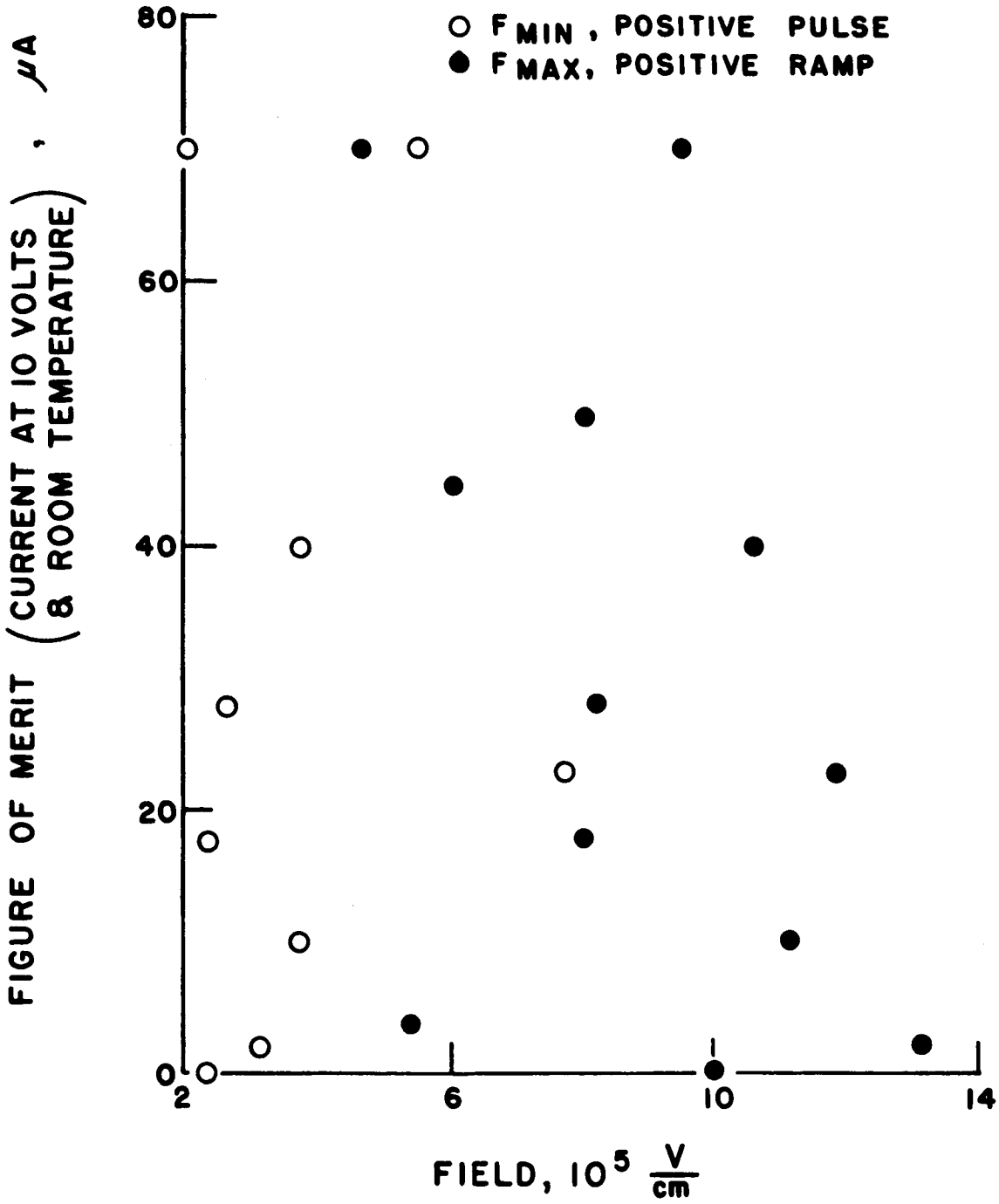

Figure 74. Comparison of experimental F_{MAX} and F_{MIN} with a figure of merit (capacitor's leakage resistance at 10 volts and room temperature.

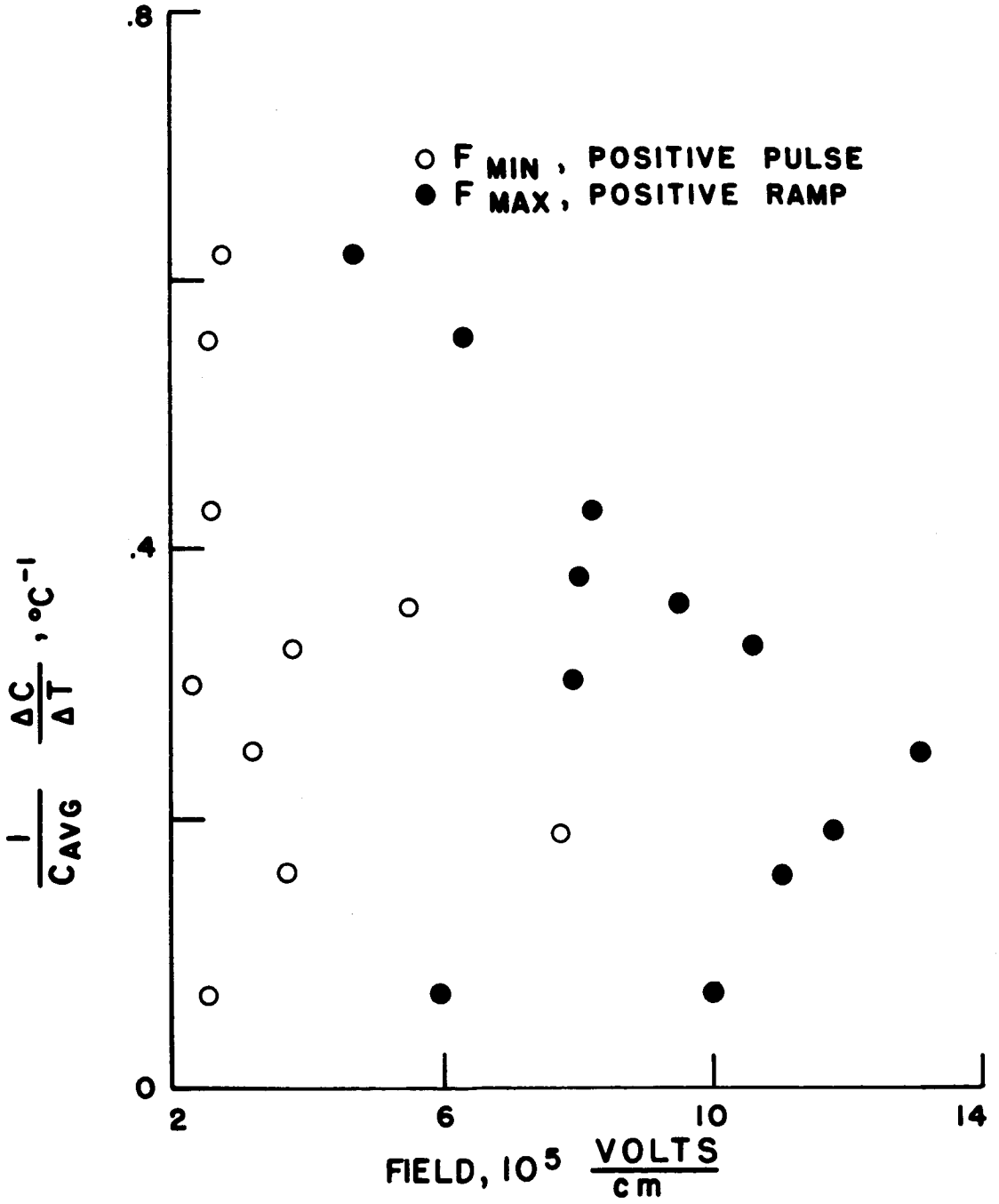

Figure 75. Comparison of F_{MAX} and F_{MIN} with the fractional temperature change in capacitance.

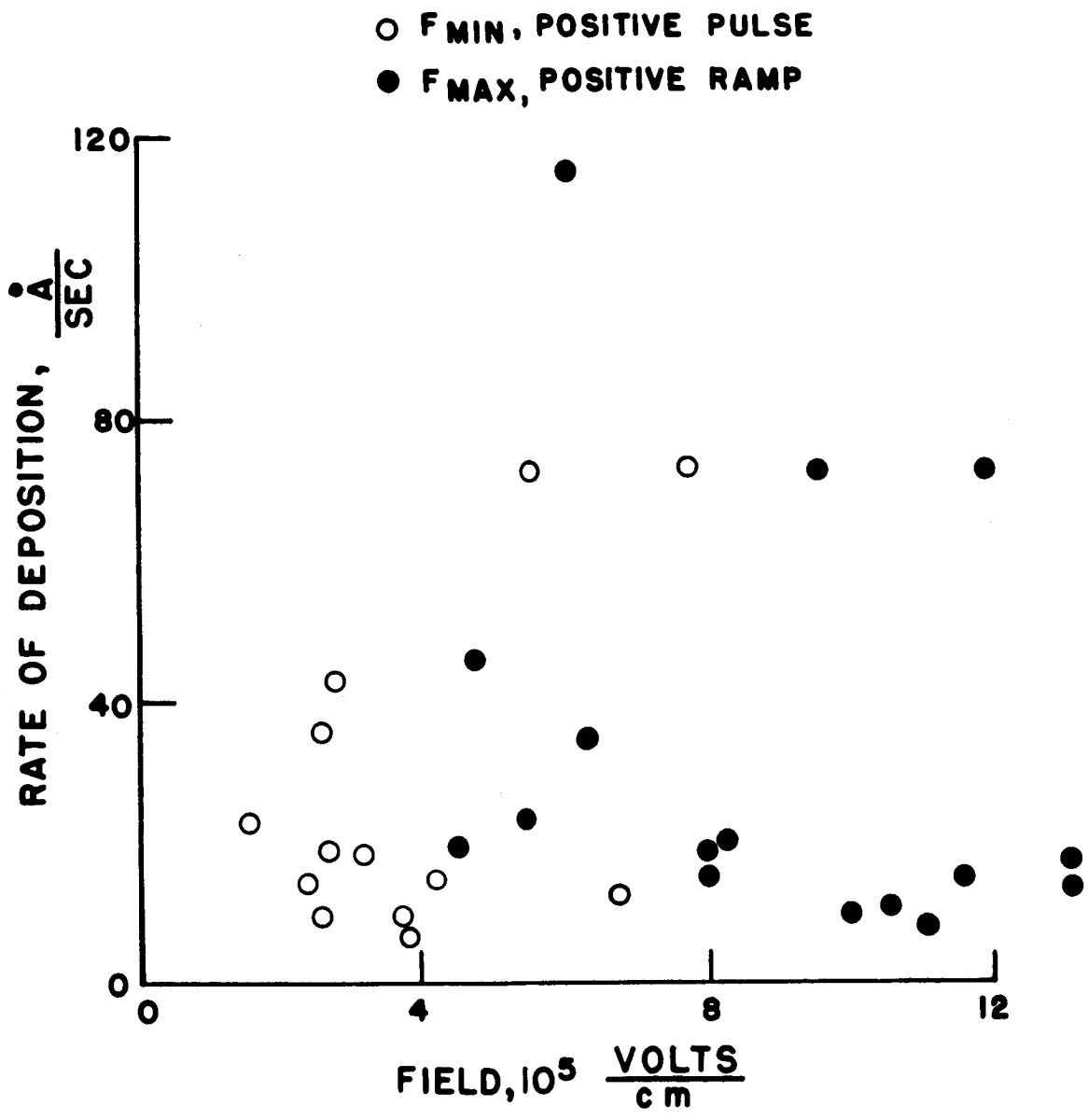

Figure 76. Comparison of F_{MAX} and F_{MIN} with rate of deposition of silicon monoxide.

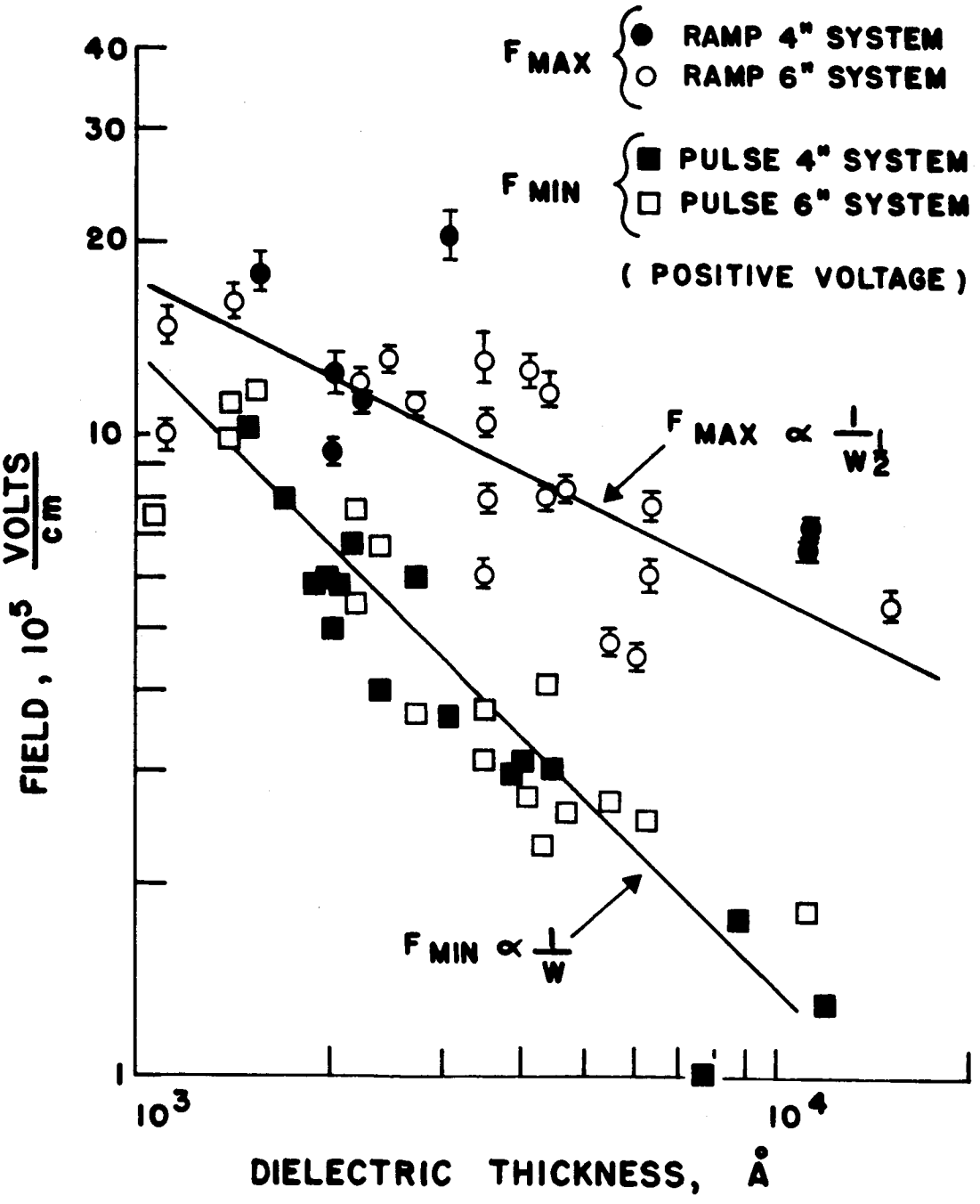

Figure 77. Comparison of F_{MAX} and F_{MIN} for the 4" and 6" vacuum system.

TABLE I

VARIATIONS IN V_{MIN}

Capacitor	SiO Thickness	Cathode Electrode	Electrode* Thickness	Electrode Metal	V_{MIN}
1019-T	2000 Å	top	200 Å	Al	7 volts
		bottom	360 "	Al	12 "
1020-T	2000 "	top	360 "	Al	6 "
		bottom	960 "	Al	11 "
1021-T	2000 "	top	1050 "	Al	5.5 "
		bottom	410 "	Al	12 "
1027-T	2400 "	top	830 "	Al	8 "
		bottom	500 "	Au	11 "
1028-T	1700 "	top	220 "	Au	16 "
		bottom	660 "	Al	15 "
1025-T	2060 "	top	770 "	Ag	12.5 "
		bottom	710 "	Ag	12.5 "

*Electrode measurements by crystal monitor.

C. Rate-of-Breakdown Tests

The randomness both in time and locality of the occurrence of breakdowns attests to its statistical nature. Siddall[38] observed that the number of breakdowns did not increase linearly as a function of time with the application of constant voltage. The increase for lower voltages would typically drop off to zero. For higher voltages the increase was more nearly linear, but apparently never reached a straight line. The capacitor illustrated had a 14,200 Å thick dielectric.

In the early part of this study, similar observations were found for all capacitors subjected to such tests. The dielectric thickness was typically 2500 Å to 3500 Å. These observations prompted an investigation of the rate-of-breakdown as the breakdown strength is exceeded. With a sudden application of an electric field greater than the breakdown strength the rate of breakdown rises to a high value and then drops off with time. Usually several seconds must elapse before the rate drops significantly. The first curve of Fig. 78 is just another way of expressing the same observation made by Siddall. It was further observed that when the voltage was removed and then suddenly reapplied the breakdown rate behaved in the same general fashion, but was somewhat lower. If sufficient time elapsed between the two voltage applications the second application of voltage would generally be more nearly like the first. This time lapse has not been carefully investigated, but seems to be of the order of several hours. Perhaps this indicates the forming of a residual polarization within the dielectric which makes the internal field less than the critical field for breakdown. The validity of such an explanation seems to be verified by the following observation. If the polarity is suddenly reversed the

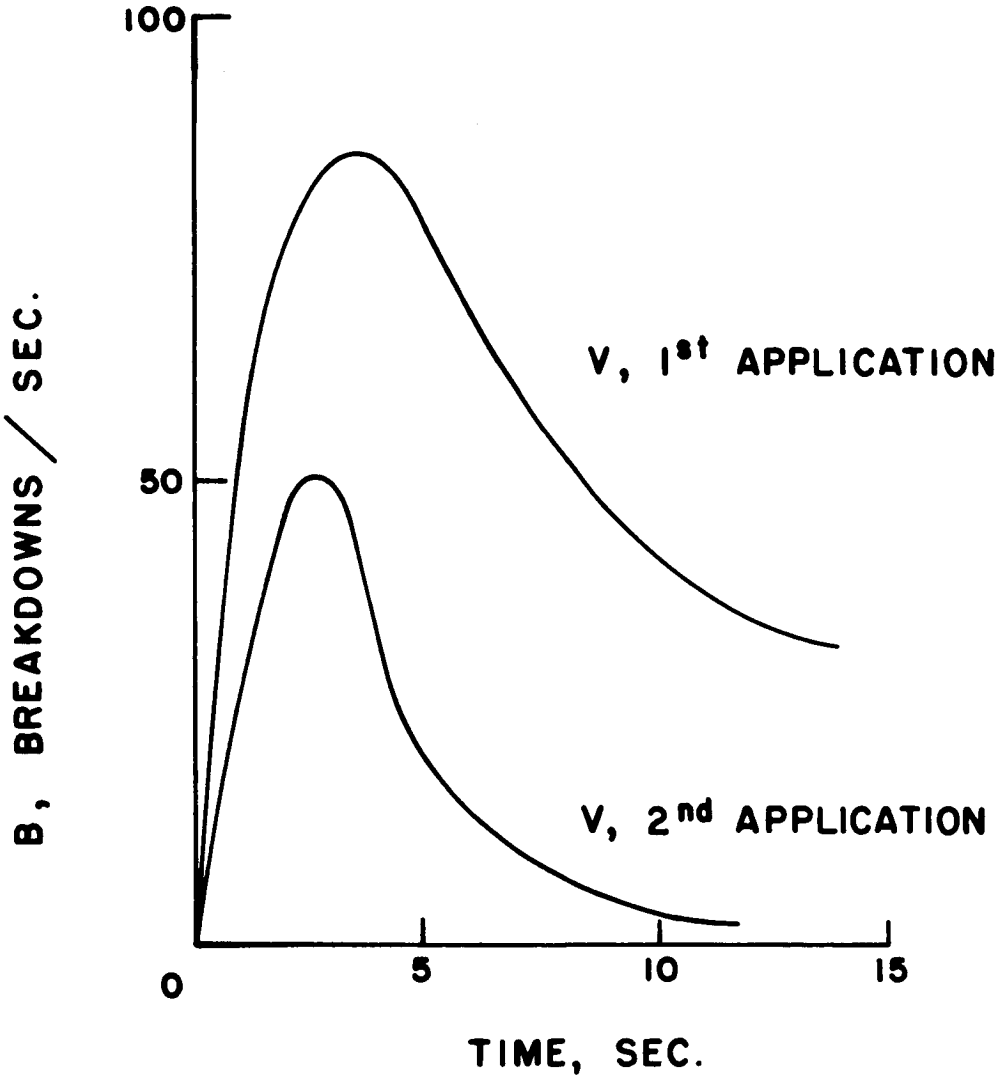

Figure 78. Characteristic breakdown rate as a function of time at a given voltage.

breakdown rate jumps back to a high value and again drops off slowly. Generally the rate goes to a higher value when the polarity is reversed than when the initial voltage is applied.

After making these observations it was felt that the application of a steadily increasing voltage, which swept through and beyond the breakdown strength, would minimize and possibly eliminate long time polarization effects so that a valid determination of breakdown rate versus voltage could be accomplished. A knowledge of the breakdown rate-voltage relationship seems important since this rate should be related to the probability of breakdown occurrence and hence to the statistics of breakdown. Fig. 79 shows that successive applications of a ramp result in a decrease in the breakdown rate. Assuming that the residual polarization explanation given above is correct, this decrease in rate indicates that the polarization effects are retained from one sweep to the next. The generation of a higher rate with polarity reversal as shown in Fig. 79 is in agreement with this explanation. When the natural logarithm of breakdown rate is plotted against voltage, it is observed that the effect of successive ramps is to shift the rate curves along the voltage axis with little change in the slopes unless the number of breakdowns has become so large that the capacitor is nearly open-circuited. Fig. 80 is a semi-logarithmic plot of the data in Fig. 79. Fig. 81 is a similar curve obtained for another capacitor.

If the ramp voltage sufficiently exceeds that corresponding to the breakdown strength, this type of test is the most destructive of all those employed in this study. This fact, coupled with the intent of measuring breakdown rate as the field was varied through the breakdown

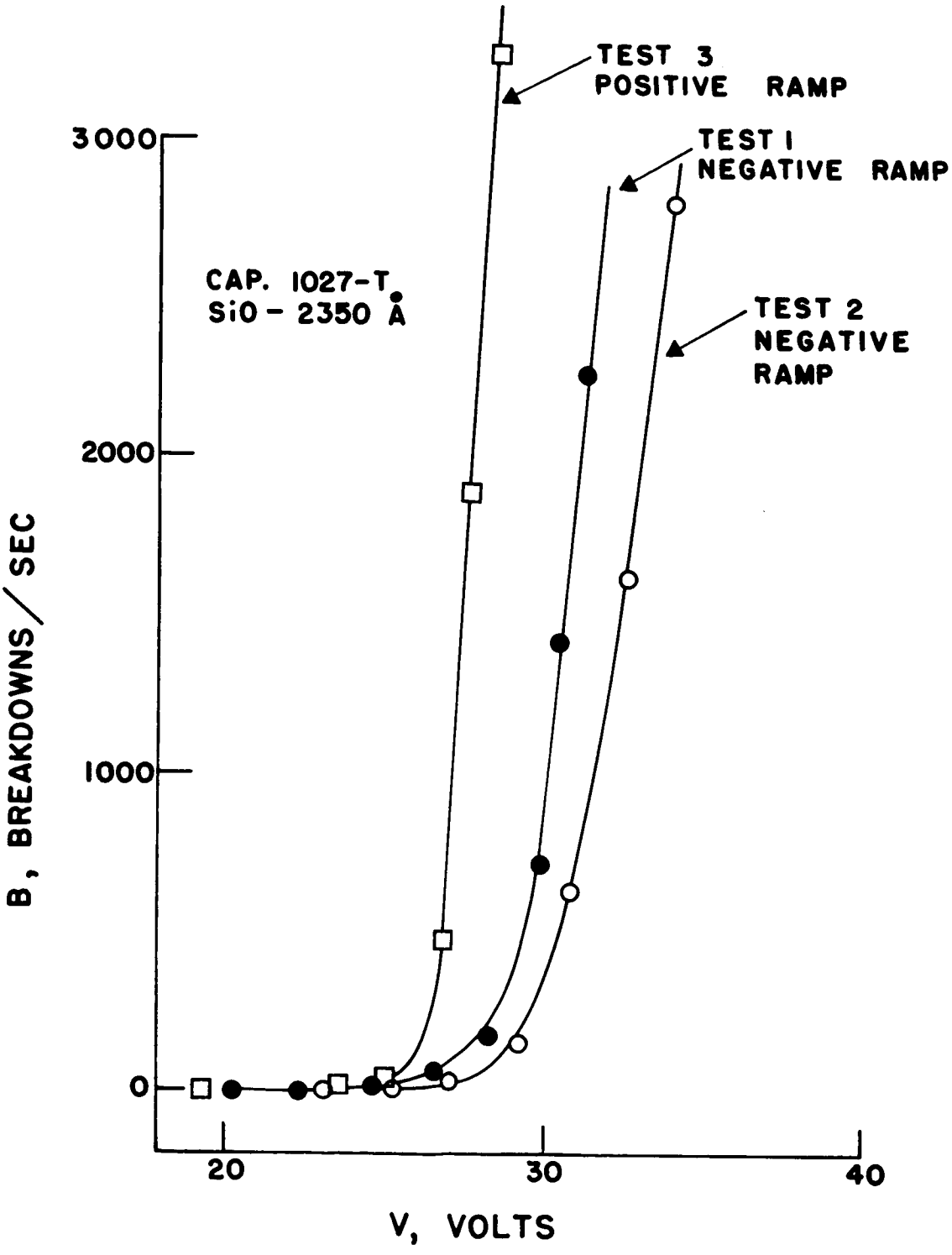

Figure 79. Effect of consecutive ramp voltages.

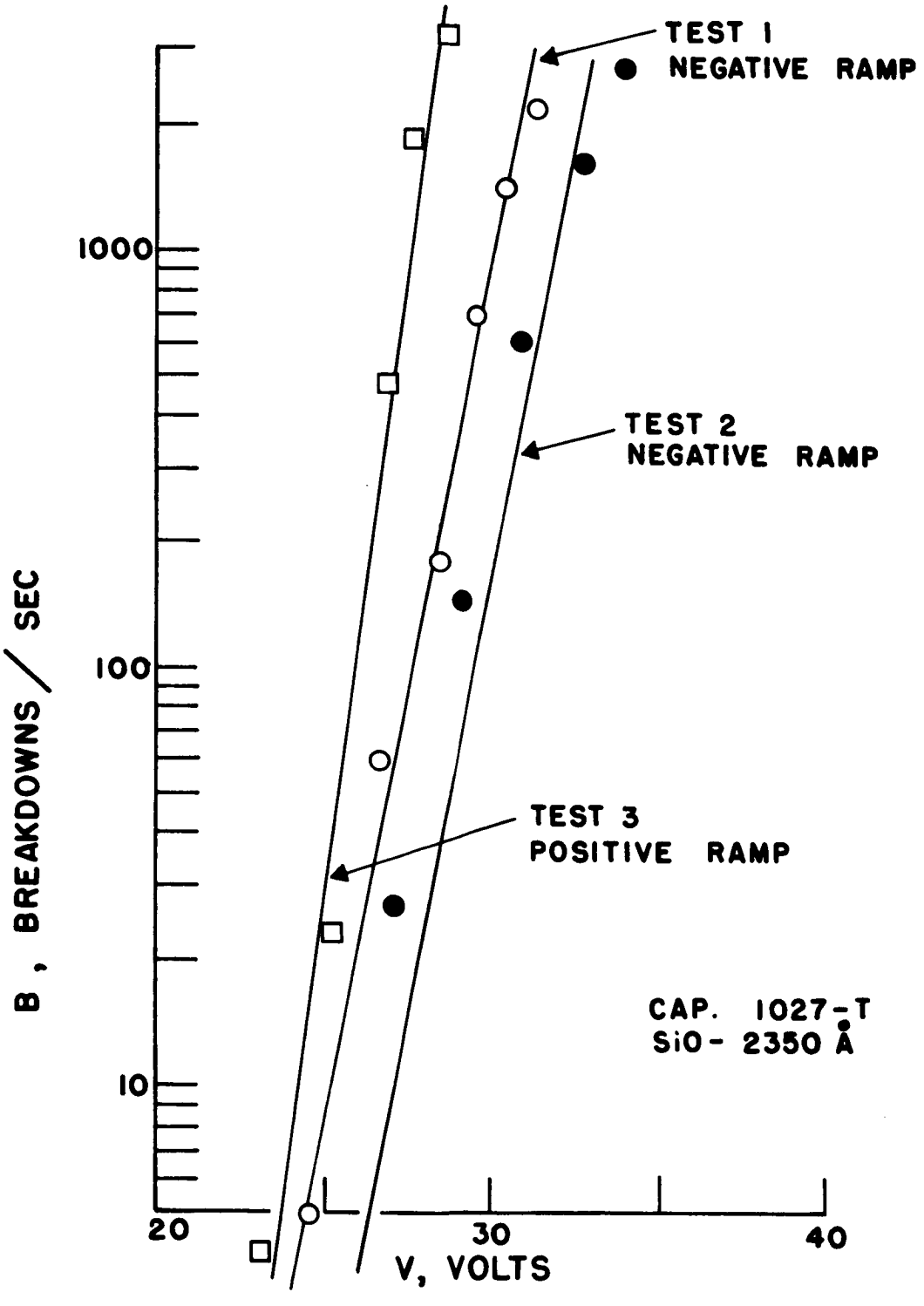

Figure 80. Breakdown rate-voltage relationship for capacitor 1027-T.

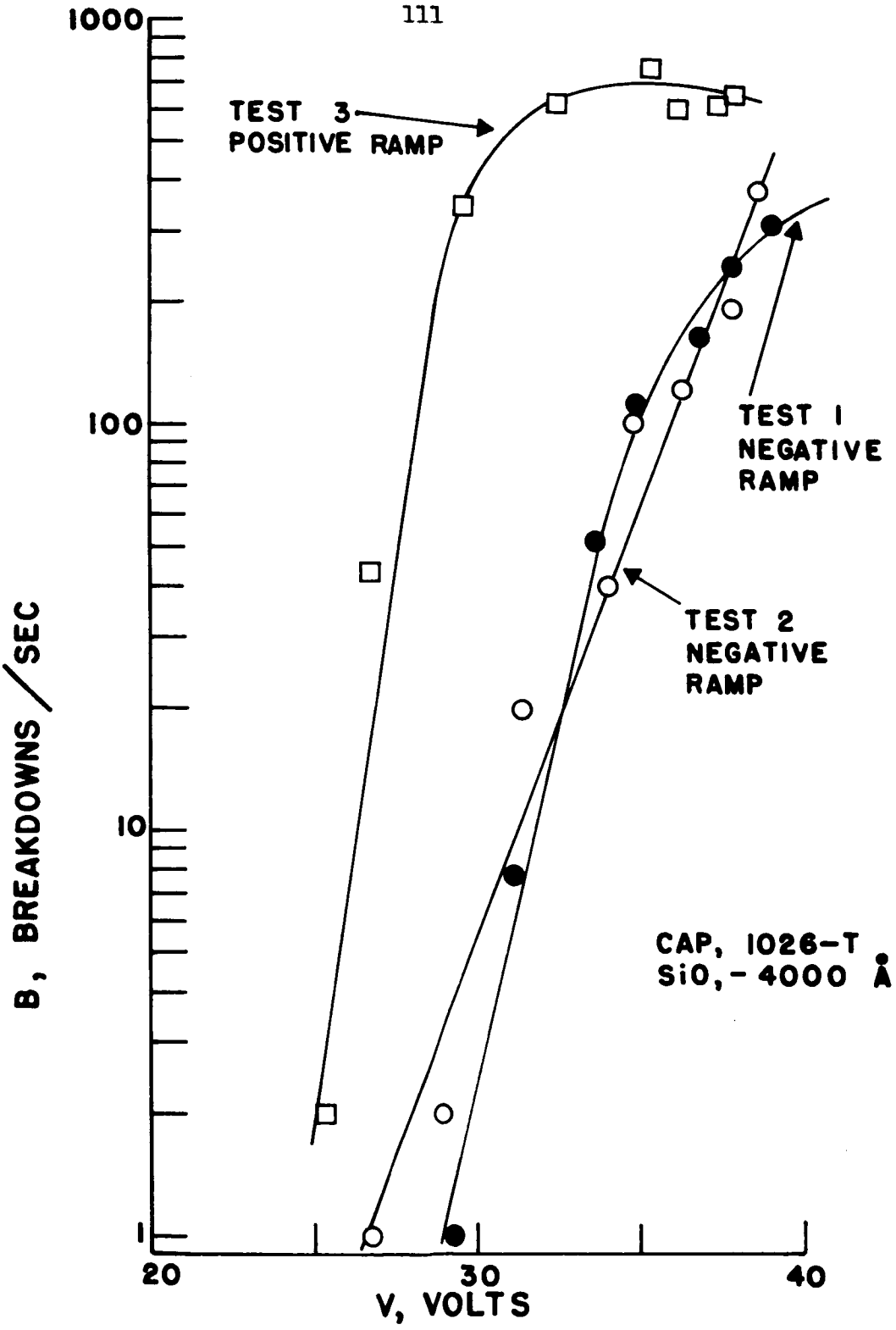

Figure 81. Breakdown rate - voltage relationship for capacitor 1026-T.

strength value, led to the use of ramps which did not greatly exceed the breakdown strength. The polarization effects then made it necessary to use higher and higher ramps while testing a particular capacitor. Figs. 82 and 83 are typical curves which were obtained in this manner. The higher ramp may be expected to yield a higher rate since it would sweep through a greater voltage range in a given time interval. The observed effect of a slightly higher ramp voltage is to shift the breakdown rate curves along the voltage axis.

Since the breakdown strength data more nearly align with the theory of electron ionization avalanche than any other theory, it seems fitting to consider the rate data in terms of that theory. In the theory given by Forlani and Minnaja, the current density which eventually reaches a value sufficient to cause breakdown is a function of tunnel-emission from the cathode into the dielectric. The current I at the cathode may be expressed

$$I \propto F^2 e^{-c/F}, \tag{18}$$

where F is the instantaneous field and c is a constant. It is of interest to compare the rate of breakdown data with the relationship

$$B \propto F^2 e^{-c/F}, \tag{19}$$

where B is the rate of breakdown. Figs. 84 through 87, semi-logarithmic plots of $\ln (B/F^2)$ versus F, show that, in some cases, the fit is very good. In cases where the breakdown voltage is somewhat higher the curves tend toward lower values of B than equation (19) predicts. In some cases this is due to the capacitor beginning to open-circuit. In others the explanation is not clear. Perhaps this is further indication of a build-up of residual polarization which is effective in reducing the field within the dielectric or, more specifically, near the cathode. It seems likely

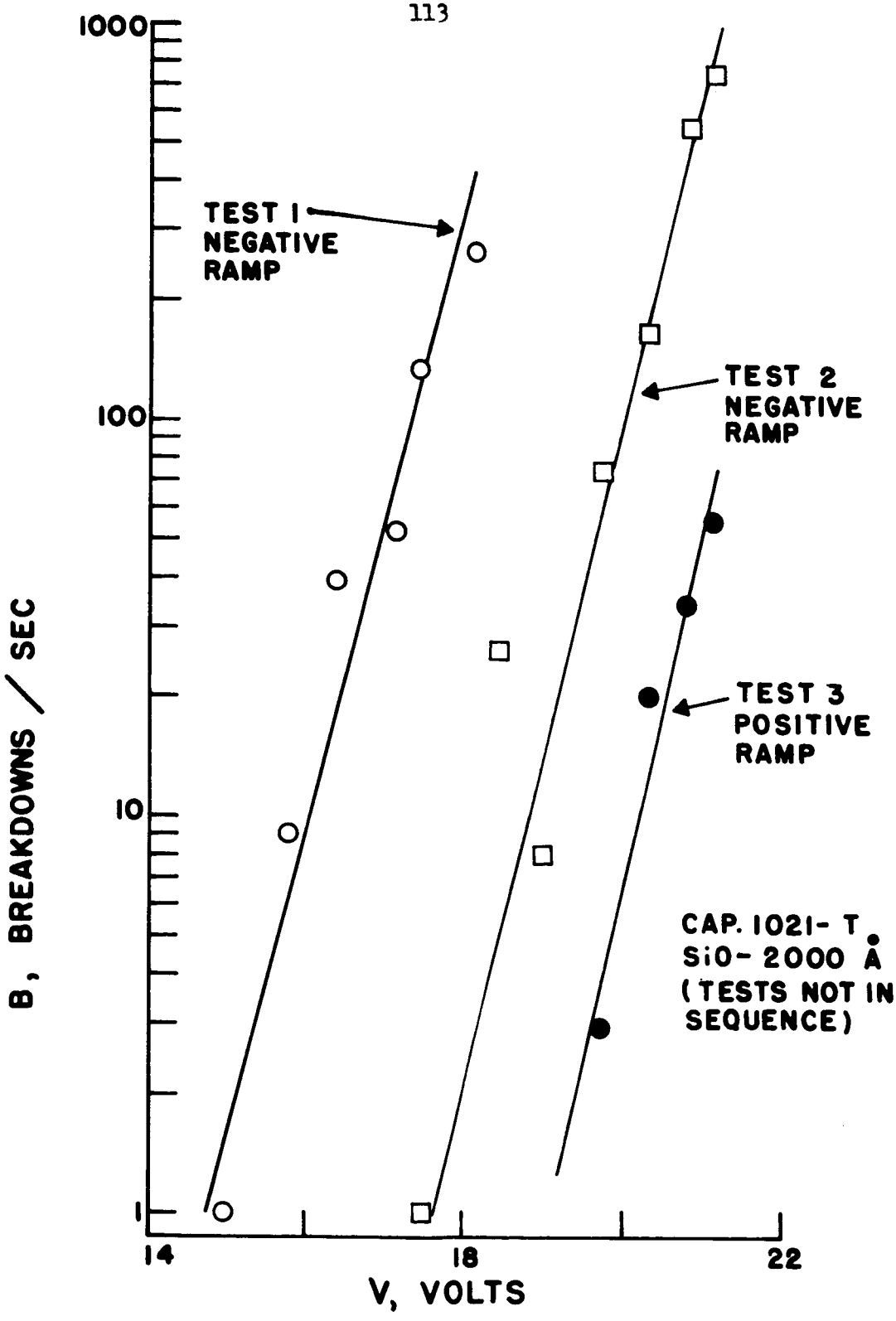

Figure 82. Breakdown rate for capacitor 1021-T.

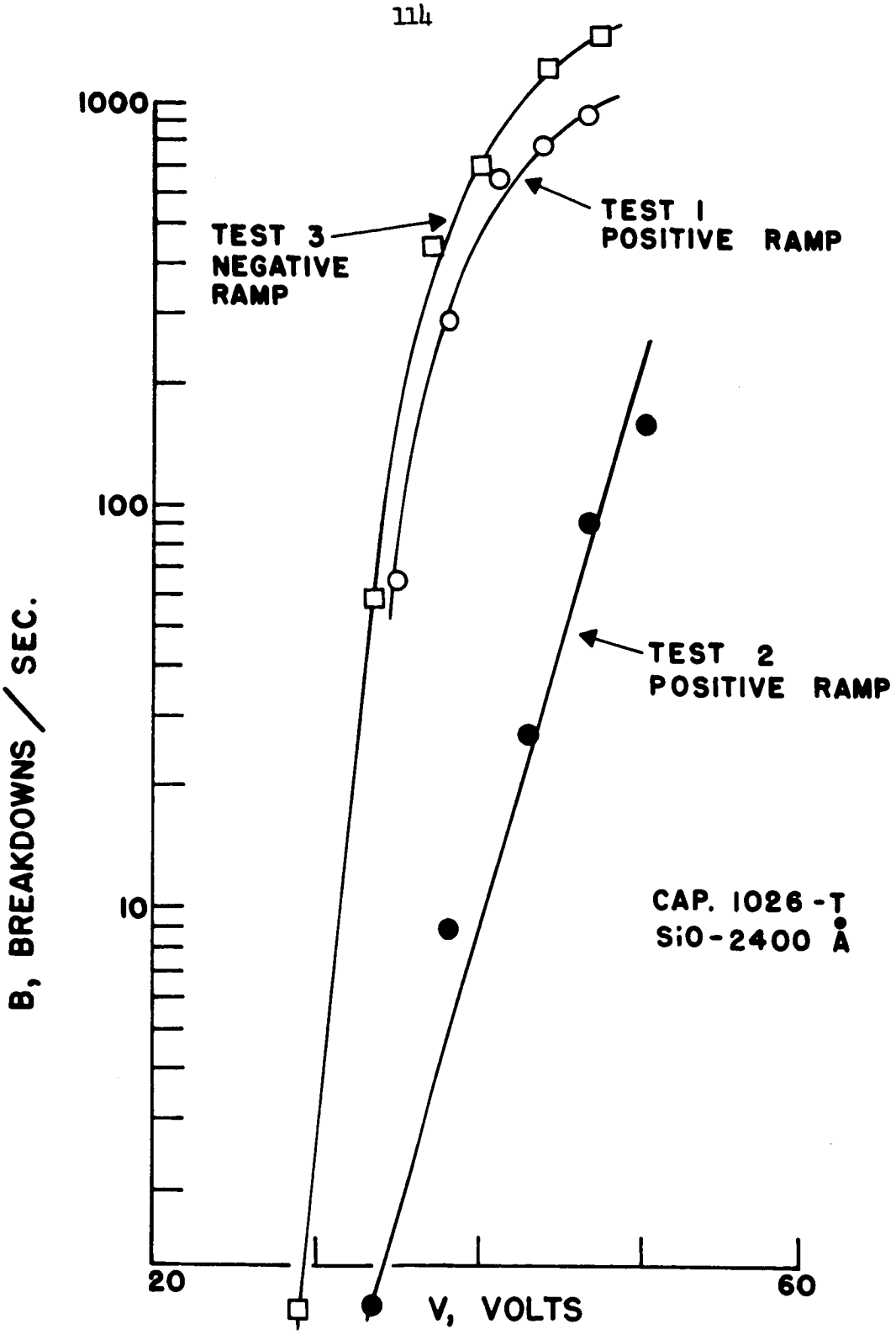

Figure 83. Breakdown rate for capacitor 1026-T.

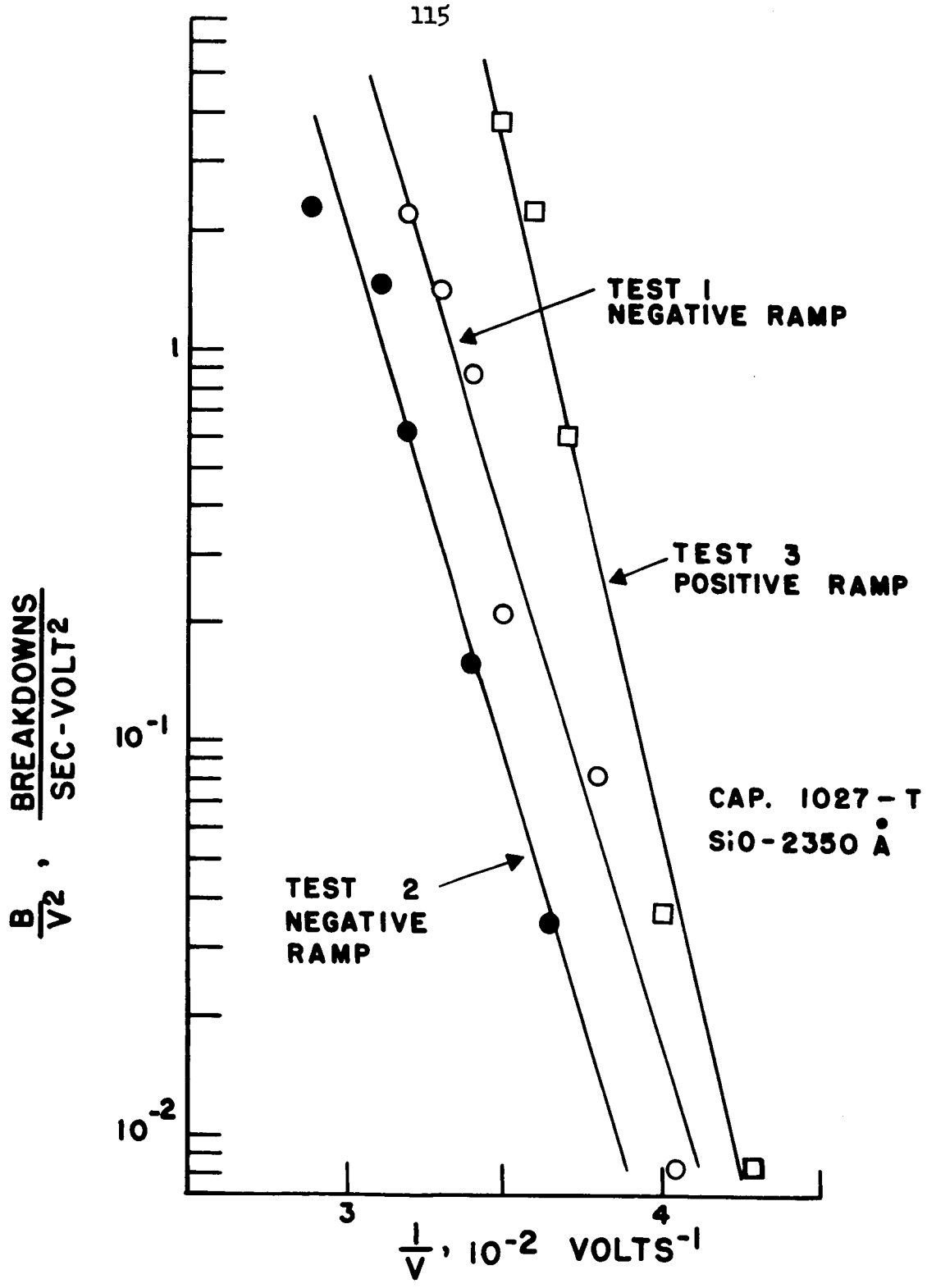

Figure 84. Comparison of breakdown rate with tunnel-emission curve--Capacitor 1027-T.

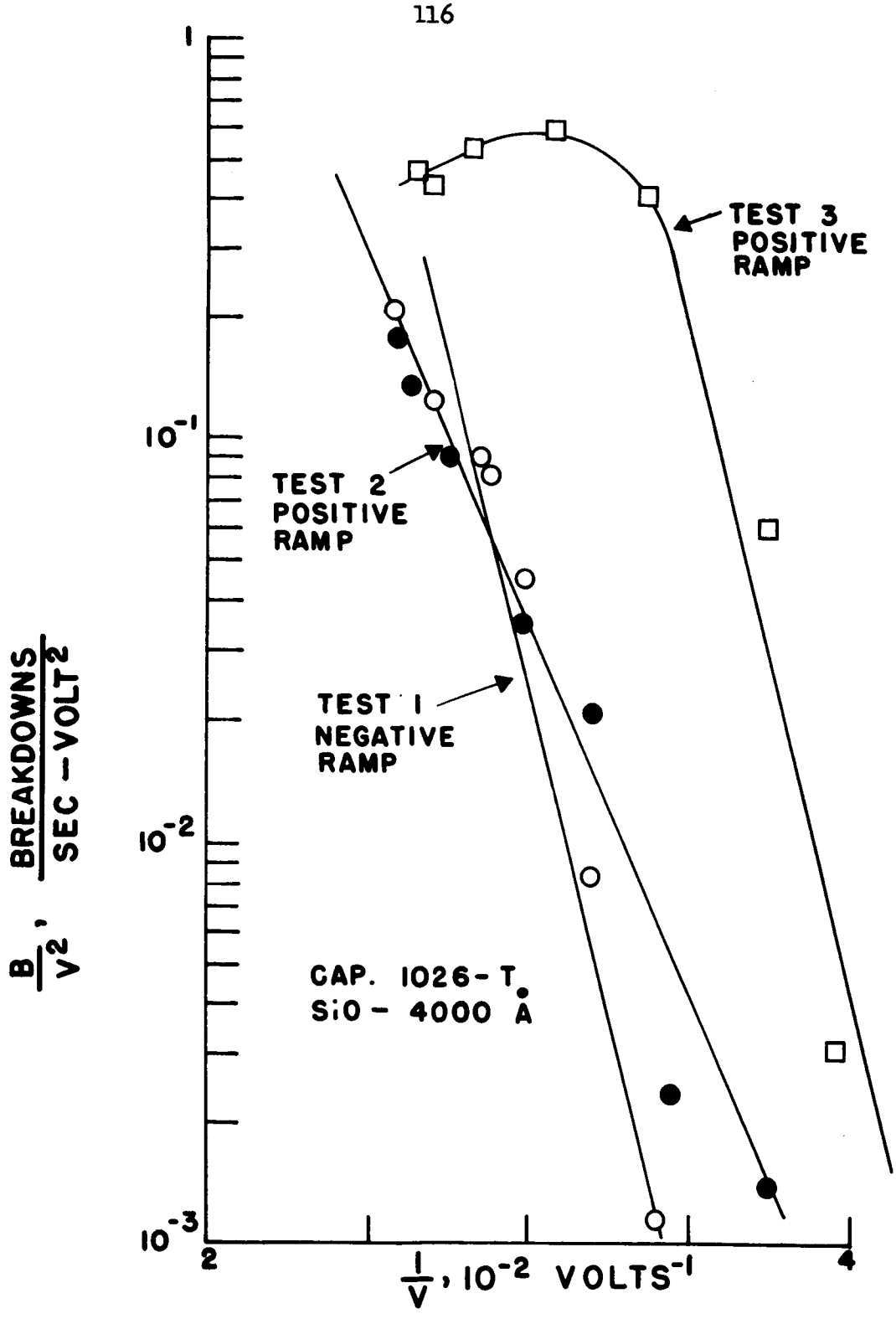

Figure 85. Comparison of breakdown rate with tunnel-emission curve--Capacitor 1026-T.

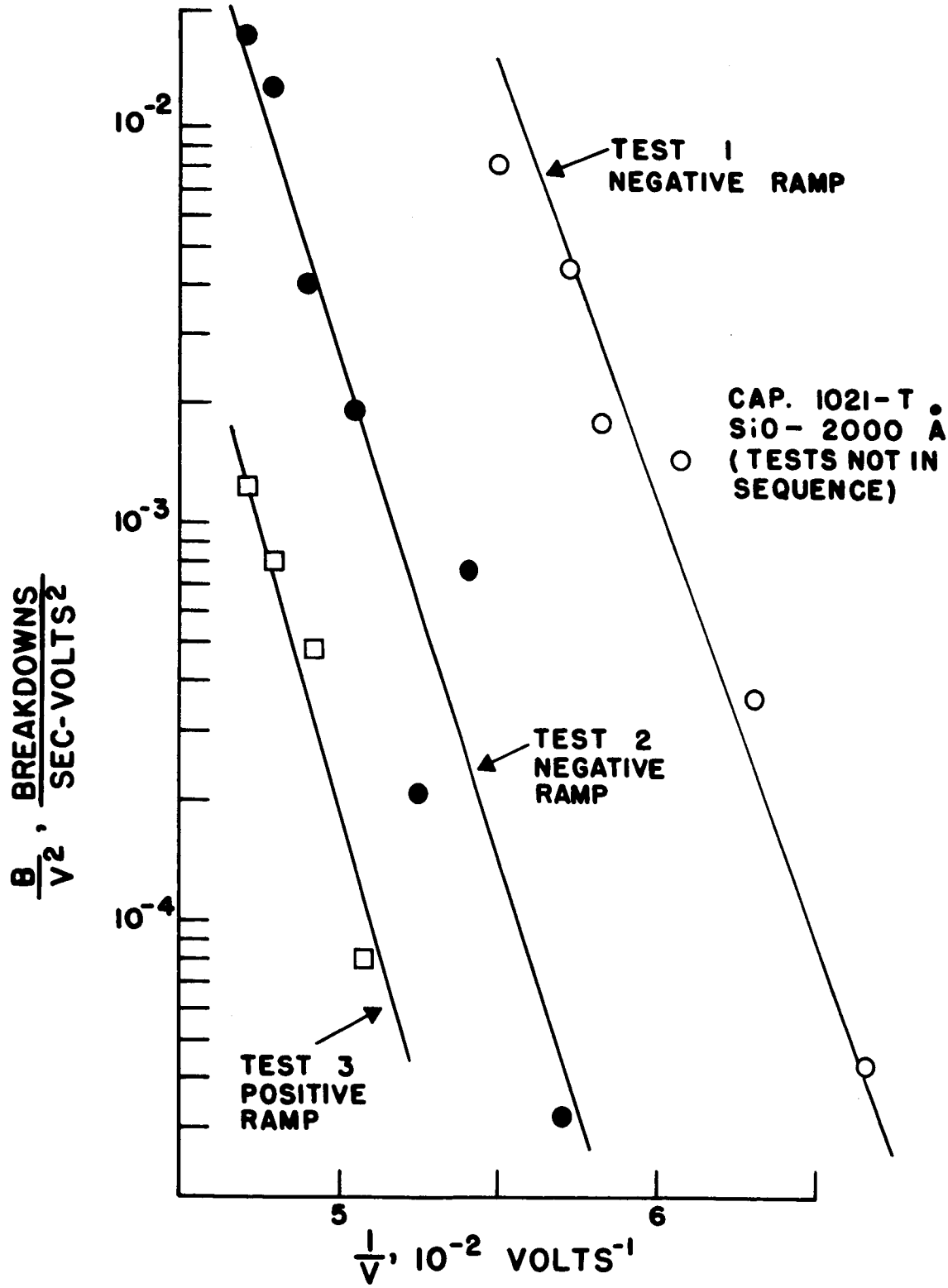

Figure 86. Comparison of breakdown rate data with tunnel-emission curve--Capacitor 1021-T.

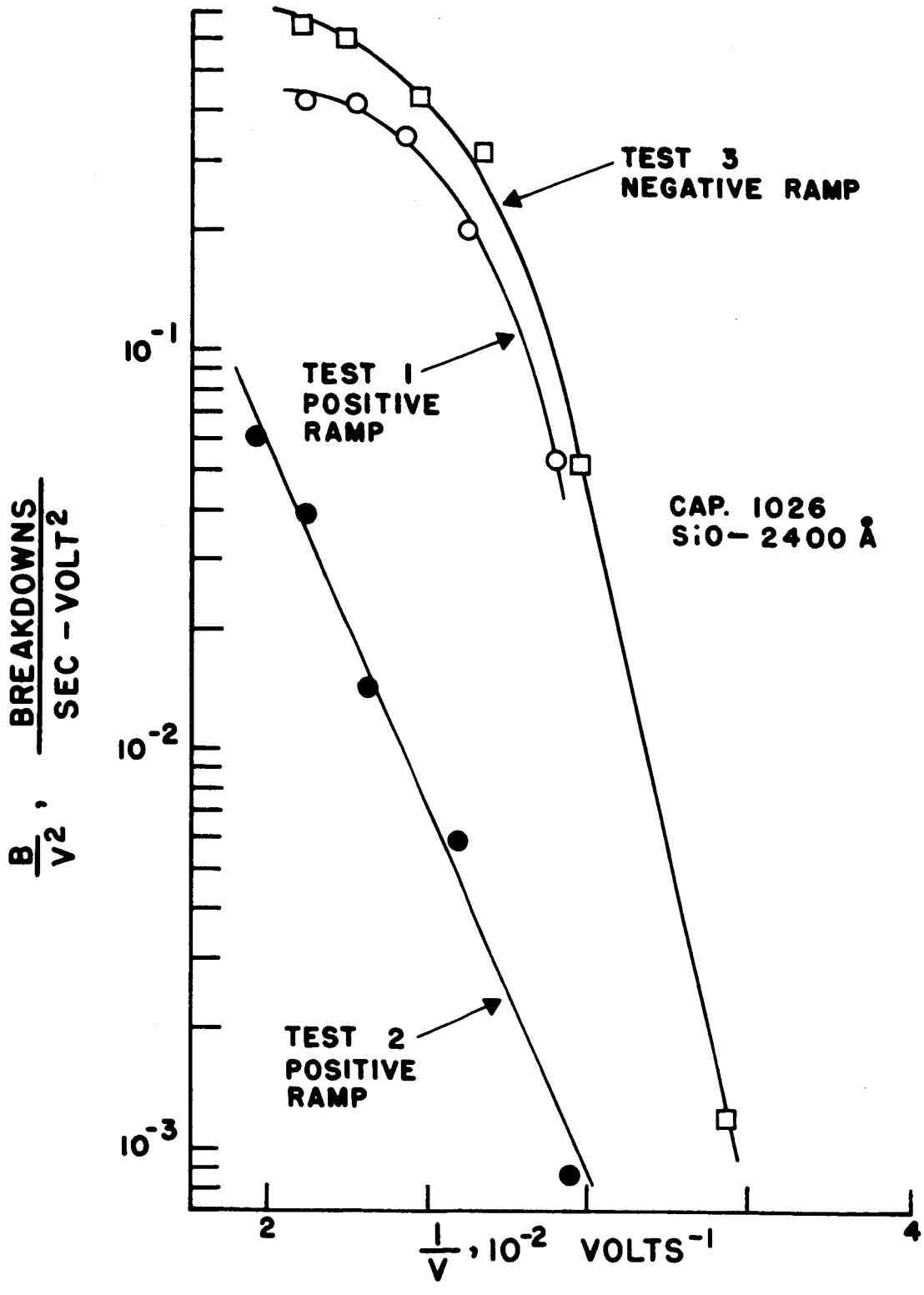

Figure 87. Comparison of breakdown rate data with tunnel-emission curve--Capacitor 102b.

that effects such as space-charge and polarization should be included and that the rate of breakdown is not simply proportional to the tunnel-emission current as given by (19).

D. Miscellaneous Effects

Several phenomena were observed in the course of this investigation, but time did not permit the study of all. In the interest of completeness it seems that these observations should be included here.

Humidity effects

Upon accidentally breathing on a capacitor which was under dc voltage stress it was noticed that the number of breakdowns increased drastically. Further pursuit of this phenomenon showed the same effect was encountered with pulse and ramp voltages as well as dc. Also, it was observed for either polarity. Other tests indicated that the important effect was not actually the humidity, but rather a changing humidity. For instance, while monitoring successive ramp applications during a breakdown strength test on a capacitor in a vacuum chamber, the breakdown strength temporarily decreased when the chamber was evacuated and also when air was let into the system.

When making breakdown rate tests, a higher rate almost always occurs if the test is made immediately after placing the capacitor in a chamber of higher humidity. However, if the capacitor is allowed to remain in the presence of the higher humidity for several minutes, a higher breakdown rate is less likely. Only erratic results were obtained in efforts to measure breakdown strength and breakdown rate as a function of humidity. To circumvent the problem and remove this variable, the capacitors have either been tested in a dessicant or in a vacuum of about 350 microns pressure.

Pulse shape of a breakdown

Using pulse voltages, it is relatively easy to observe the waveform of individual breakdown pulses. A thorough study of these individual waveforms could lead to a better understanding of the various breakdown patterns which are observed. Fig. 88 illustrates four patterns which have been observed and there is no reason to expect there are not others. In (a) the waveform is a linear decrease in voltage to V_{MIN} where the breakdown very smoothly ends and the capacitor begins to charge again. In (b) there is a similar decrease in voltage from initiation of breakdown to A and a region of even slower decrease from A to B. At B the breakdown is over and the capacitor begins to recharge. The details of the section of the pulse from A to B vary somewhat. In (c) a rapid decrease in voltage is terminated by a very irregular pattern before the capacitor breakdown is terminated. The breakdown pulse in (d) has been seen in only a few capacitors, but is believed to result in the long streaky breakdowns which are observed. The time t varies, but is occasionally of the order of milliseconds. This type of pulse gives a clear indication of V_{MIN}.

Spontaneous shorts

Siddall[39] reported the occurrence of spontaneous short circuits which could be removed by discharging a rather large (few microfarads) capacitor through the thin film capacitor. The short circuit regions are destroyed and the leakage resistance of the capacitor increases by many orders of magnitude. This procedure is sometimes called "forming".

Similar shorts have occasionally occurred in the capacitors made in both the four-inch and six-inch vacuum systems. As mentioned in Chapter I above, these may be attributed to highly doped bridges through the

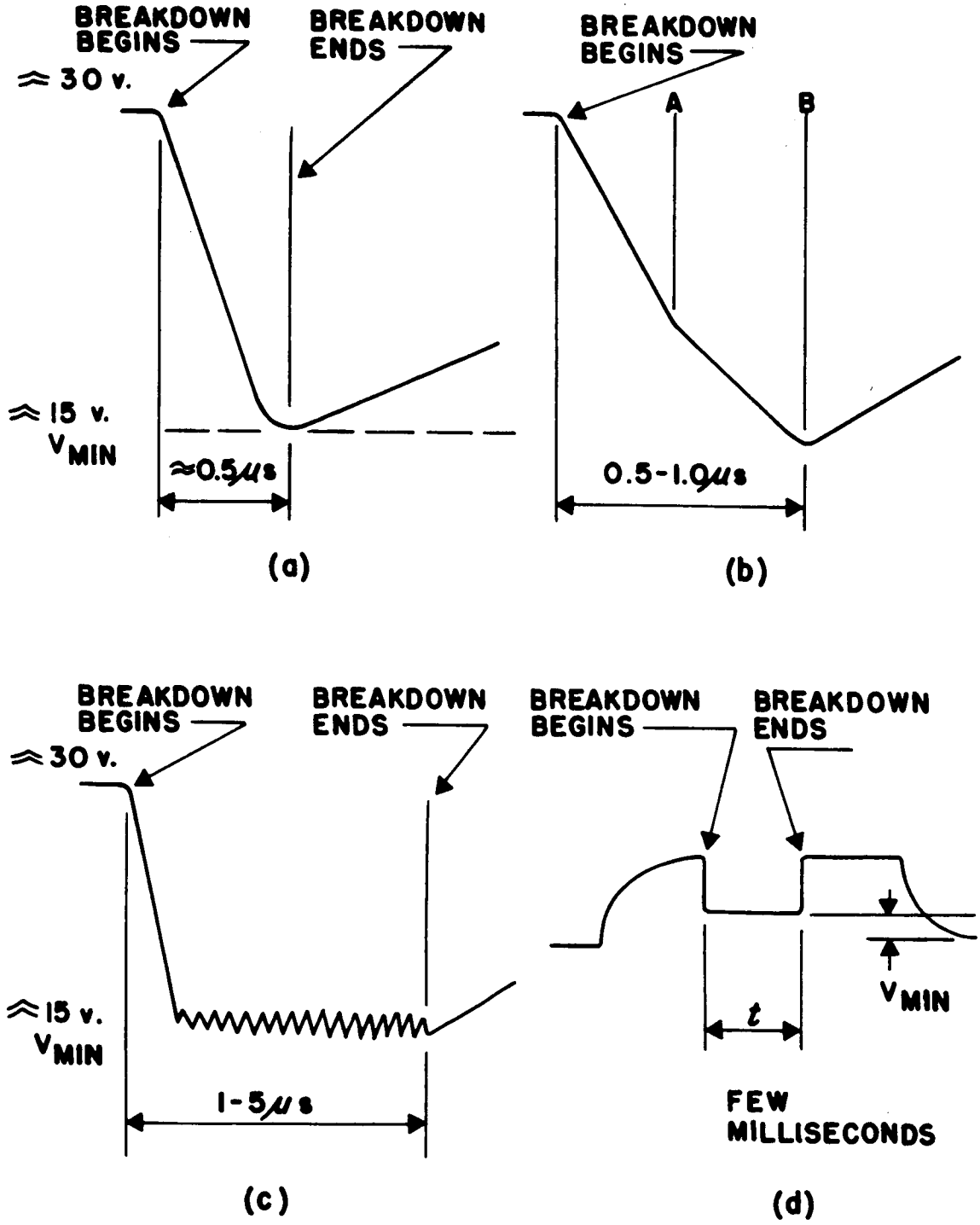

Figure 88. Some characteristic breakdown pulses.

dielectric. It should be noted that the destroyed regions which result by the forming procedure very closely resemble the breakdowns which occur in the absence of spontaneous shorts.

In the few capacitors made using two silver electrodes or two gold electrodes, the problem of spontaneous shorts has been very severe.

Equilibrium condition for a breakdown

There is a noticeable limitation on breakdown which relates to pulse voltages, very fast ramps, and ac voltages. Breakdowns do not occur until the capacitor is essentially in an equilibrium relationship with the applied voltage. In other words, the capacitor does not break down while the capacitor is in the process of charging or discharging even if the voltage greatly exceeds that corresponding to the breakdown strength. This effect is illustrated in Fig. 89. The voltages are shown in a typical relationship. Breakdowns do not occur until the instantaneous capacitor voltage is greater than about ninety per cent of V_p. After a breakdown occurs the voltage must again charge to a value very near V_p before another breakdown will occur. Fig. 43 shows a rather long pulse which is over twice the value of V_{MIN} and hence a large number of breakdowns result. The first one did not occur until the capacitor was completely charged. Fig. 90 illustrates the same phenomenon. The lower curve shows the whole pulse, while the upper curve is a simultaneous magnification of the plateau of the pulse.

In ramp voltage applications if the sweep is sufficiently fast no breakdowns will occur. In one particular capacitor of capacitance 0.043 uf the circuit time constant was 4.5 microseconds. V_{MIN} was twenty volts and V_{MAX} was approximately fifty volts. A ramp voltage of 150 volts

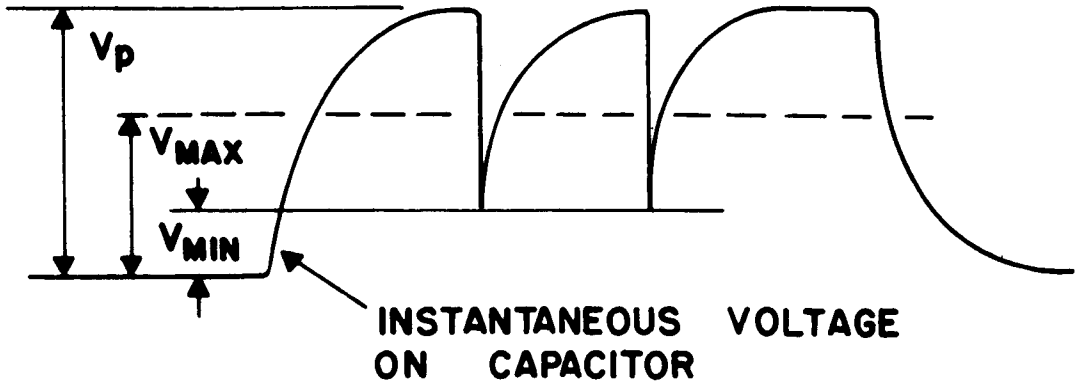

Figure 89. Diagram illustrating the equilibrium condition for a breakdown.

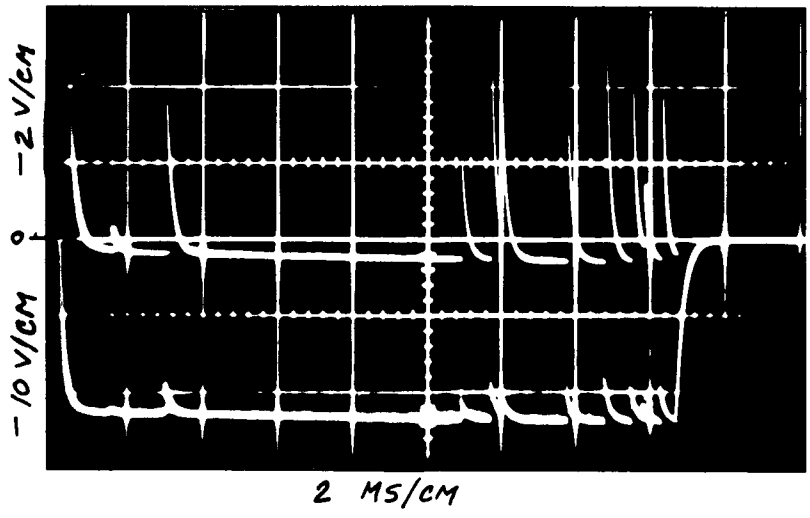

Figure 90. Oscillogram of pulse applied to capacitor #9/30b.

maximum was applied at varying sweep speeds. If the total sweep time was less than two milliseconds no breakdowns were observed. As the sweep time was increased the breakdowns began to appear at lower and lower positions on the ramp. Sweep times of greater than two seconds did not appear to affect the instantaneous voltage of the ramp at which breakdowns first occurred.

This phenomenon is clearly demonstrated by the use of ac voltages for there the breakdowns appear only in the immediate vicinity of the sine wave peaks as shown in Fig. 91. This feature was used by Chaikin and St. John[40] in detecting the breakdown strength of similar capacitors. They observed breakdown pips at the regions of a Lissajous pattern which corresponded to the sine wave peaks.

E. Optical Microscopic Examination of Breakdown

An optical microscopic study was made of the breakdown patterns of large capacitors. This included color photomicrographs of all capacitors, as well as many black and white pictures. A comparison of the size of the breakdowns was then made. The diameter of a breakdown depends upon capacitor thickness and the energy dissipated in the creation of the breakdown. Fig. 92 gives a plot of dielectric thickness versus the typical energy release of a breakdown. If the breakdown occurs at the breakdown field strength the energy release, ΔW, is given by

$$\Delta W = \tfrac{1}{2} C \left(V_{MAX}^{2} - V_{MIN}^{2} \right) \qquad (20)$$

where C is the capacitance. Since the actual voltage at which the measured breakdown occurred is not known, it will be assumed that it occurred at V_{MAX}. The curve in Fig. 92 is rough since, on most capacitors,

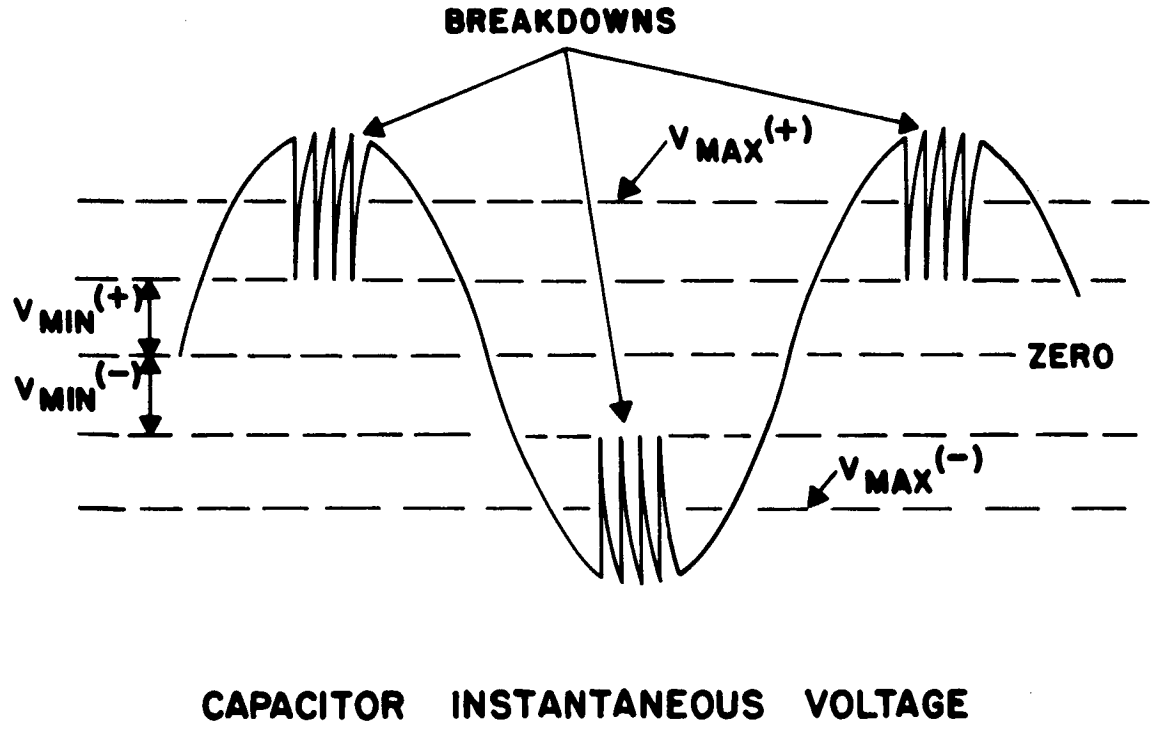

Figure 91. Diagram of breakdowns resulting from a sine wave voltage stress.

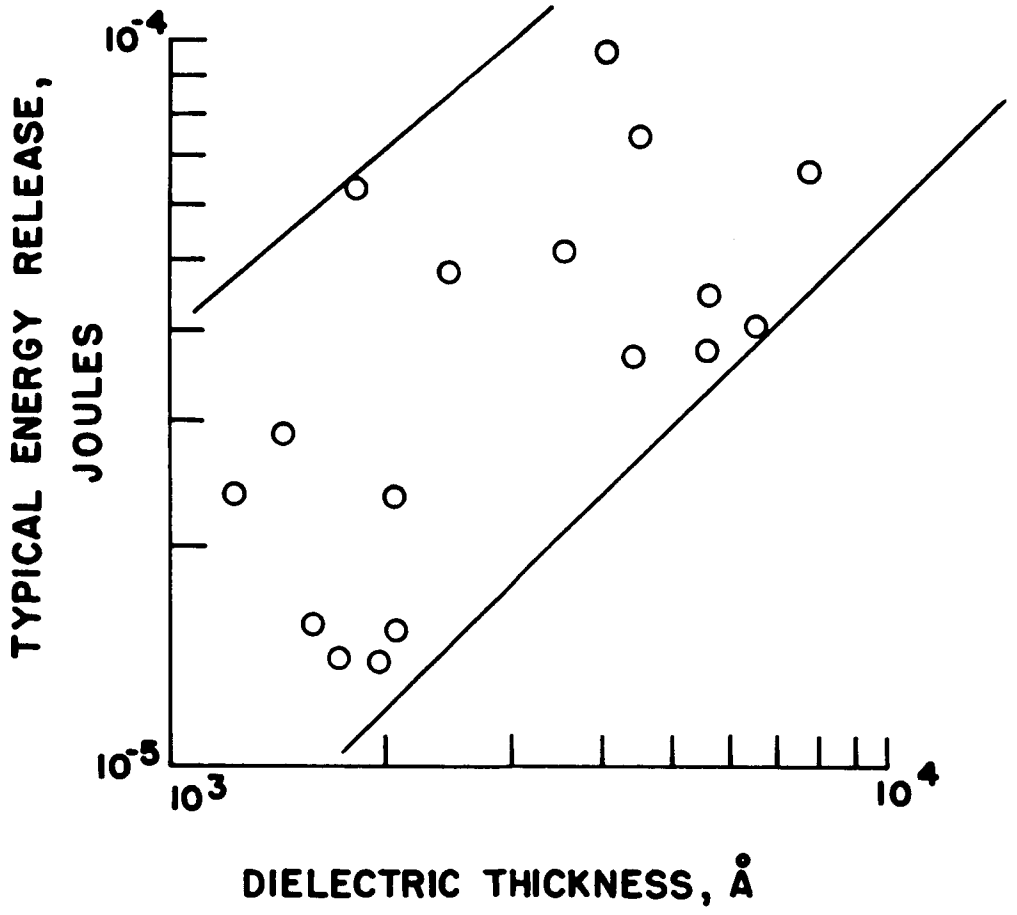

Figure 92. Comparison of the energy released during breakdown with dielectric thickness.

a range of breakdown sizes was found. Fig. 93 illustrates the relationship of the energy released during breakdown and the volume of dielectric destroyed. A representative point in the center of the data gives an energy density of 40,000 joules/cm^3. If electrode destruction and radiative energy are included this value will be reduced slightly. Approximately the same value was observed in connection with the electron microscopy where much smaller capacitors were used.

A number of pictures are included to illustrate the variety of breakdown structures. Except where indicated, both transmitted and reflected light were used to capture a maximum amount of detail.

For ease of discussion three forms of breakdown patterns will be distinguished. Breakdowns which are not actually connected to adjacent breakdowns are called "isolated breakdowns". Fig. 94 is an example of isolated breakdowns. Connected breakdowns, such as those in Fig. 95, will be designated as "breakdown patches". Streaking patterns such as that in Fig. 96 are referred to as "filament damage".

Referring back to Fig. 94, the isolated breakdown is probably the most common type. The details depend strongly on the thicknesses of the various layers of the capacitor and also on the type of electrode material. A general feature is a transparent central region with much structure as shown in Fig. 97. The structure within the transparent region always consists of lumps and balls which range in diameter from about ten microns to much less than one micron. A low reflectance is usually observed at the top of the balls. Because of the high energy release during the breakdown the balls may be strongly bonded to the glass slide. Just outside the transparent region is an area in which

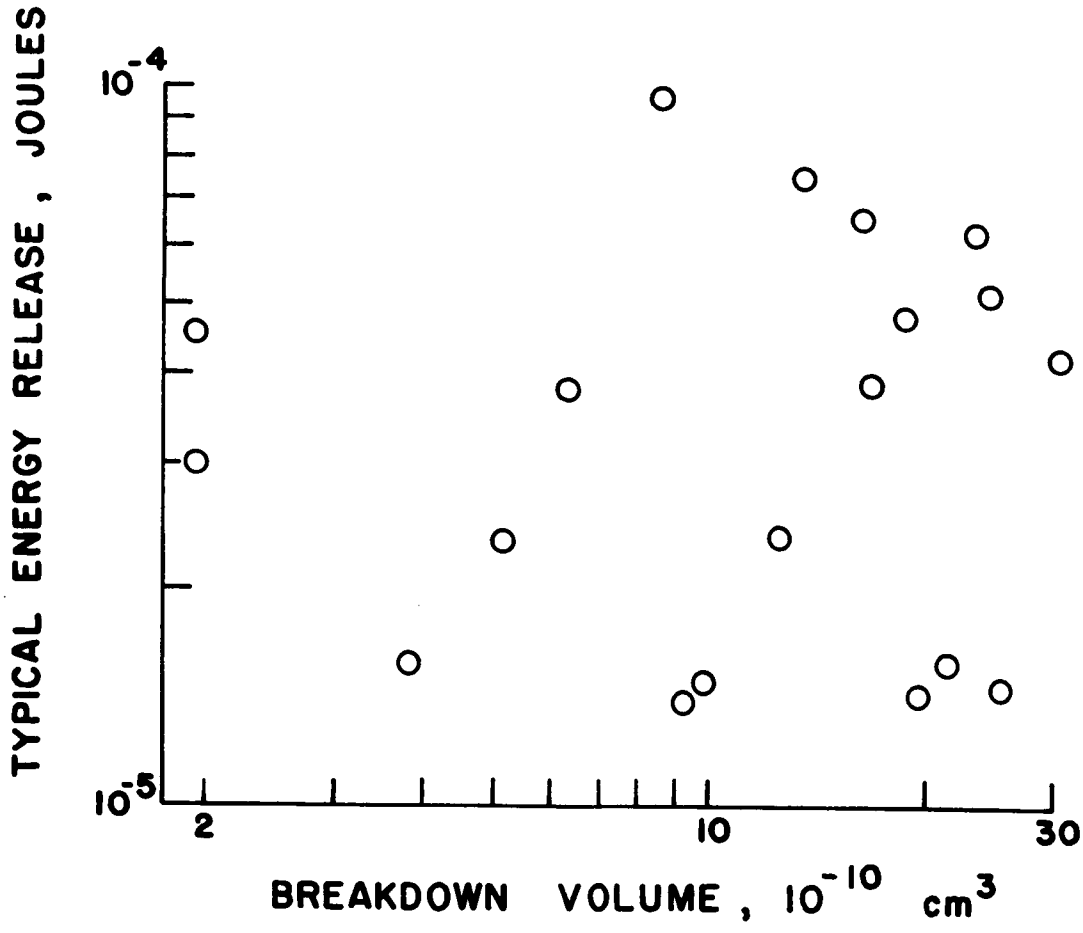

Figure 93. Comparison of the energy release of a breakdown with the destroyed volume of the capacitor.

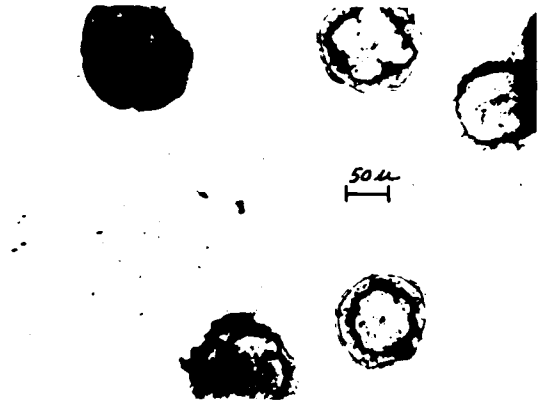

Figure 94. Capacitor 1029-T.

Figure 95. Capacitor 1030-T.

Figure 96. Capacitor 1036-T.

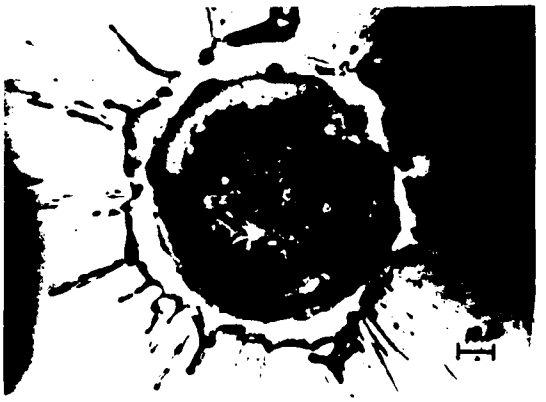

Figure 97. Capacitor 12/29b.

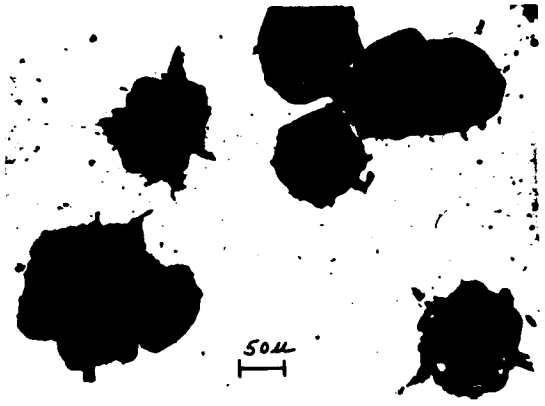

Figure 98. Capacitor 1026-T.

Figure 99. Capacitor 102b.

the dielectric appears unaffected. Except for the region bordering with the transparent area the color is the same as the dielectric. An electron microscopic examination of portions of some of these large capacitors showed the ball and lump structure (same type of structure identified as silicon in the electron microscopy) at the immediate edge of the transparent region. Surrounding the exposed dielectric is a ridge of the upper electrode and radial streaks which indicate that molten pieces are thrown out during the breakdown.

Fig. 98 shows mostly isolated breakdowns. There is no region here with the dielectric uncovered. One of the breakdowns is shown at higher magnification in Fig. 99. Again the ball formation is seen within the central transparent region.

Fig. 100 shows isolated breakdowns, again with transparent centers. The buckling of the capacitors around the breakdown edges seems to indicate compressional stresses within the films. Breakdowns in this particular capacitor generally occurred in patches as shown in Fig. 101. The structure within the transparent area is very evident in this picture. These patches of breakdowns are interpreted as a series of individual breakdowns. The circular structure normally found in the transparent area of isolated breakdowns occurs repeatedly in the transparent area shown in this picture.

Figs. 102, 103, and 104 show, for three different capacitors, both isolated breakdowns and patches. Both electrodes of the capacitor shown in Fig. 103 were silver. The long streaks also resulted from the breakdowns, but are present only in the upper electrode. The streaks probably indicate stresses within the upper electrode. The capacitor of Fig. 104

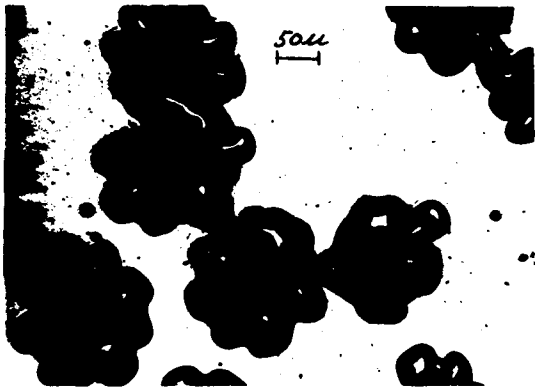

Figure 100. Capacitor 9/12a.

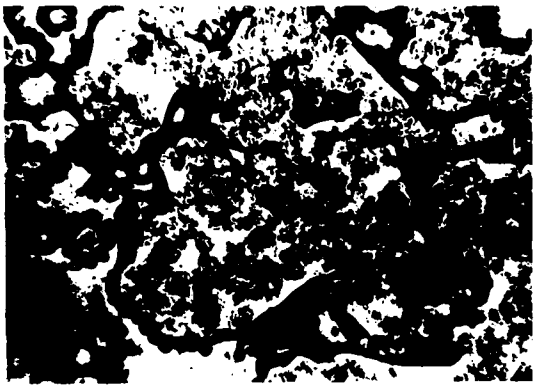

Figure 101. Capacitor 9/12a.

Figure 102. Capacitor 1014-T.

Figure 103. Capacitor 1024-T.

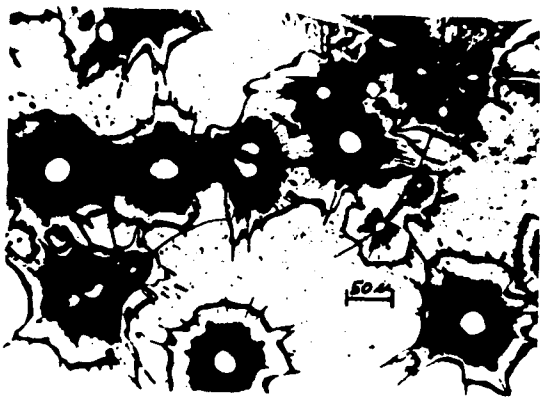

Figure 104. Capacitor 1004-T.

Figure 105. Capacitor 1028-T.

had a gold counter electrode and an aluminum bottom electrode. An isolated breakdown in another capacitor, which also had a gold counter electrode is shown in Fig. 105. Judging from the pink and blue interference colors, there is a thin layer of gold surrounding the central transparent region. The gold electrode is destroyed in a quite irregular pattern of radial streaks.

Many breakdown patterns indicate that the occurrence of one tends to promote the occurrence of another, thus giving a spreading or fanning effect. This spreading is illustrated in Fig. 106. The transparent region seems to be a long string of breakdowns. The adjacent dark structure is green and is a form of filament damage. Occasionally this filament damage occurs in regions outside the active portion of the capacitor. Fig. 107 shows a close-up view of the same pattern. The formation of dark balls is shown within a dark yellow area between the transparent region and the unaffected part of the electrode. A similar effect with smaller transparent regions is shown in Fig. 108.

Figs. 109 and 110 show breakdowns which blew large portions of the capacitor off the glass. Pieces of the capacitor are seen in both pictures. By the explosive removal of large chunks off the glass, broad areas of transparency are formed. The radial pattern in Fig. 109 is more typical of thicker capacitors.

While studying the effects of humidity, one capacitor was partially over-coated with a 5000 Å layer of silicon monoxide. The humidity tests were inconclusive, but an interesting breakdown feature was noted. Figs. 111 and 112 show the same view of a typical breakdown which occurred in the uncoated part of the capacitor. Fig. 112 is made with transmitted

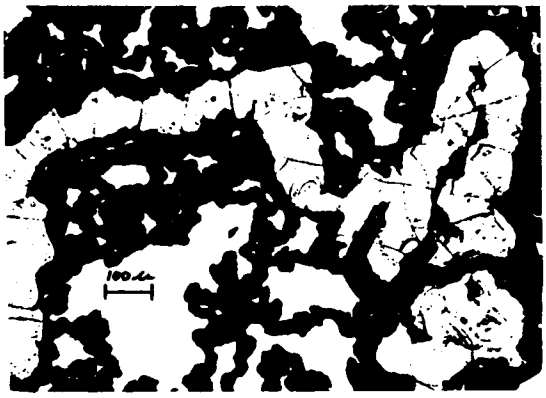

Figure 106. Capacitor 114a.

Figure 107. Capacitor 114a.

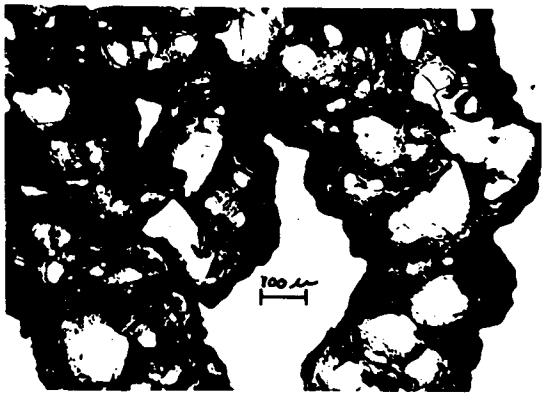

Figure 108. Capacitor 113a.

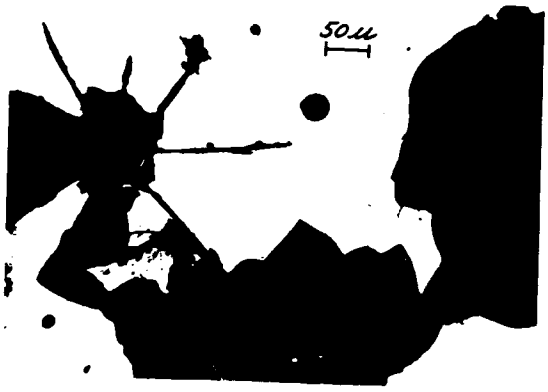

Figure 109. Capacitor 7/7a.

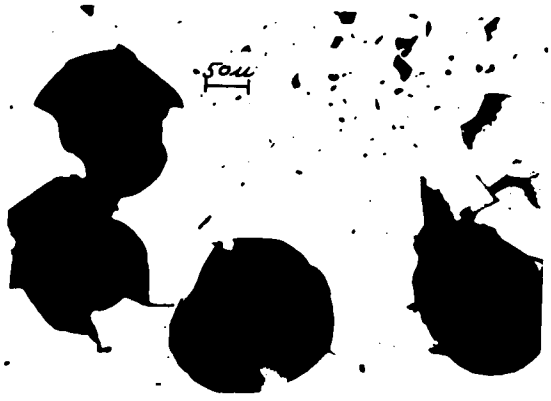

Figure 110. Capacitor 7/7b.

Figure 111. Capacitor 1016-T.

Figure 112. Capacitor 1016-T.

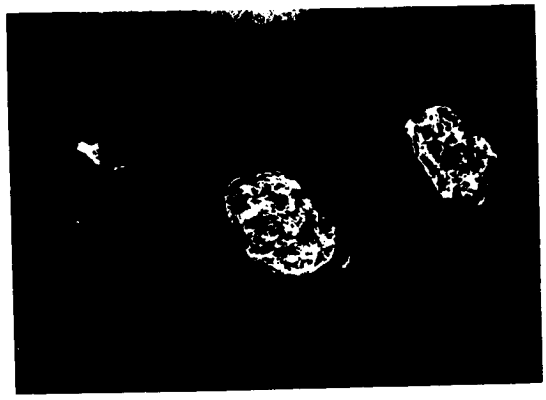

Figure 113. Capacitor 1016-T.

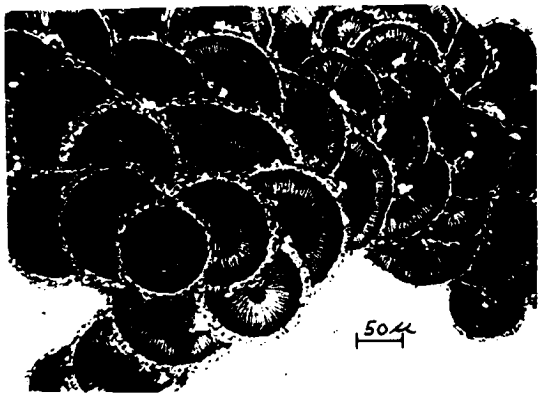

Figure 114. Capacitor 1020-T.

Figure 115. Capacitor 1020-T.

Figure 116. Capacitor 1020-T.

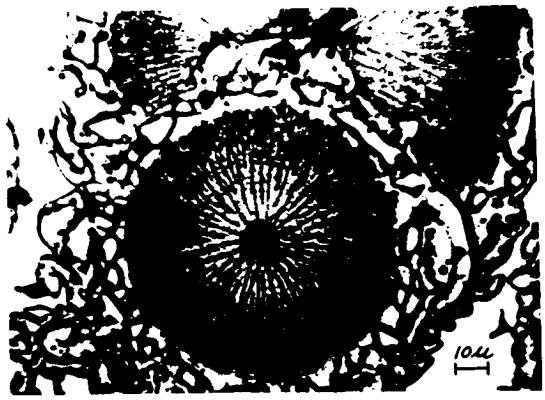

Figure 117. Capacitor 1020-T.

light only. Each of the little bubbles surrounding the breakdown has a small hole, generally on the side of the bubble. Just how this array of bubbles and holes is related to the large breakdown is not known. In the region over-coated with silicon monoxide the breakdowns have a much different appearance as shown in Fig. 113. The breakdowns are a little smaller and the bubbles and associated holes are missing.

Figs. 114 and 115 show breakdowns which exhibit much structure. The periphery of the radial pattern is yellow; thus, indicating that the dielectric is intact. Only very small portions (the centers) of the breakdowns are transparent. Three breakdowns in Fig. 115 have a green color near their perimeter. The green is the same color as the interference color at the edge of the top electrode. It is probably a thin layer of aluminum which was not vaporized in the breakdown. This breakdown pattern is further illustrated in Figs. 116 and 117. The extent of the radial pattern varies somewhat as does the size of the exposed dielectric region at the edge of the breakdown. A concentric pattern is observed at the center of the breakdowns. The characteristic dark balls of, presumably, silicon are also present in the exposed part of the dielectric. There are only occasional breakdowns found on the capacitor which form a full circle such as those shown in Figs. 116 and 117. Extending from the circular breakdown are numerous breakdowns, each with its center at the edge of another. This feature is further evidence to support the idea that new breakdown center defects are formed by breakdowns. The rate of breakdown for these capacitors became higher that 1000 per second when V_{MIN} was only slightly exceeded. Figs. 118 through 120 show similar patterns in other capacitors.

Figure 118. Capacitor 105a.

Figure 119. Capacitor 1019-T.

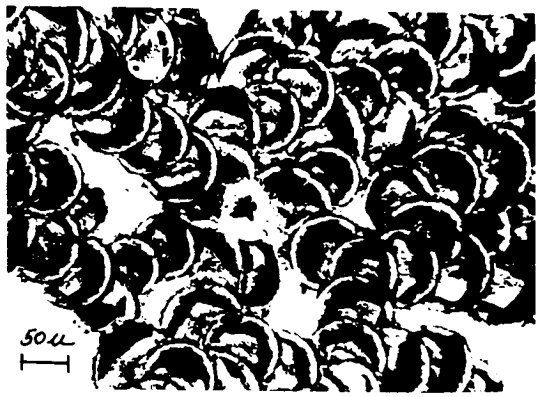

Figure 120. Capacitor 1022-T.

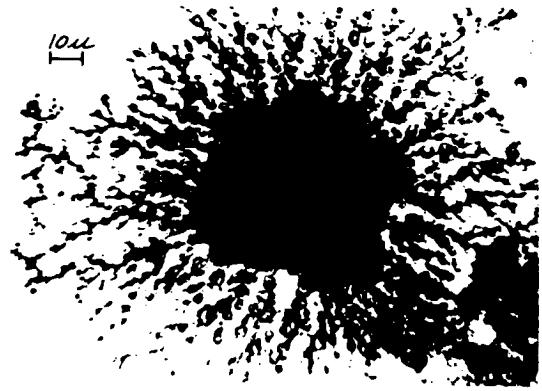

Figure 121. Capacitor 1031-T.

Figure 122. Capacitor 1031-T.

Figure 123. Capacitor 1015-T.

Figs. 121 and 122 also show a radial pattern, but the streaks are somewhat less organized. Fig. 122 is made with transmitted light only and very closely resembles the Lichtenberg patterns observed in the electron microscope. The streaks are made of numerous holes through the capacitor. The streaks near the periphery of the breakdown in Fig. 121 are of the same form of those shown in Fig. 123. A region similar to that shown in Fig. 123 was stripped and examined in the electron microscope.

Fig. 124 shows an area of much destruction by several breakdowns. Areas where the dielectric has been uncovered, but otherwise unharmed, are also shown. Filament damage is characterized by the streaky pattern.

Occasionally there are large areas of destruction surrounding circular regions which are apparently unaffected. For the sake of notation these unaffected regions have been termed "anti-breakdowns". Several such areas are shown in Figs. 125, 126, 127, and 128. The dark destroyed regions of these capacitors appear to be primarily due to electrode damage. The anti-breakdown is always characterized by a defect at the center. If several such defects are close together, the anti-breakdowns join as shown in all four of these figures. Whether the defect associated with the anti-breakdown is the same type as the breakdown center defect has not yet been established.

Circular patterns of dark spots, of about the same size as the anti-breakdowns of Fig. 128, have been found in several capacitors. These are not necessarily in the active region of the capacitor. Frequently they are located outside the area of the top electrode. None have been found in regions where there is neither electrode. Further, these circular

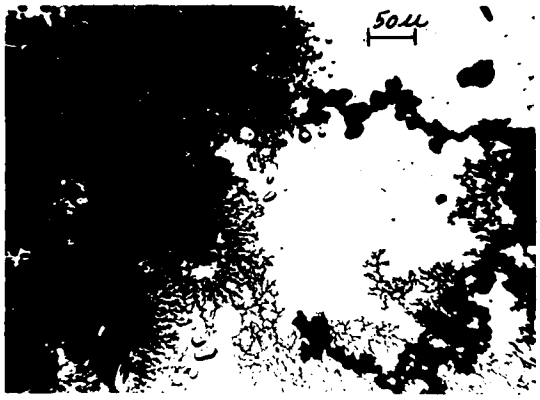

Figure 124. Capacitor 1032-T.

Figure 125. Capacitor 112a.

Figure 126. Capacitor 1027-T.

Figure 127. Capacitor 115a.

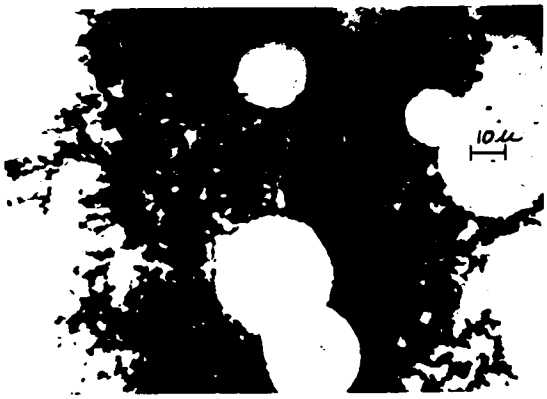

Figure 128. Capacitor 107a.

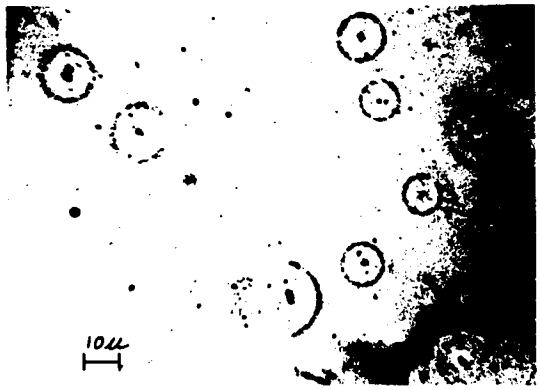

Figure 129. Capacitor 10/2a.

defects have not been observed in plain dielectric or plain electrode films. These observations suggest that dielectric-electrode reactions generate the defects. Fig. 129 depicts these defects at the edge of the top electrode. More of these defects are shown in Fig. 130. Occasionally there will be found tiny holes through the capacitor at the defects in these circular patterns. A plausible way in which this circular array of defects could yield an anti-breakdown is by the first breakdowns occurring at the defects in the circles, thus isolating the central spot from the electrode.

Figs. 131 and 132 show isolated breakdowns with adjacent filament damage. Buckling around the edge of the breakdowns is also evident.

Fig. 133 illustrates several isolated breakdowns amid much filament damage. The large dark areas are green, which indicates that a thin layer of aluminum remains.

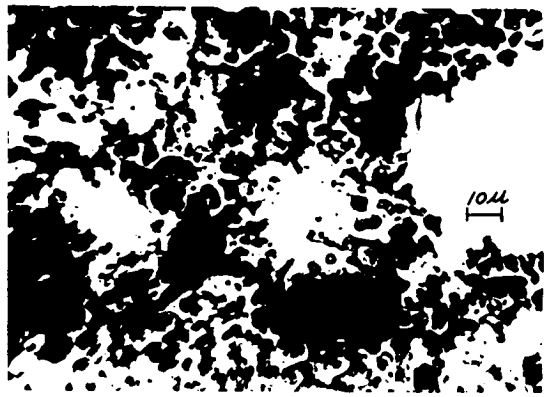

Figure 130. Capacitor 8/3b.

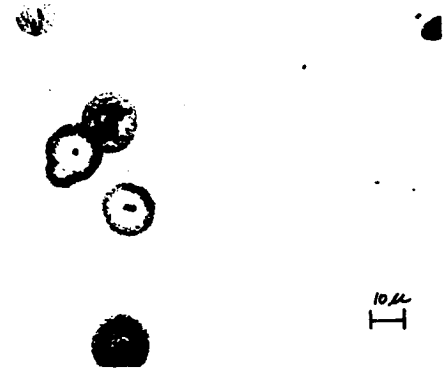

Figure 131. Capacitor 1028-T.

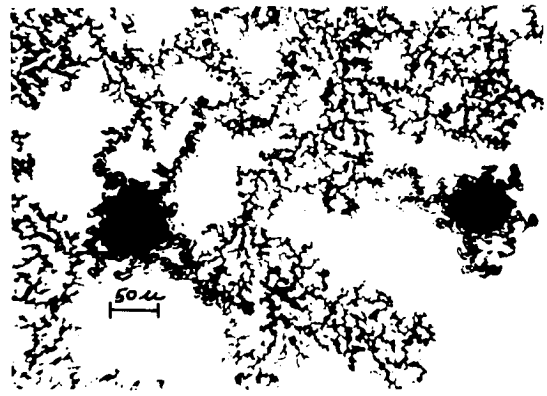

Figure 132. Capacitor 1028-T.

Figure 133. Capacitor 112b.

V. CONCLUSIONS

A. Summary of Results

A technique was developed whereby thin film silicon monoxide capacitors could be vacuum deposited and subsequently removed from the substrate intact. This development enabled an electron microscope study of the capacitors while under electrical stress. Resulting from this study was the discovery of breakdown center defects of about one half micron diameter. Furthermore, it was established that during breakdown the silicon monoxide decomposes, leaving free crystalline silicon. A number of types of breakdown patterns were observed, all of which contribute toward a better understanding of the breakdown process.

The breakdown strength was found to be almost independent of temperature between $80^{\circ}K$ and $363^{\circ}K$ with a slight increase in breakdown strength with decreasing temperature. This is in marked contrast with the strong temperature dependence in dc conductivity at low voltages (below V_{MAX}).

A comparison of the breakdown strength data with published theories showed that the best agreement was obtained with the electron ionization avalanche model as developed by Forlani and Minnaja.[41] Although their model is based upon an ionic crystalline dielectric, their $1/W^{\frac{1}{2}}$ breakdown strength dependence on thickness roughly fits the experimental data of silicon monoxide capacitors. Their theory is based purely on field emission and is essentially temperature independent. Other

theories of breakdown (intrinsic, thermal, and avalanche) are not nearly in agreement with the data.

It was found that the voltage across the capacitor does not drop to zero volts during a breakdown, but to a value V_{MIN} which is a constant for a given polarity and a given capacitor. This minimum voltage is independent of temperature. It is of significance that no breakdowns were ever observed below a given capacitor's V_{MIN}. The field corresponding to the experimental value of V_{MIN} appears to depend on the reciprocal of dielectric thickness over the range investigated.

A study was made of the rate-of-breakdown as the voltage across a capacitor is steadily increased to and above the voltage corresponding to the breakdown strength. Since the rate-of-breakdown should be closely related to the probability of a breakdown, the results are compared with tunnel-emission injection of current into the dielectric at the cathode, an inherent part of the electron ionization avalanche breakdown. Agreement is good in some cases, but not as good for higher voltages.

Several observations related to breakdown pulse characteristics and measurements were made.

A broad range of breakdown structure is discussed in connection with an optical microscopic examination of the breakdowns which occurred in the capacitors on glass slides.

No correlation between breakdown strength and deposition parameters was established. Neither was any correlation found between substrate irregularities and breakdown strength.

B. Suggestions for Further Work

There is one area of this study which remains incomplete--identification of the breakdown center defects and their source. The spots are too thick to give a detectable diffraction ring pattern in the 50,000 volt microscope which is available. They are too scarce to be detected by x-ray examination. If they are crystalline it may be possible to observe their diffraction pattern in a higher voltage electron microscope. The microprobe is another instrument which affords good possibilities in making the identification.

A more detailed study of the breakdown pulse shape is suggested. Such an investigation may explain the details of the breakdown structure and shed more light on the mechanism. A closer study of the effects of humidity on breakdown also seems desirable.

An improvement of the breakdown strength apparatus would be to replace the relays with electronic switches. This change would shorten the time between the occurrence of the first breakdown and the removal of the applied voltage and reduce the problem of open-circuiting the capacitor with a large number of breakdowns.

The most obvious suggestion, perhaps, is that the same general plan of investigation be used in a study of other dielectrics, both amorphous and crystalline.

In the area of theoretical work, it seems that a suitable theory of breakdown using an amorphous model has not yet been developed. Inherent within the theory should be an explanation of F_{MIN} and its relation to F_{MAX}. It seems that the rate-of-breakdown observations should also be intimately related with, possibly, both F_{MIN} and F_{MAX}.

LIST OF REFERENCES

1. M. A. Novice, Vacuum 14, 385-391 (1964).

2. M. A. Novice, Brit. J. Appl. Phys. 13, 561 (1962).

3. J. Priest, H. L. Caswell, and Y. Budo, Vacuum 12, 580 (1961).

4. J. Priest, H. L. Caswell, and Y. Budo, J. Appl. Phys. 34, 347 (1963).

5. L. Holland, Vacuum Deposition of Thin Films (Chapman & Hall, Ltd., London, 1963), pp. 485-487.

6. H. Hirose and Y. Wada, Japan J. Appl. Phys. 3, 179 (1964).

7. I. T. Johansen, J. Appl. Phys. 37, 499 (1966).

8. F. W. Schnekel, IEEE Trans. CP-11, 94-102 (1964).

9. G. Siddall, Vacuum 9, 274 (1960).

10. T. E. Hartman, J. C. Blair, and R. Bauer, J. Appl. Phys. 37, 2468 (1966).

11. P. P. Budenstein (private communication).

12. S. W. Chaikin and G. A. St. John, Electrochem. Technology 1, 291 (1963).

13. Holland, op.cit., pp. 71-72.

14. A. R. Wolter, J. Appl. Phys. 36, 2377 (1965).

15. Progress Report 33, Laboratory for Insulation Research, MIT, pp. 21-22.

16. S. Tolansky, Multiple Beam Interferometry of Surfaces and Films (Oxford University Press, London, 1945), p. 224.

17. R. C. Williams and R. C. Backus, J. Appl. Phys. 20, 98-106 (1949).

18. G. Thomas, Transmission Electron Microscopy of Metals. (John Wiley & Sons, New York, 1964), pp. 134-139.

19. G. E. Bradley, Brit. J. Appl. Phys. 5, 65-66 (1954).

20. Specimen holder designed by P. P. Budenstein, Auburn University.

21. L. Glassman made micrographs, used to identify silicon in the breakdown area, with an RCA-EMU-3 100 KV electron microscope at the Georgia Tech Experimental Station.

22. G. Marsh of NASA, (Huntsville, Alabama) identified silicon in the breakdown area using an RCA-EMU-3 100 KV electron microscope.

23. P. P. Budenstein (private communication).

24. Siddall, loc. cit.

25. P. P. Budenstein (private communication).

26. F. H. Merrill and A. von Hippel, J. Appl. Phys. 10, 873-887 (1939).

27. S. Whitehead, Dielectric Breakdown of Solids, (Oxford University Press, Great Britain, 1953), pp. 236-244.

28. F. Forlani and N. Minnaja, Phys. Stat. Sol. 4, 311, (1964).

29. W. Franz, Handbuch der Physik 17, 153 (1956) cited by F. Forlani and N. Minnaja, Phys. Stat. Sol. 4, 311 (1964).

30. J. J. O'Dwyer, The Theory of Dielectric Breakdown of Solids, (Oxford University Press, Great Britain, 1964) pp. 60-62.

31. Ibid., pp. 14-24.

32. Ibid., pp. 41-45.

33. Ibid., pp. 85-86.

34. Ibid., pp. 54-55.

35. P. P. Budenstein (private communication).

36. P. P. Budenstein (private communication).

37. P. P. Budenstein (private communication).

38. Siddall, loc. cit.

39. Siddall, loc. cit.

40. Chaikin and St. John, loc. cit.

41. Forlani and Minnaja, loc. cit.

APPENDIX A

SAWTOOTH GENERATOR FOR BREAKDOWN STRENGTH STUDY

A sawtooth generator, illustrated by the circuit in Fig. 134, has been constructed to supply a ramp voltage with a maximum amplitude of 300 volts. The power supply used to energize this circuit has a floating ground, thus the COMMON terminal may be at the high voltage (+V) side of the circuit.

The circuit employs a 6AU6A pentode to provide a constant current to a selected (through switch S1) charging capacitor. The sweep time of the ramp is determined by the selected capacitance and the PENTODE BIAS.

With S2 at INT and S1 positioned at one of the capacitors, the voltage at the OUT terminal, relative to the COMMON terminal, decreases from an initial value of about minus ten volts toward minus 350 volts. Thus a negative-going ramp is produced. At some voltage above GRD potential, (determined by the THYRATRON BIAS), the 2D21 grid-controlled Thyratron triggers and discharges the capacitor. This cycle continues repetitively with S2 set at INT.

With S2 positioned at EXT the repetition of the ramp is controlled by the external relay switches S3 and S4. These are appropriately energized by the occurrence of a breakdown pulse in the test capacitor. Thus the ramp may be terminated by a breakdown in the test capacitor (see Fig.13).

This circuit has been used to test silicon monoxide capacitors having a breakdown voltage greater than 100 volts.

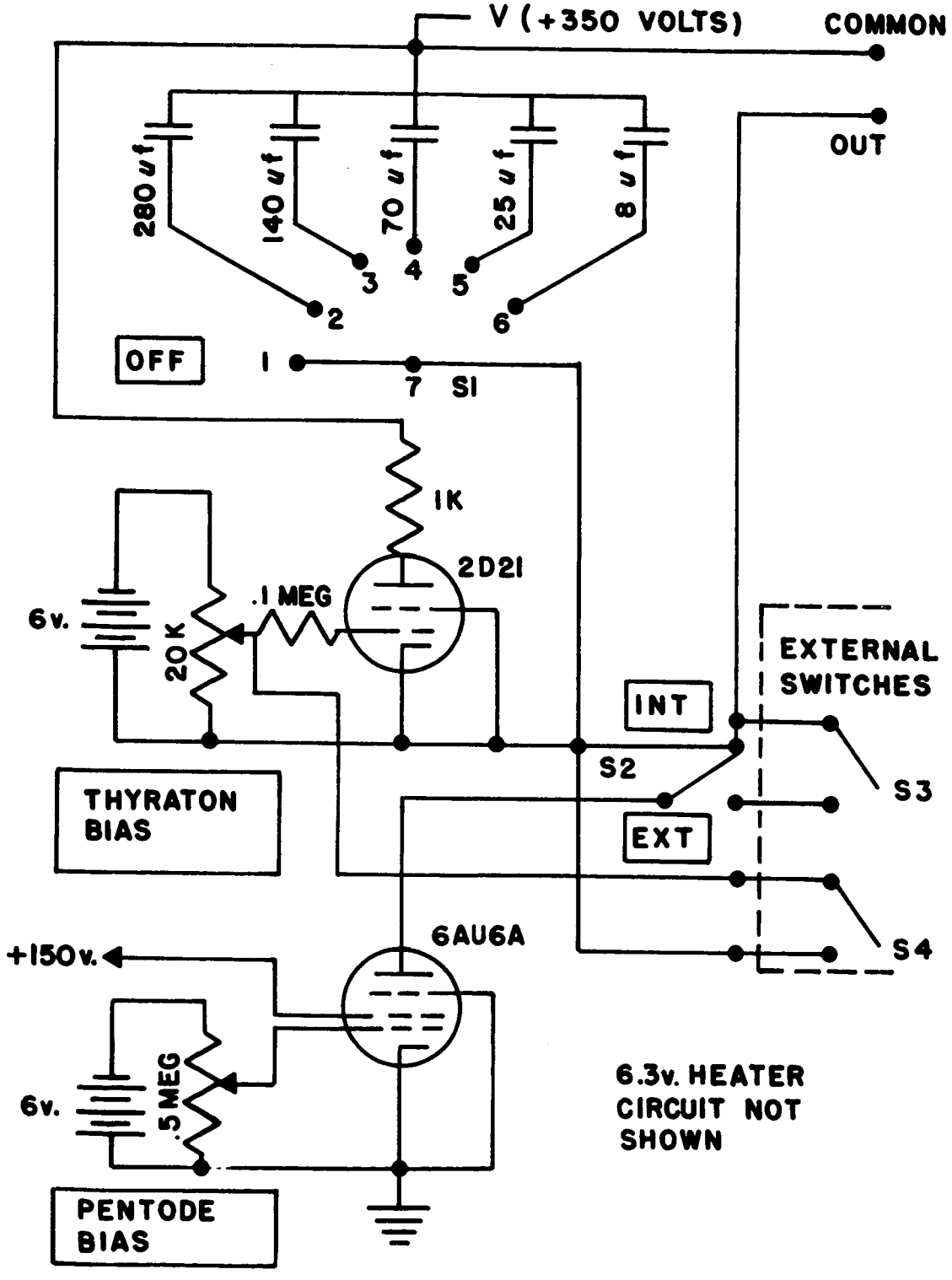

Figure 134. Sawtooth generator schematic.

APPENDIX B

AMPLIFIER CIRCUIT

A three stage, transistorized amplifier was constructed to amplify the breakdown pulse to a level sufficient to trigger the Hewlett-Packard Pulse Generator. The circuit shown in Fig. 135 has an amplification of twenty. The first and last stages are emitter followers. The second stage provides the amplification.

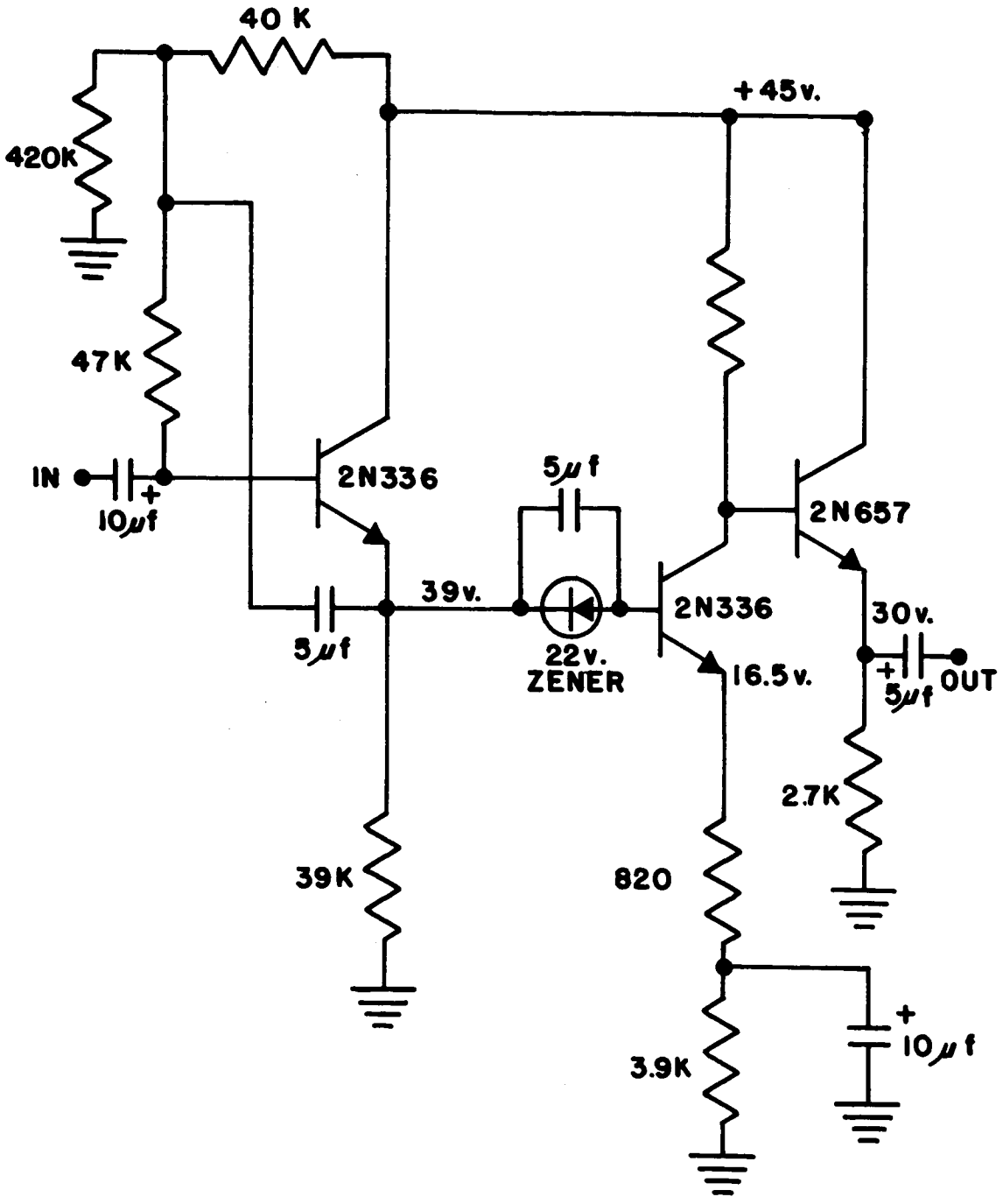

Figure 135. Amplifier circuit.